

QUANTIFICATION OF SPHEROID FORMATION MECHANISM BY
SIZE AND SHAPE ANALYSIS

CHUA SIANG MENG

B.Sc.(Pharm.)(Hons.), NUS

A THESIS SUBMITTED FOR THE DEGREE OF
DOCTOR OF PHILOSOPHY
DEPARTMENT OF PHARMACY
NATIONAL UNIVERSITY OF SINGAPORE

2008

ACKNOWLEDGEMENTS

I am deeply grateful to my supervisors, Assoc Prof Paul Heng and Dr Celine Liew for their unyielding support and guidance provided during the course of my study.

I wish to thank the National University of Singapore, for providing me with the opportunity for postgraduate study with a research scholarship.

My appreciation goes to Assoc Prof Chan Lai Wah for her advices on my research and also for being a supportive mentor to pharmacy's postgraduate community.

My thanks also go to Ms Teresa Ang, Ms Wong Mei Yin and Mr Peter Leong who have maintained the laboratories excellently and provided assistance whenever I needed. Mr Peter Leong has also become a good friend and I cherish this friendship.

My fellow postgraduates in GEA-NUS Pharmaceutical Processing and Research Laboratory have been a wonderful company to be with. Their kindness and support have always helped me overcome my many tough challenges. My thanks to my senior Dr Gu Li for her guidance. I am fortunate to be in the company of Dr Cheong Wai See, Ms Elaine Tang and Mr Goh Cheong Hian. I will not forget their friendship and selfless support during the course of my research.

Last but not least, I am indebted to my parents and Zheng Lin for believing in me and supporting me in whatever I do.

Siang Meng

2008

TABLE OF CONTENTS

	Page
ACKNOWLEDGEMENTS.....	i
TABLE OF CONTENTS.....	ii
SUMMARY.....	vi
LIST OF TABLES.....	ix
LIST OF FIGURES.....	xi
LIST OF ABBREVIATIONS.....	xiii
PART 1. INTRODUCTION.....	1
1. Spheroids.....	1
2. Methods of spheroid production.....	2
2.1. Extrusion-spheronization.....	2
2.2. Rotary processing.....	6
3. Process and formulation parameters influencing spheroid formation.....	7
3.1. Parameters affecting extrusion-spheronization.....	7
3.2. Parameters affecting rotary processing.....	9
3.3. Parameters affecting extrusion-spheronization and rotary processing.....	9
3.4. Influence of formulation.....	10
4. Contrasting extrusion-spheronization and rotary processing.....	12
5. Spheroid formation and growth.....	12
6. Characterization of spheroids.....	14
6.1. Spheroid size and size distribution.....	15

6.2. Spheroid shape	22
7. Size distribution in other particulate systems	23
8. Log normal, normal and mixed Gaussian distributions	24
PART 2. OBJECTIVES	27
PART 3. MATERIALS AND METHODS	29
1. Materials	29
2. Methods	29
2.1. Preparation of spheroids	29
2.2. Spheroid production by ES	31
2.3. Spheroid production by RP	33
2.4. Formation process during ES	33
2.5. Controlled spheroid agglomeration during RP	34
2.6. Drying of spheroids	35
2.7. Characterization of spheroids	35
2.7.1. Size analysis by sieving	35
2.7.2. Sizing by image analysis	36
2.7.3. Roundness quantification by image analysis	38
2.7.4. Crushing strength analysis	39
2.7.5. Moisture content determination	40
2.7.6. Surface roughness analysis	40
2.8. Statistical analysis on spheroid size distributions	41
3. Illustration and quantification of simulated spheroid images	42

PART 4. RESULTS AND DISCUSSION	44
1. Equivalency in process between ES and RP	44
1.1. Equivalency in spheronization conditions between different frictional surfaces	46
1.2. Producing RP spheroids of equivalent size and size distribution to ES spheroids	48
1.3. Effect of processes on size and size distribution of spheroids.....	49
1.4. Shape of size distribution between ES and RP spheroids.....	56
1.5. Effect of processes on spheroid roundness	56
1.6. Role of moisture in spheroid formation	57
1.7. Crushing strength of ES and RP spheroids.....	59
1.8. Visual examination of spheroid formation	61
1.9. Comparison of observed spheroid formation with existing theories	68
2. Mathematical quantification of spheroid formation process	75
2.1. Conventional size and shape characterization methods.....	75
2.1.1. Sieving	75
2.1.2. Image analysis.....	76
2.2. Representing ES spheroid size with MG distribution.....	85
2.2.1. Verifying size distribution of ES spheroids statistically.....	86
2.2.2. Quantifying spheroid formation with MG distribution.....	88
3. Relationship between size and roundness of ES spheroids	91
3.1. Sensitivity of roundness descriptors in characterizing spheronization.....	94

TABLE OF CONTENTS

3.2. Correlation between roundness descriptors	95
3.3. Shape heterogeneity within ES spheroid population during spheroid formation.....	97
3.4. Novel method in spheroid shape analysis.....	101
3.4.1. Predominant spheroid shape during spheronization	108
4. Controlled spheroid agglomeration in rotary processor.....	110
4.1. Representation of RP spheroids with MG distribution.....	113
4.2. Effects of AGL on spheroid size.....	116
4.3. Effects of AGL on spheroid roundness.....	124
4.3.1. Applicability of roundness correlations with RP spheroids.....	124
4.3.2. Choosing robust spheroid roundness descriptors.....	127
4.4. Surface changes during spheronization with addition of AGL.....	132
4.5. Yield.....	139
PART 5. CONCLUSIONS.....	142
PART 6. REFERENCES	146
LIST OF PUBLICATIONS/POSTER PRESENTATIONS	163

SUMMARY

During extrusion-spheronization, extrudates readily break down into fines and broken cores. The breakdown of the extrudates is followed by extensive layering of the fines. Extensive layering of fines would occur during spheronization. In contrast, spheroids produced by rotary processing are formed mainly by nucleation and agglomeration. In this study, rotary processing produced spheroids used lesser amounts of water for granulation, as compared to extrusion-spheronization. By appropriate choice of the spheronization duration and peripheral tip speed, a teardrop studded rotating frictional plate could produce spheroids with properties equivalent to those produced by the cross-hatch textured rotational frictional plate. The possible of equivalency between 2 frictional plates that differ in plate surface design allows process engineers to explore new grounds in equipment design and to transfer know-how in production from extrusion-spheronization to rotary processing. The loss of moisture during spheronization was not found to be critical in spheroid formation. Although rotary processing is a less robust process compared to extrusion-spheronization, good quality spheroids could still be produced if the distribution of granulation liquid and movement of powder during wet massing could be improved. The mechanism of spheroid formation by extrusion-spheronization was found to be related to surface remodelling and fines layering.

Size analysis of spheroids using sieves was found in this study to lack sensitivity in detecting subtle size differences as compared to sizing using image analysis. Size

distribution of spheroids produced by extrusion-spheronization and rotary processing did not follow normal or log normal distribution. Instead, both processes produced spheroids which followed a mix Gaussian distribution. These findings offered direct evidence of spheroid size heterogeneity within a population. During extrusion-spheronization, dumbbell intermediates were not likely to be formed. Instead, observations of dumbbells could be a result of coalescence between spheroids of similar sizes. Compared to conventional methods for computation of spheroid size, subtle but significant spheroid size changes could be detected if size was represented by mix Gaussian distribution.

When used alone, circularity (C) was not critical in detecting improvement in roundness during spheronization. Data from both processes suggested strongly that eccentricity factor (e_R) and aspect ratio (AR) were highly correlated with each other. Therefore, due to mathematical simplicity, AR could be used as a roundness descriptor instead of e_R without being less critical in quantifying roundness. The novel method of using R values of AR -projected sphericity (PS) and AR - C correlations to distinguish shapes of spheroids such as oval, ellipse and rectangle with round ends were found to be applicable in both extrusion-spheronization and rotary processing spheroids. At the end of spheronization, the smaller extrusion-spheronization spheroids within the population were rounder and these smaller spheroids were also more variable in shapes, indicating that these spheroids participated actively in mass

transfer or remodelling. This observation further supported the hypothesis that within a spheroid population, the size and shape heterogeneity are related.

Prolonged spheronization would alter the surface morphology of spheroids. Addition of granulating liquid after spheroids were formed would definitely increase the size of spheroids and also cause a decrease in roundness.

LIST OF TABLES

	Page
Table 1. Recent studies on spheronization and the respective methods used for size, size distribution and shape characterization.	16
Table 2. Details of equipment used for spheronization of extrudates by ESC and EST.	32
Table 3. Process parameters for ESC and EST batches.....	32
Table 4. Process parameters for RT batches.....	33
Table 5. Process parameters and formulations used for controlled agglomeration of RP spheroids.	35
Table 6. Size, size distribution, roundness, moisture content and crushing strength of ESC, EST and RT spheroids.....	46
Table 7. One way ANOVA and post hoc LSD test for variables of ESC, EST, and RT batches.....	50
Table 8. Statistical descriptors for size distribution of ESC, EST931 and RT36% spheroids.	54
Table 9. Mean size and size distribution of ESC(TS) spheroids derived from size analysis using sieves.	76
Table 10. Mean size and size distribution of ESC(TS) spheroids derived from image analysis.....	77
Table 11. One way ANOVA and post hoc test for size and roundness of ESC(TS) spheroids.	83
Table 12. P values from Chi square curve fitting of size distribution of ESC(TS) spheroids to various distributions.	86
Table 13. Size distribution of ESC(TS) spheroids as defined by 3cMG distribution..	88
Table 15. Correlation coefficient (R) of roundness against ECD of ESC(TS) spheroids.	92
Table 16. Roundness values for different shapes.....	103

LIST OF TABLES

Table 17. Correlation between roundness descriptors for ellipse, oval and RRE.....	105
Table 18. Size and size distribution of RT(SR) spheroids as characterized by sieving.	112
Table 19 One way ANOVA of size and size distribution of RT(SR) spheroids.	113
Table 20. P values for Chi square curves fitting of size distribution of RT(SR) spheroids to statistical distributions.	114
Table 21. Size distribution of RT(SR) spheroids as defined by 3cMG distribution..	118

LIST OF FIGURES

	Page
Figure 1. Schematic diagrams of (a) a spheronizer and (b) a rotary processor	4
Figure 2. Dimensions of the surface protuberances of (a) cross-hatch and (b) teardrop studded frictional plates.	5
Figure 3. Schematics showing processes leading to spheroid formation.....	30
Figure 4. Photographs of time-sampled spheroids depicting stages of spheroid formation in ESC, EST931 and RT36%.	62
Figure 5. Sequential frames of ESC spheroid formation captured <i>in situ</i> using high speed video camera.	67
Figure 6. Model of spheroid formation by (a) ES and (b) RP.	72
Figure 7. Effect of spheronization duration on (a) e_R , (b) AR, (c) PS and (d) C of ESC(TS) spheroids.....	78
Figure 8. PDF of ESC(TS) spheroids.	79
Figure 9. R values of correlations among roundness descriptors for ESC(TS) spheroids.	95
Figure 10. Intra lot R values of AR- e_R and C-AR correlations against ECD of spheroids (μm).	98
Figure 11. e_R , AR, PS, C of simulated images plotted against one another.	106
Figure 12. Moisture content of RT(SR) spheroids during RP.	111
Figure 13. Average DI of RT(SR)20 batches and respective DI % changed after AGL addition.	117
Figure 14. Roundness RT(SR)20 batches and respective roundness % changed upon AGL addition.	125
Figure 15. R values of roundness correlations for RT(SR) spheroids.	128
Figure 16. Surface roughness of RT(SR) spheroids.	133

LIST OF FIGURES

Figure 17. Surface morphology of RT(SR) spheroids as observed under scanning probe microscopy.....	135
Figure 18. Yield for RT(SR) processes.....	140

LIST OF ABBREVIATIONS

AGL	–	Additional granulation liquid
AR	–	Aspect ratio
C	–	Circularity
cMG	–	Components mixed Gaussian
DI	–	Arithmetic mean diameter
DI _{geo}	–	Geometric mean diameter
DI _{med}	–	Median diameter
D _{warith}	–	Arithmetic weight mean diameter
D _{wgeo}	–	Geometric weight mean diameter
D _{wmed}	–	Mass median diameter
ECD	–	Equivalent circle diameter
e _R	–	Eccentricity factor
ES	–	Extrusion-spheronization
ESC	–	Extrusion-spheronization with cross-hatch plate
ESC(TS)	–	Extrusion-spheronization with cross-hatch plate (Time sampling)
EST	–	Extrusion-spheronization with teardrop studded plate
LSD	–	Least square difference
MCC	–	Microcrystalline cellulose
PDF	–	Population density function
PS	–	Projected sphericity

LIST OF ABBREVIATIONS

RP	–	Rotary processing
RT	–	Rotary processing with teardrop studded plate
RT(SR)	–	Rotary processing with teardrop studded plate (Spray rate)
S630	–	Copovidone
SDI	–	Arithmetic standard deviation
SDarith	–	Arithmetic weight standard deviation
SDwgeo	–	Geometric weight standard deviation
SpanI	–	Span derived from image data
Spanw	–	Span derived for sieving data
R	–	Pearson correlation
Ra	–	Arithmetic average roughness
RRC	–	Rectangles with round corners
RRE	–	Rectangles with round ends
Tween 80	–	Polysorbate 80

PART 1.
INTRODUCTION

PART 1. INTRODUCTION

1. Spheroids

Granules are generally physically and chemically less prone to changes compared to powders. Granules are easier to handle, possess better flow and are less likely to cake or harden on storage (Schwartz, 1988). Spheroids are a subset of granules. They are free flowing spherical granules, commonly of size between 0.5-1.5 mm (Sellassie, 1989a). Hence they possess certain properties which are advantageous over irregularly shaped granules. These properties include narrow size distribution, uniformity in shape, low friability, better packing and better flow (Conine and Hadley, 1970; Reynolds, 1970; Robinson and Hollenbeck, 1991). Spheroids are the desirable choice for capsule filling as they possess good flow properties and are resistant to breakdown during handling.

The spherical shape allows spheroid coating to be carried out efficiently. Controlled released dosage forms can be made with drug-loaded cores and release modifying coatings. Drugs which are incompatible with one another can be placed in the same capsule by first formulating the different drugs into different spheroids and subsequently applying coating on the spheroids to function as a protective layer.

Compared to single unit dosage forms, these multiparticulate systems offer advantages such as improved bioavailability, consistency in gastric emptying rate and

less variability in intra-subject and inter-subject drug plasma profiles. Occurrences of dose dumping effects can also be minimized (Sellassie et al., 1985; Sellassie, 1994).

2. Methods of spheroid production

Depending on the ways particles are brought together, spheroids could be produced by three general techniques (Sherrington and Oliver, 1981a; Sellassie, 1989b),

- a) globulation - spray drying, spray congealing, cryopelletization,
- b) compaction, and
- c) agitation - solution or suspension layering, powder layering, balling, high shear pelletization and rotary processing.

Being a multi-step process, extrusion-spheronization (ES) can be classified as a combination of compaction and agitation. ES is currently one of the most popular methods of producing spheroids.

2.1. Extrusion-spheronization

ES could be broadly described by these steps: wet massing, extrusion, spheronization and drying. In general, powders are premixed prior to wet massing. Mixing and wet massing could be carried out simultaneously in mixer granulators such as planetary mixers, sigma blade mixers, high shear mixers and continuous granulators (Vervaet et al., 1995). During wet massing, a moistening agent is added to the powder mixture in

order to produce a homogenous wet mass. The moistening agent is usually water but other binders have also been used to produce spheroids (Umprayn et al., 1999). The wet massing step is usually followed by extrusion within a short time interval.

However, some research groups have also allowed the wet mass to stand for a few hours to facilitate moisture equilibration prior to extrusion (Fielden et al., 1989; Newton et al., 1992).

In the extrusion step, pressure is exerted on the wet mass, forcing it to flow through orifices of the extrusion die. As such, the wet mass is densified and shaped into cylindrical aggregates termed as extrudates. Types of extruders are classified according to the design of the die and the wet mass conveying mechanism (Fielden and Newton, 1992). The different types of extruders include ram, screw, radial screen, roll, gravity feed, sieve and basket extruders. Different types of extruders would exert varying degree of densification onto the wet mass (Sherrington and Oliver, 1981b). Specialized equipment such as the twin screw extruder could carry out mixing, wet massing and extrusion in a single step (Linder and Kleinebudde, 1994).

Spheronization is carried out in a spheronizer after extrudates are produced.

Extrudates within the product chamber of the spheronizer experience frictional forces exerted by the rotating frictional plate (Figure 1).

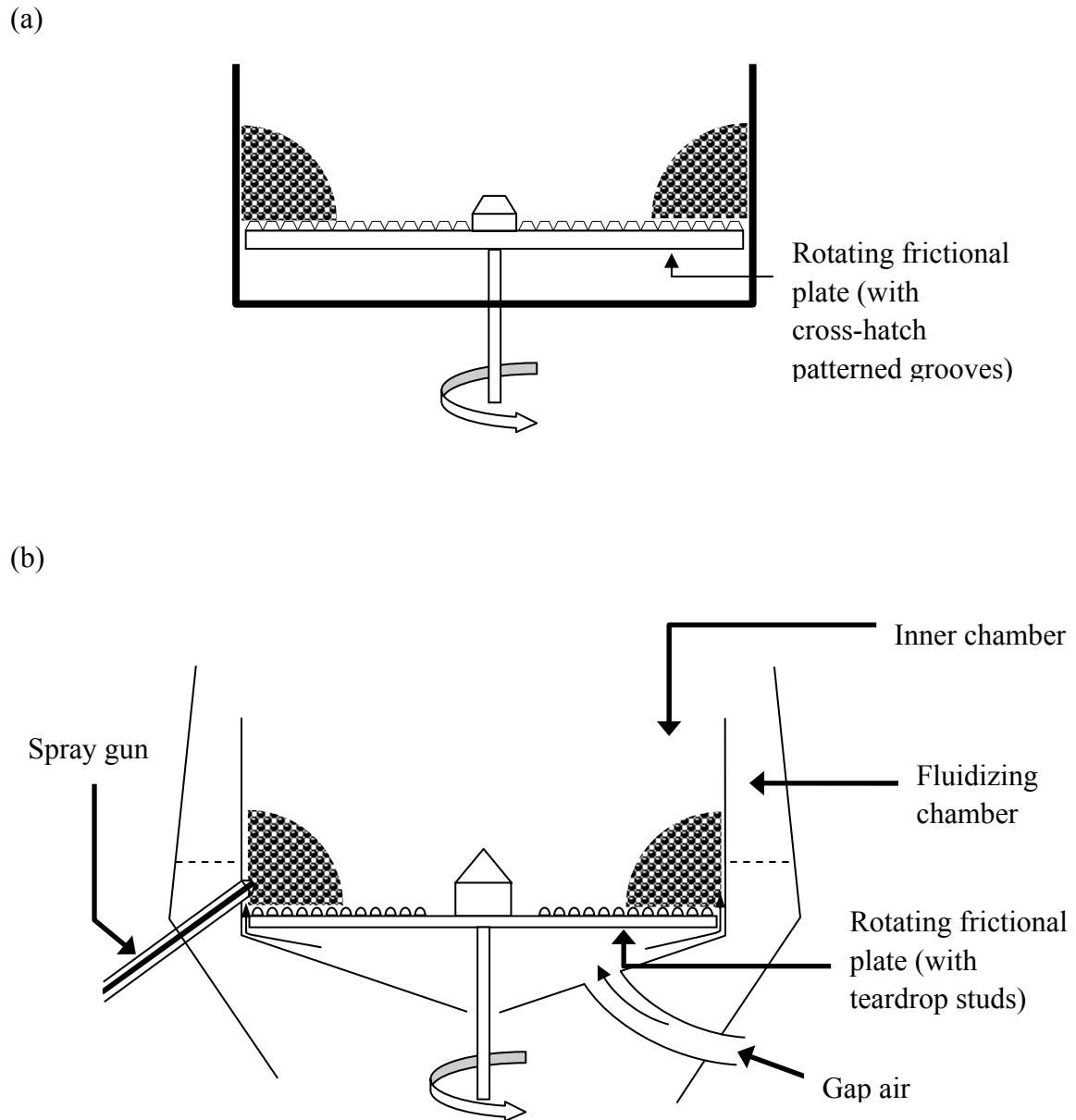


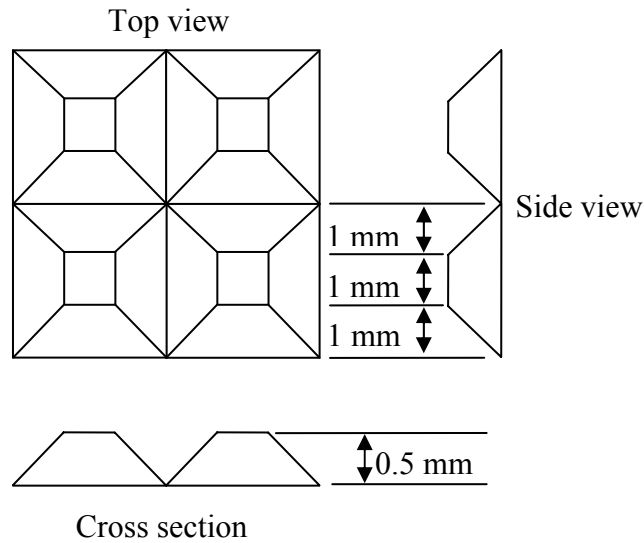
Figure 1. Schematic diagrams of (a) a spheronizer and (b) a rotary processor

Typically, the surface texture of the rotating frictional plates is made up of a cross-hatch pattern of square pyramidal studs with rectangular grooves (Figure 2).

The plate can also be of a radial pattern, consisting of rectangular grooves radiating from the center of the plate. It has been reported that cross-hatch or radial textured rotating frictional plates did not affect spheroid quality unless the extrudates were of

poor quality (Newton et al., 1995a). During spheronization, the sharp edged texture of the rotating frictional plate breaks up the cylindrical extrudates into shorter segments as they tumble around the spheronizer in a rope like motion. With prolonged tumbling, these shorter segments would be rounded, forming spheroids.

(a)



(b)

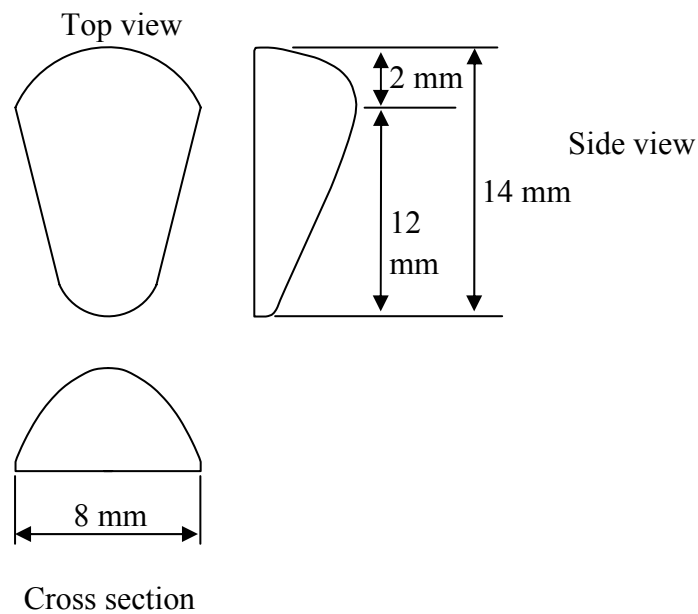


Figure 2. Dimensions of the surface protuberances of (a) cross-hatch and (b) teardrop studded frictional plates.

Spheroids are commonly dried either by using hot air ovens or by fluid-bed driers. These two methods have been compared by Dyer et al. (1994). Other drying methods include microwave drying (Bataille et al., 1993) and freeze drying (Kleinebudde, 1994).

2.2. Rotary processing

Rotary processing (RP) is alternative method to produce spheroids. The main difference between ES and RP is that the former is a multi-step process while the latter is a “one pot” process. Different terms have been used to describe the equipment for RP. These include centrifugal equipment/granulator, rotary fluidized bed granulator, rotary processor and rotor granulator (Figure 1). During RP, liquid addition, wet massing, agglomeration and spheronization would take place simultaneously. Like the spheronizer, the rotary processor has a product chamber with a rotating frictional plate located at the bottom (Figure 1). However, the texture of its rotating frictional plate differs from that of the typical spheronizer. The protrusions on the plates of the rotary processor are generally rounded with less well-defined edges, e.g. in the shape of teardrops (Figure 2) or truncated pyramids. Unlike the spheronizer, the rotating frictional plate of rotary processor has been designed to fulfill a wider range of requirements: transporting powders around the rotary processor, transporting aggregates around the rotary processor, densifying aggregates, breaking down excessively large aggregates and rounding of aggregates. Within the product chamber, the rotary processor has a spray gun to introduce granulating liquid to the powder

mixture. The wall of the product chamber can be elevated, allowing materials to move outwards by centrifugal forces when they are agitated around the product chamber by the rotating frictional plate to the fluidizing zone. Hot fluidizing air is passed through the fluidizing zone to dry the materials. Another difference between a rotary processor and a spheronizer is the presence of gap air in a rotary processor. Pressurized air, termed gap air, is introduced from the bottom of the product chamber of the rotary processor through the clearance between rotating friction plate and the product chamber wall. At the beginning of RP when the powder mixture is still dry, the powder mixture can slip through the clearance between the rotating frictional plate and the product chamber when the plate rotates. The gap air prevents the slippage of powders through the clearance.

3. Process and formulation parameters influencing spheroid formation

The parameters affecting spheroid formation can be divided into three groups. The first group affects exclusively ES. The second group affects exclusively RP. The third group affects both ES and RP.

3.1. Parameters affecting extrusion-spheronization

The type of extruder used can affect the resultant spheroids. Compared to a rotary ring die press, a twin-screw extruder required a higher amount of water for producing

spheroids of equivalent size (Schmidt and Kleinebudde, 1998). Using a radial extruder, Vervaet and Remon (1996) investigated the effects of two different impeller designs and three different screen perforation geometries on the quality of spheroids produced. Their results showed that the impeller design and screen perforation geometry affected the maximum amount of lactose to be used as filler. Thoma and Ziegler (1998) researched on the optimum amount of water required for making spheroids using roll, axial and radial extruders. Among these types of extruders, the roll extruder required the least amount of water for successful spheroid formation. While the axial extruder tolerated the widest range of water concentration for successful spheroid formation, the maximum allowable water concentration for extrusion for the axial extruder was also the highest among the three extruders. Extrudates produced by the axial extruder were the densest, thus improving their ability to retain water within the matrix, resulting in a decrease in the amount of excess water on spheroid surfaces. This, in turn, reduced the tendency for excessive agglomeration during spheronization. Larger spheroids could be produced if a thicker screen was used (Hellen et al., 1993). Instead of evaluating extrusion performance by assessing the quality of spheroids produced, Shah et al. (1994 and 1995) investigated extrusion performance using an instrumented extruder. Extrudability of wet mass could be determined by the screen temperature and pressure (Shah et al., 1994). The yield of spheroids of size 710-1000 μm could be controlled by the screen pressure. Yield and tensile strength of wet mass were also able to affect the shape factor of spheroids (Shah et al., 1995).

3.2. Parameters affecting rotary processing

With sufficient amount of water for spheronization, an increase in spray rate would increase the spheroid size (Wan et al., 1994) whereas the rate of water addition during wet massing would not be an issue with ES. An increase in gap air pressure reduced the size of spheroids produced (Wan et al., 1994). Vertommen et al. (1998) attributed the influence of gap air pressure to the amount of water loss during water addition.

3.3. Parameters affecting extrusion-spheronization and rotary processing

A longer duration for spheronization allows an increased opportunity for agglomeration to take place. However, longer durations might cause spheroid size to decrease if spheronization speed is excessively high, promoting breakdown (Wan et al., 1993).

Spheronization at low speed would yield spheroids with poor form factor due to insufficient frictional forces to round them. Above a certain threshold speed, generally round spheroids can be formed (Wan et al., 1993). As spheronization speed increases, spheroid size increases to a maximum. Interplay of agglomeration and breakdown govern the size of resultant spheroids. Increase in spheronization speed promotes agglomeration. However, if spheronization speed is excessively high, the tendency for spheroids to breakdown is greater than to agglomerate, leading to a decrease in spheroid size (Wan et al., 1993).

Liew et al. (2000) used a “low-high-low” speed variation during rotary processing to produce spheroids with narrow size distribution, minimizing the production of oversize agglomerates. In that study, powder mixture was first agitated with a lower spheronization speed for the initial 2 min of water addition. Subsequently, the higher spheronization speed aimed to improve the water distribution within the wet mass. Upon completion of water addition or to prevent excessive agglomeration, the spheroids were allowed to tumble at a low speed to effect roundening.

Using teardrop studded plates with different heights, Heng et al. (2002) showed that an increase in the protuberance of teardrop studs on rotating frictional plate would increase the size and roundness of spheroids produced, at the expense of lowered yield due to increased adhesion of wetted powder mass onto the plate.

3.4. Influence of formulation

Regardless of ES or RP, the formulation for spheronization requires a balance between rigidity and plasticity. If the formulation is skewed towards rigidity, spheroids formed would be dumbbell shaped and the product would also have large amount of fines. On the other hand, a formulation which is extremely plastic would instead allow excessive agglomeration, resulting in excessively large spheroids (Harris and Sellassie, 1989). Extrudates with the right balance of rigidity and plasticity would break up into appropriate length, undergo minimal agglomeration and

allow rounding, yielding spheroids of desirable size and roundness. During RP, aggregates are formed when the granulating liquid is added to the powder mixture. With adequate plasticity, agglomeration between aggregates would take place. The right balance of rigidity and plasticity prevents uncontrolled agglomeration while allowing rounding of agglomerates, yielding spheroids.

Usually a spheronization aid has to be added into the formulation in order to achieve the right balance of plasticity and rigidity. Presently, microcrystalline cellulose (MCC) remains the spheronization aid of choice. Studies have been carried out to investigate the properties of MCC with the intention of elucidating the reasons for its superior “spheronization aid” properties (Koo and Heng, 2001; Heng and Koo, 2001; Soh et al., 2006).

Newton et al. (1992) demonstrated that equivalent grades of MCC between brands required different amount of water for spheroid production. Regardless of brands and grades of MCC, an increase in void volume of MCC was found to increase the amount of water required for spheronization while MCC:lactose with higher packing densities required a lower amount of water for spheronization (Heng and Koo, 2001). MCC having high bulk density, low porosity and low water retentive capacity required less water to produce spheroids. However these spheroids had lower roundness and also wider range in roundness (Koo and Heng, 2001).

Spheroid formulations containing soluble fillers, such as lactose, required less water than formulations having insoluble fillers, such as dicalcium phosphate, to produce spheroids (Holm et al., 1996).

4. Contrasting extrusion-spheronization and rotary processing

To date, there have not been many reports comparing ES and RP on spheroid production. Using the same formulation but with differing amounts of water for both processes, Pisek et al. (2001) reported that RP spheroids were of broader size distributions but higher densities. These spheroids were also more brittle. However, the comparisons were made between spheroids of different mean sizes. By varying rotor speed, spray rate and drug loading, Robinson and Hollenbeck (1991) produced RP spheroids which had similar dissolution rates and crushing strengths as those produced by ES.

5. Spheroid formation and growth

The formation of spheroids could be described from different approaches: bonding between individual particles, basic growth mechanism of aggregates, and breakage and remodelling of aggregates. Particles at close proximity with one another experience attractive forces such as valence forces, Van der Waals forces, electrostatic forces or magnetic forces. During wet granulation, liquid bridges are

formed between particles. The degree of liquid bridging depends on the amount of granulating liquid and the inter-particulate void volume. Classical models on liquid saturation of granules defined 4 states of liquid saturation as pendular, funicular, capillary and droplet (Iveson et al., 2001).

Theories have been proposed on how spheroids are formed and enlarged. These theories were based on experimental results and visual observations (Sastry and Fuerstenau, 1973; Sastry and Fuerstenau, 1977; Leuenberger and Imanidis, 1986; Mehrotra and Sastry, 1986). Experiments involving the use of tracers provided more convincing data which led to the proposal of the following spheroid growth mechanisms: nucleation, coalescence, layering and abrasion transfer (Sastry and Fuerstenau, 1973; Linkson et al., 1973; Bhrany et al., 1962).

Two prominent theories have been put forward to explain how the extrudates develop into spheroids via ES. Rowe (1985) proposed that extrudates would rapidly break up at the initial 20 s of spheronization, producing cylindrical-like aggregates with rounded ends. The shape of these aggregates would be remodelled sequentially into dumbbells, proceeding to ellipses, and eventually into spheroids. Upon observation of spheroid formation using plasticine as a starting material, the alternative theory which was proposed by Baert and Remon (1993) suggested that because extrudates were subjected to rope folding forces, these extrudates were twisted, resulting in the development of dumbbell shaped aggregates. Under this rope folding force, the

dumbbell shaped aggregates would break apart in the middle into 2 spheroid precursors. These precursors would eventually be rounded into 2 spheroids. The existence of a central cavity within each spheroid was postulated to be caused by folding at the point of dumbbell separation.

Unlike ES, RP has characteristics of high shear granulation, fluidized bed granulation and spheronization. Granulating liquid is added to the powder mixture tumbling on a rotating frictional plate. Nuclei progressively form, coalesce, consolidate, densify and eventually round off to form spheroids (Liew et al., 1998). Unlike in ES, wet massing, agglomeration and spheronization occur simultaneously during RP. The interplay of these process steps results in spheroid formation (Liew et al., 1998).

6. Characterization of spheroids

Spheroid quality is mainly determined by evaluating spheroid size, roundness, friability, dissolution rate, hardness, surface morphology, flowability and porosity (Vervaet et al., 1995). In general, spheroids could be analyzed by 2 approaches: their functional or process efficiencies. For example, on functional efficiency, drug can be included into the formulation and dissolution tests carried out to evaluate the dissolution profile (Chatchawalsaisin et al., 2004). Besides the dissolution profile, uniformity in drug content could also be inferred.

Percentage yield is often reported when process efficiency is considered to be more important. Yield is commonly defined by authors as percentage of spheroids within a desired size fraction. Percentage of oversized spheroids (Gu et al., 2006) or fines (Howard et al., 2006) have also been used to characterize process efficiency.

Homogenous spheroids of narrow size distribution are desired for capsule filling. Highly rounded spheroids with narrow size distribution generally have good flow properties. It is therefore important that spheroid quality should be evaluated by characterizing their size, size distribution and shape. Table 1 provides a list on recent publications on spheronization and respective methods used to characterize mean size, size distribution and shape.

During the last 4 years, there have been more publications on ES than on RP. Selected publications on RP which are not recent were also included in Table 1 as they are relevant in the review of methods used to characterize the size, size distribution and shape of spheroids.

6.1. Spheroid size and size distribution

Predominantly, sieving is the method of choice for characterizing spheroid size. Mass mean diameter has been used to represent the average size of spheroids produced by ES (Table 1). MacRitchie et al. (2002) and Boutell et al. (2002) used sieves of $\sqrt{2}$ size progression to compute the mass median diameter and interquartile range of spheroids. Tomer et al. (2002) similarly reported mass median diameter. The size

Table 1. Recent studies on spheronization and the respective methods used for size, size distribution and shape characterization.

Reference	Focus of research	Characterization methods and descriptors		Remarks
		Size and size distribution	Shape	
Pinto et al., 2006	Evaluation of quality of spheroids produced by a continuous spheronizer.	(Sieving) Median and interquartile range	(Image analysis) Aspect ratio	
Bommareddy et al., 2006	Inclusion of Carbopol® 974P in spheroids produced by ES.	(Sieving) 840 – 1410 µm size fraction reported as yield	(Image analysis) $"roundness" = \frac{P^2}{4\pi A \times 1.064}$	
Podczeczek and Knight, 2006	Relating rheological properties and fluid mobility of wet mass to quality of spheroids produced by ES.	(Sieving) Median and interquartile range	One plane critical stability	
Howard et al., 2006	Feasibility of replacing MCC with polyethylene oxide and methoxypolyethylene to produce spheroids by ES.	(Sieving) 707-1190 µm size fraction reported as percentage yield. < 707 µm size fraction reported as percentage fines.	(Image analysis) $"roundness" = \frac{P^2}{4\pi A}$	
Rough and Wilson, 2005	Extrudate defects, induced by varying extruder parameters, were related to the quality of spheroids produced by ES.	(Sieving) Sieve fractions individually reported, depicting size distribution	(Image analysis) Qualitative descriptions	

Table 1 (Continued). Recent studies on spheronization and the respective methods used for size, size distribution and shape characterization.

Reference	Focus of research	Characterization methods and descriptors		Remarks
		Size and size distribution	Shape	
Almeida-Prieto et al., 2006	Effects of process variables of ES on shape of spheroids produced, as described by circularity, aspect ratio, e_R , V_r and V_p .	(Image analysis) Mean size	(Image analysis)	Aspect ratio, e_R , V_r and V_p
Chukwumezie et al., 2004	Effects of formulation and process variables on ibuprofen spheroid production in a rotary processor.	(Sieving) Geometric weight mean diameter and geometric weight standard deviation	(Image analysis)	"sphericity" = $\frac{4A \times 3.142}{p^2}$
Agrawal et al., 2004	Using chitosan as a spheronization aid in spheroid production by ES.	(Sieving) Weight mean diameter	(Image analysis)	"sphericity" = $\frac{4A}{\pi d^2}$
Gu et al., 2006	Comparing the quality of spheroids produced by rotary processing using unblended and blended powder mixtures.	(Sieving) Percentage over 2.8 mm, mass mean diameter and span	(Image analysis)	Circularity, aspect ratio and e_R

Table 1 (Continued). Recent studies on spheronization and the respective methods used for size, size distribution and shape characterization.

Reference	Focus of research	Characterization methods and descriptors		Remarks
		Size and size distribution	Shape	
Liew et al., 2005	Feasibility study of using cross-linked polyvinylpyrrolidone as a spheronization aid in producing spheroids using ES.	(Sieving) Percentage over 2.8 mm size, mass mean diameter and span	(Image analysis) Circularity, aspect ratio and e_R	
Galland et al., 2005	The hydro-textural and morpho-granular characteristics of the products at various stages of ES were monitored and compared to quality of spheroids produced.	(Sieving) Mass mean diameter and interquartile range	(Image analysis) Elongation ratio = $\frac{d_{\min}}{d_{\max}}$	
Chatchawalsaisin et al., 2004	The quality of spheroids produced by ES when chitosan and/or sodium alginate were included in the formulation.	(Sieving) Mass mean diameter and interquartile range	(Image analysis) e_R and aspect ratio	Commented that aspect ratio was inferior.
Kristensen, 2005	The effects of different grades of lactose and MCC on quality of spheroids produced by RP.	(Sieving) Geometric weight mean diameter and geometric weight standard deviation	(Image analysis) Aspect ratio and "roundness" = $\frac{4\pi A}{p^2}$	Commented that size distribution was in good agreement with log normal distribution.

Table 1 (Continued). Recent studies on spheronization and the respective methods used for size, size distribution and shape characterization.

Reference	Focus of research	Characterization methods and descriptors		Remarks
		Size and size distribution	Shape	
Tho et al., 2005	Spheroids containing amidated low-methoxylated pectin were produced by ES and their quality investigated.	(Image analysis) Mean diameter	(Image analysis) Aspect ratio	
Krejcova et al., 2006	The influence of particle size and solubility of drug on the quality of spheroids produced by RP.	(Sieving) Mass mean diameter	(Image analysis) $"sphericity" = \frac{4\pi A}{p^2}$	
Steckel and Mindermann-Nogly, 2004	Effects of different amount of chitosan on the quality of spheroids produced by ES.	(Image analysis) Mean diameter	(Image analysis) Aspect ratio	Spheroids > 500 μm not included in size or shape analysis.
Chatchawalsaisin et al., 2005	Influence of glyceryl monostearate on the quality of spheroids produced by extrusion-spheronization.	(Sieving) Mass mean diameter	(Image analysis) e_R and aspect ratio	
Bornhoft et al., 2005	Feasibility study using carrageenan as a spheronization aid in spheroid produced by ES.	(Image analysis) Mean diameter	(Image analysis) Aspect ratio	

Table 1 (Continued). Recent studies on spheronization and the respective methods used for size, size distribution and shape characterization.

Reference	Focus of research	Characterization methods and descriptors		Remarks
		Size and size distribution	Shape	
Thommes and Kleinebudde, 2006a and Thommes and Kleinebudde, 2006b	With κ -carrageenan as spheronizing aid, spheroids containing different fillers and drug of differing solubilities were produced by ES and assessed.	(Sieving) 1.0 – 1.6 mm size fraction as yield	(Image analysis) Aspect ratio	
		(Image analysis) Mean diameter Proportion of spheroids within 10% of the mean spheroid diameter.		
Kristensen and Schæfer, 2000	Feasibility of using torque as a RP end point was investigated with varying amount of MCC in formulation.	(Sieving) Geometric weight mean diameter and geometric weight standard deviation	(Image analysis) Aspect ratio	
Kristensen et al., 2000	Feasibility of using torque as a RP end point was investigated with varying rotational plate speed, gap air pressure and batch size.	(Sieving) Geometric weight mean diameter and geometric weight standard deviation	(Image analysis) Aspect ratio	

distribution of spheroids was represented as percentage of spheroids in the 0.71-1.7 mm size fraction. Sousa et al. (2002) presented the mass median diameter and percentage weight retained between 1-1.4 mm aperture size sieves. Tho et al. (2002) presented spheroid size distribution as percentages of spheroids in the 0.7-1.0 mm, 1.0-1.7 mm and >1.7 mm size fractions.

Average size of spheroids has also been presented as the average maximum and minimum feret diameters obtained from image analyses of 400 ± 50 spheroids. (Tho et al., 2005). D25%-D75% of feret diameter (the difference between the 25th and 75th percentile spheroid diameters) was reported to provide information on the spread of size distribution. From the choice of calculation method used to represent average size of spheroids, it would seem that spheroids either followed a normal distribution, a symmetrical distribution or did not follow any distribution. Apart from mass mean diameter, geometric weight mean diameter has been used to represent the average size of spheroids produced by RP (Table 1). The size distribution of spheroids could be log normal which consequently require the use of geometric weight mean diameter as the choice parameter to represent the average size (Kristensen, 2005). Liew et al. (2002) observed that sieved fractions of spheroids produced by RP resembled log normal distribution. Therefore, size of spheroids was presented as geometric weight mean diameter and the size distribution as geometric weight standard deviation.

However, to date, there has been no report on statistical significance tests carried out to verify if spheroids, either produced by ES or RP, follow any size distribution.

6.2. Spheroid shape

In shape characterization of spheroids, aspect ratio (AR) could be the most popular (Table 1). Other descriptors which have been used included e_R and formulas resembling Circularity (C). e_R was proposed by Podczeczek and Newton (1994) as a superior shape descriptor for spheroids. Chatchawalsaisin et al., 2004 commented that AR showed results in agreement with those by e_R . Nevertheless, they believed that AR was less critical in distinguishing spheroids produced by different formulations. Almeida-Prieto et al. (2004) introduced V_r and V_p as new shape descriptors for ES spheroids. Almeida-Prieto et al. (2004) did not give a name to these new shape descriptors but it should be reasonable to describe V_r and V_p as “Radius variability” and “Perimeter variability” shape factors. V_r measures radius variability which therefore is more sensitive to changes in shape. V_p measures perimeter and can be affected by surface roughness. It was reported that V_r and V_p were able to show predominant shape texture and in the spheroid population only when they used in combination (Almeida-Prieto et al., 2004).

7. Size distribution in other particulate systems

In contrast to spheroids, studies concerning other particulate systems have defined size distribution by curve fitting to mathematical equations. For example, size distribution of cyclodextrins was found to be log normally distributed by using Chi square goodness of fit test (MunozRuiz and Paronen, 1997). Size distribution of unicores and multicores three-walled microcapsules could be curve fitted, by least square minimization, to a two log normal distribution (Morris and Warburton, 1984).

Theories on spheroid formation by Rowe (1985) and Baert and Remon (1993) were derived based on qualitatively observed evidences. In contrast, Sastry and Fuerstenau (1973) mathematically analyzed the rate of spheroid growth in order to explain the underlying spheroid growth mechanism. In high shear melt granulation, heterogeneity has been observed in the particle size distribution of granules and heterogeneity could be correlated to the different methods of binder addition, which in turn was used to explain agglomerate formation by different mechanisms (Scott et al., 2000). The appropriate use of descriptors to represent the size distribution of particles can aid in finding relationships between particle populations to process or particle properties (Alderliesten, 2004). In unimodal distribution, location parameter of Rosin-Rammler distribution was used to quantify the outcome of grinding experiments (Alderliesten, 2004). Bimodal or multiple modal distributions have been used to represent heterogeneity within a population, such as disease mapping, meta-analysis and texture modeling (Bohning and Seidel, 2003). For these reasons, the mathematical analysis of

spheroid size distribution will be useful, allowing greater understanding of spheroid growth and formation.

8. Log normal, normal and mixed Gaussian distributions

Log normal distribution, one of the many well-known statistical distributions, is a probability model which is used to represent the uncertainty of an occurrence. In this case, using the statistical model, the amount of fines and oversized spheroids can be predicted and should tally with actual experimental results. In the field of engineering, statistical distributions are commonly used to describe and predict chances of occurrence. Normal distribution, for instance, describes any occurrence as a result of the summation of many random independent reasons. Repeated measurements using an instrument might give readings which follow a normal distribution (Bury, 1999).

Mixed Gaussian distribution is a distribution resulting from summation of multiple normal distributions. A normal distribution is defined by mean μ and standard deviation σ . For a 2 components mixed Gaussian distribution, let $f(x)$ be the population density function (PDF) of a mixed Gaussian distribution

$$f(x) = \alpha_1 f_1(x) + \alpha_2 f_2(x) \dots (1)$$

$$\alpha_1 + \alpha_2 = 1 \dots (2)$$

where $f_1(x)$ and $f_2(x)$ represent the PDF of first and second normal distributions with probability p_1 and p_2 respectively. Since a normal distribution PDF is defined by parameter mean μ and standard deviation σ , a 2 components mixed Gaussian distribution $f(x)$ is defined by parameter $\alpha_1, \mu_1, \sigma_1$ and $\alpha_2, \mu_2, \sigma_2$. A 3 components mixed Gaussian distribution $f(x)$ would be defined by parameter $\alpha_1, \mu_1, \sigma_1, \alpha_2, \mu_2, \sigma_2$ and $\alpha_3, \mu_3, \sigma_3$.

In order to have a better understanding of spheroid growth mechanism, size distributions of spheroids have to be defined. The size distribution would then have to be examined together with the shape and size of individual spheroids so as to reveal information on how spheroids are formed during spheronization.

PART 2.
OBJECTIVES

PART 2. OBJECTIVES

The main hypothesis of this study is that in spheroid formation, spheroid growth and shape changes would reflect a heterogeneous particulate population undergoing transformation in a non-random manner.

In order to test the hypothesis:

- 1) ES and RP would have to produce spheroids of similar quality and size. These spheroids have to be produced under identical or equivalent process conditions and formulation in order for fair comparison to be made.
- 2) Growth of spheroids should be observed visually. In addition, spheroid growth and shape changes during spheronization have to be described quantitatively in order to substantiate visual observation.
- 3) Spheroid growth during spheronization should be induced. This act as an experimental intervention to verify if quantification of spheroids growth could be reproducible.
- 4) ES and RP spheroid formation would have to be compared.

PART 3.
MATERIALS AND METHODS

PART 3. MATERIALS AND METHODS

1. Materials

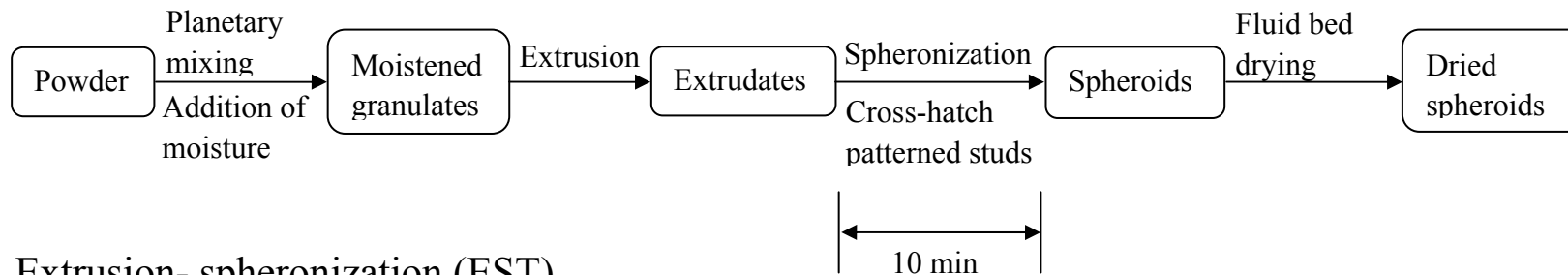
In this study, MCC (Avicel PH101, Asahi Chemical, Japan) was used as the spheronization aid and lactose monohydrate (Pharmatose 200M, De Melkindustrie Veghel, The Netherlands) as the bulk material in the preparation of spheroids. The 1:3 MCC:lactose powder was pre-blended for an hour at 40 rpm using a twin cone mixer (AR401, Erweka, Germany). Unless otherwise specified, distilled water was used as the granulating liquid. Ten % w/v copovidone (Plasdone S630, International Specialty Product, US) in distilled water and 0.001%w/v polysorbate 80 (Tween 80, ICI Surfactants, US) in distilled water were 2 types of granulating liquids used.

2. Methods

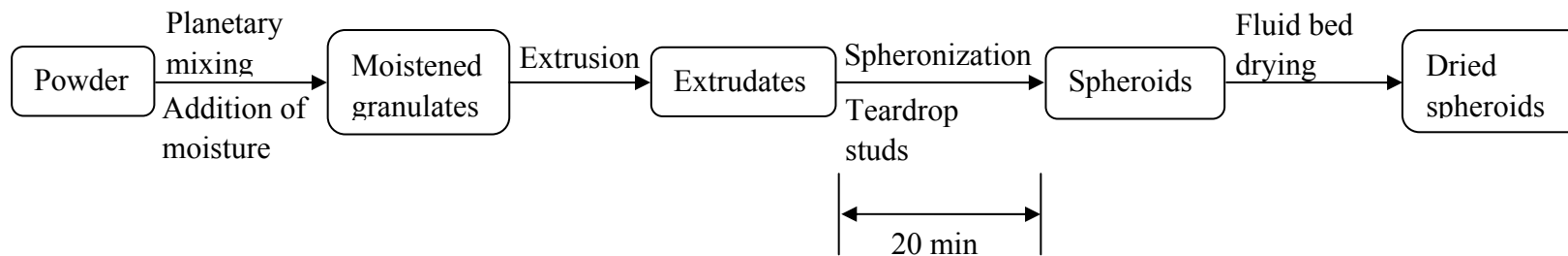
2.1. Preparation of spheroids

Spheroids were produced by 3 different spheronization processes: ES with cross-hatch plate (ESC), ES with teardrop studded plate (EST), and RP with teardrop studded plate (RT) (Figure 3).

Extrusion- spheronization (ESC)



Extrusion- spheronization (EST)



Rotary-processing (RT)

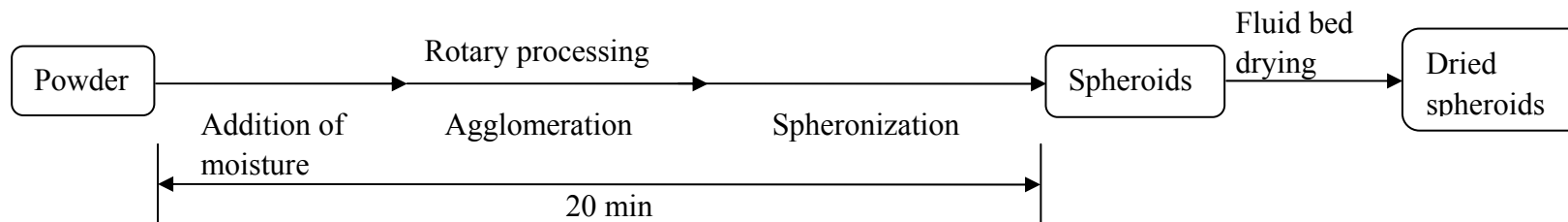


Figure 3. Schematics showing processes leading to spheroid formation.

2.2. Spheroid production by ES

For ESC and EST, 1 kg of MCC:lactose powder mixture was wet massed using a planetary mixer (Kenwood Major, Kenwood, UK). During wet massing, 380 ml of water, used as granulating liquid, was delivered at a flow rate of about 40 ml/min by a peristaltic pump (502S, Watson-Marlow, England). The wet mass was extruded by a radial extruder (E140, GEA-Niro, UK) fitted with an extrusion screen of 1 mm aperture diameter and thickness. The extrusion feed rate and the extrusion speed were set at 60 rpm and 47 rpm respectively. The extrudates produced were subsequently spheronized using 2 different equipments.

For ESC, extrudates were spheronized on a cross-hatch frictional plate in a spheronizer (S320, GEA-Niro, UK). For EST, extrudates were spheronized on a teardrop studded frictional plate in a rotary processor module connected to a multi-system air handling unit (MP1, Aeromatic-Fielder, UK). Details on the frictional plates are presented in Figure 2 and Table 2. Conditions for spheronization for ESC and EST batches are presented in Table 3.

Table 2. Details of equipment used for spheronization of extrudates by ESC and EST.

Process	Spheronizing equipment	Diameter of frictional plate (mm)	Texture of frictional plate
ESC	Spheronizer (GEA-Niro S320, UK)	320	Cross-hatch design plate (Grooves with well-defined and sharp edges)
EST	Rotary processor (MP1, Aeromatic–Fielder, UK)	275	Teardrop studded plate (Stud height, 2.75 mm. Rounded edges.)

Table 3. Process parameters for ESC and EST batches.

Batch	Rotational speed of frictional plate (rpm)	Equivalent tip speed (cms^{-1})	Gap air (bar)	Duration of spheronization (min)
ESC	600	10.1	Not applicable	10
EST793	793	11.4	1.2	20
EST862	862	12.4	1.2	20
EST931	931	13.4	1.2	20
EST1000	1000	14.4	1.2	20

For each batch, spheroids were sampled at half minute intervals during spheronization for size and shape analysis. All runs were carried out in triplicates and results averaged. The batches were coded according to the processes used and the “revolutions per minute” (rpm) of the frictional plate.

For ESC spheroids, video footage of the first 20 s of spheronization was captured using a high speed camera (MotionPro HS-3, Redlake, US) at 1000 fps and shutter speed at 86 μs .

2.3. Spheroid production by RP

RP was carried out in the rotary processor module, coupled to a multi-system air handling unit (MP1, Aeromatic-Fielder, UK). The same rotating frictional plate used for EST was used in RP. One kg load of the MCC:lactose powder mixture was used per batch. The amount of water used ranged from 360 to 380 ml. RP batches were coded according to the amount of water used (RT36%, RT37%, and RT38%).

During RP, spheroids were sampled at half minute intervals after completion of water addition for size and shape analysis. The process parameters used are shown in Table 4 and runs were triplicated.

Table 4. Process parameters for RT batches.

Process parameters	Parameter values
Equivalent tip speed (cms^{-1})	7.2 (first 2 min) 13.4 (after 2 min)
Gap air (bar)	1.2
Duration of process (min)	20
Inlet air temperature ($^{\circ}\text{C}$)	30
Atomizing air pressure (bar)	1.2
Spray nozzle diameter (mm)	0.8
Spray rate (g/min)	41

2.4. Formation process during ES

In order to investigate spheroid formation during ES and RP, spheroids were produced with identical process parameters and formulation to ESC (Table 3). For each batch, spheroids were sampled at 2 min intervals during spheronization for size and shape analysis. Spheroids sampled during spheronization were coded as

xESC(TS)_y where “x” is the experiment repeats and “y” is the spheronization time.

All runs were carried out in triplicates and results averaged.

2.5. Controlled spheroid agglomeration during RP

RP batches were produced to investigate spheroid agglomeration behavior when additional amount of granulating liquid was added to well-formed spheroids during spheronization. These batches were coded RT(SR). “SR” represented “spray rate”. RT(SR) were produced with process parameters and formulation identical to those of RT36%. Process duration for RT36% was 20 min. However, for RT(SR) batches, the process was extended for 30 min. During the 30 min extended process period, spheroids were spheronized at the same spheronization speed of 931 rpm and additional granulation liquid (AGL) was added to the spheroids at a constant rate throughout that period. Spheroids were sampled at 10 min interval during the additional 30 min.

AGL was added at 4 different spray rates, i.e. 0, 2, 4, 6 ml/min. Apart from using only distilled water as granulating liquid, solutions containing copovidone (S630) and polysorbate 80 (Tween 80) were also used. Details of process parameters and formulations used are listed in Table 5. All runs were carried out in triplicates. Runs with S630 and Tween 80 solutions were carried out in duplicates. Batch codes were assigned according to spray rate and additional excipient present in AGL.

Time-sampled spheroids were coded with suffix representing time of sampling (20, 30, 40, and 50). Time of sampling also represented process lapsed in minutes.

Table 5. Process parameters and formulations used for controlled agglomeration of RP spheroids.

Batch	Spray rate (g/min)	Atomizing air pressure (bar)	Gap air (bar)	AGL
RT(SR0)	0	0	1.2	Nil
RT(SR2)	2	1.2	1.2	Distilled water
RT(SR4)	4	1.2	1.2	Distilled water
RT(SR6)	6	1.2	1.2	Distilled water
RT(SR4S630)	4	1.2	1.2	10% w/v S630 in distilled water
RT(SR4TWN)	4	1.2	1.2	0.001% w/v Tween 80 in distilled water

2.6. Drying of spheroids

Unless otherwise stated, ESC, EST and RT spheroids were dried in a fluid bed dryer (Strea-1, GEA-Aeromatic, Switzerland) with an inlet drying air temperature of 60 °C.

Drying was deemed completed when outlet air reached 50 °C, which took approximately 30 min. ESC(TS) and RT(SR) spheroids were dried in a convection oven (Modell 600, Memmert, Germany) at 60 °C for 8 h.

2.7. Characterization of spheroids

2.7.1. Size analysis by sieving

The spheroid batches were subdivided using a riffler (PT, Retsch, Germany) into 8 portions. A portion, approximately 120 g, was sized using a nest of sieves of aperture sizes in a $\sqrt[4]{2}$ progression, ranging from 250 μm to 4.00 mm. The nest of sieves was vibrated at amplitude of 1 mm for 15 min on a sieve shaker (VS1000, Retsch, Germany).

The size and size distribution of the spheroids were described using geometric weight mean diameter (D_{wgeo}), geometric weight standard deviation (SD_{wgeo}) (Liew et al., 2002), arithmetic weight mean diameter (D_{warith}), arithmetic weight standard deviation (SD_{warith}) (Agrawal et al., 2004), mass median diameter (D_{wmed}) and span ($Span_w$) (Heng et al., 2002). The equations for the size and size distribution of spheroids are as follows,

$$D_{wgeo} = \frac{\sum (w_i \times \lg d_i)}{\sum w_i} \dots(3)$$

$$SD_{wgeo} = \sqrt{\frac{\sum [w_i \times (\lg d_i)^2]}{\sum w_i} - \left(\frac{\sum (w_i \times \lg d_i)}{\sum w_i} \right)^2} \dots(4)$$

$$D_{warith} = \frac{\sum (w_i \times d_i)}{\sum w_i} \dots(5)$$

$$SD_{warith} = \sqrt{\frac{\sum (w_i \times d_i^2)}{\sum w_i} - \left(\frac{\sum (w_i \times d_i)}{\sum w_i} \right)^2} \dots(6)$$

where,

d_i = midpoint of size intervals according to the aperture size of the sieves, and

w_i = weight of spheroids retained in the respective size interval.

2.7.2. Sizing by image analysis

For every lot of time-sampled spheroids, at least 625 spheroids were randomly selected for image analysis. The time-sampled spheroids were visually examined

under 20X magnification using a stereomicroscope (SZH, Olympus, Japan) and images captured using a digital colour video camera (DXC-390P, Sony, Japan) and imaging analysis software (Micro Image ver. 4.5, Media Cybernetics, US). The spheroids were mounted manually to ensure that all images taken represented discrete spheroids. Image analysis quantified the area of silhouette of each spheroid. All images of the spheroids were calibrated, ensuring that 1 mm was represented by at least 100 pixels.

The size of each spheroid was represented by the equivalent circle diameter (ECD) (Schmidt and Kleinebudde, 1998) calculated from the area of the spheroid silhouette. For each lot of sampled spheroids, 625 ECD values were used to define its size distribution. The size and size distribution of spheroids were described by geometric mean diameter (DI_{geo}), geometric standard deviation (SDI_{geo}), arithmetic mean diameter (DI), arithmetic standard deviation (SDI), median diameter (DI_{med}) and span (SpanI) as obtained from the image analysis data. The equations are as follows,

$$ECD_i = \sqrt{\frac{4 \times a}{\pi}} \dots(7)$$

where

$i = 1, \dots, 625$, representing ECD values in ascending order, and

a = area of silhouette of spheroid.

$$DI_{geo} = \left(\frac{1}{625} \sum_{i=1}^{625} \lg ECD_i \right)^{10} \dots(8)$$

$$SDI_{geo} = \left(\frac{1}{625} \sum_{i=1}^{625} (\lg ECD_i - \lg DI_{geo})^2 \right)^{10} \dots\dots(9)$$

$$DI = \frac{1}{625} \sum_{i=1}^{625} ECD_i \dots\dots(10)$$

$$SDI = \frac{1}{625} \sum_{i=1}^{625} (ECD_i - DI)^2 \dots\dots(11)$$

$$DI_{med} = \frac{ECD_{312} + ECD_{313}}{2} \dots\dots(12)$$

$$SpanI = \frac{ECD_{562} + ECD_{563} - ECD_{62} - ECD_{63}}{2DI_{med}} \dots\dots(13)$$

where SpanI is computed by taking the difference between ECD of the 90th % and 10th %, divided by DI_{med}.

2.7.3. Roundness quantification by image analysis

Using data obtained from image analysis, spheroid shape was quantified using the following shape factors: aspect ratio (AR) and eccentricity factor (e_R) (Eriksson et al., 1997; Podczec et al., 1999), projected sphericity (PS) and circularity (C). f is a correction factor for e_R . Their equations are given as follows:

$$AR = \frac{l_f}{b_f} \dots\dots(14)$$

$$e_R = \frac{2\pi r_e}{p f} - \sqrt{1 - \left(\frac{b}{l}\right)^2} \dots\dots(15)$$

$$f = 1.008 - 0.231 \left(1 - \frac{b}{l} \right) \dots\dots(16)$$

$$PS = \frac{4a}{\pi l_f^2} \dots\dots(17)$$

$$C = \frac{4\pi a}{p^2} \dots\dots(18)$$

where

l_f = maximum feret diameter of image,

b_f = feret diameter of image, in the direction perpendicular to l_f ,

r_e = mean radius derived from the average distances between the center of gravity of the image to the perimeter,

p = perimeter of image,

l = length of image outline,

b = breadth of image outline, taken perpendicular to l , and

a = projected image area of the particle.

2.7.4. Crushing strength analysis

For ESC, EST and RT, 25 spheroids within the 850 – 1000 μm size fraction were randomly selected from each batch for assessment of crushing strength. A tensile tester (EZ Tester, Shimadzu, Japan) affixed with a platen of diameter 25 mm was used to compress each spheroid at a rate of 3 mm/min. The force required to crush the spheroid was measured by a load cell connected to the platen and recorded using data

acquisition software (WinAGS ver 2.01, Shimadzu, Japan). For each batch, average crushing strength was computed. RT38% was excluded from the test as there was negligible amount of spheroids in the specified size fraction.

2.7.5. Moisture content determination

Approximately 25g of MCC:lactose powder mixture was accurately weighed and oven-dried (Modell600, Memmert, Germany) at 70 °C till constant weight. The percentage weight lost was taken to be the percentage amount of moisture present in the starting material of MCC:lactose powder mixture (W_0). Experiments were carried out in triplicates and results averaged. In a similar manner, approximately 25 g of sampled spheroids were oven-dried at 70 °C till constant weight. Percentage weight lost was calculated (W_1). The percentage moisture content of spheroids attributed to the amount of water added was (W_1-W_0).

2.7.6. Surface roughness analysis

For every time-sampled lot of RT(SR) spheroids, 12 randomly chosen spheroids were used for surface roughness measurement. The surface roughness was measured using a scanning probe microscope (SPM-9500J, Shimadzu, Japan). Spheroid surface was scanned at a frequency of 1 Hz over a scan area of 25 x 25 μm using the dynamic mode and a Z value of 10 μm . The arithmetic average roughness (Ra) of individual spheroids was obtained.

2.8. Statistical analysis on spheroid size distributions

Statistical programs (SPSS version 12.0, SPSS Inc., US) and (Minitab release 14.1, Minitab Inc., US) were used to carry out the statistical calculations. Computing environment software (Matlab version 6.5 release 13, The MathWorks Inc., US) was used in statistical curve fitting of mixed Gaussian distribution.

Mean, standard deviation skewness and kurtosis of individual size distribution were computed using 625 ECD of each lot of spheroids. The size distributions of spheroids were statistically fitted to normal, log normal and mixed Gaussian (MG) distributions. Statistical distribution fitting required 2 steps: estimating the parameters of an ideal distribution to be fitted, and testing the goodness of fit. The parameters for the mean and standard deviation for the ideal normal distribution are taken to be DI and SDI respectively. For log normal fitting, lg ECD values were fitted to normal distribution.

A Matlab script, written to perform expectation maximization algorithm (Verbeek et al., 2003) was used to compute 2, 3, and 4 components MG distributions which approximated the size distribution of spheroids. PDF graphs were also plotted using the same software.

Per sampled lot, 625 ECD were divided into 65 intervals to compute Chi square goodness of fit for normal, log normal and 2, 3 and 4 MG distributions.

3. Illustration and quantification of simulated spheroid images

Images of circle, ellipses, ovals, rectangles with round ends (RRE), rectangles with round corners (RRC), and dumbbells were drawn (Macromedia Freehand MX, Adobe Systems Incorporated, US) and rasterized (Photoshop CS, Adobe Systems Incorporated, US) and saved in jpeg (Joint Photographic Experts Group) format. Breadth of individual rasterized image was represented by about 100 pixels. The images were assessed using the same method and software as that used for image analysis of the spheroids.

PART 4.
RESULTS AND DISCUSSION

PART 4. RESULTS AND DISCUSSION

1. Equivalency in process between ES and RP

The main similarity between ES and RP would be the use of a rotational frictional plate to round and shape agglomerates into spheroids. The magnitude of forces exerted by the rotating frictional plates onto agglomerates would generally be related to the surface texture and the speed of the rotational frictional plate. In order to compare ES and RP, process and formulation parameters between them have to be kept identical, if not equivalent. As the frictional forces exerted by surface texture onto agglomerates could not be measured realistically, the effect of the rotational frictional plates has to be measured qualitatively. The inclusion of EST into the experimental design allowed the possibility of establishing equivalency in the effect of the frictional plate between ES and RP. RP would usually require a duration of 20 min to produce spheroids, inclusive of time for water addition. Both the peripheral tip speed and the duration of spheronization have to be considered together in order to achieve equivalency. The forces experienced by agglomerates during spheronization by RP versus ESC and EST could translate roughly to a spheronization duration of 20 min for EST. For the initial part of the study, one of the objectives would be to establish standardization in spheronization conditions between ESC, EST and RP (Tables 3 and 4).

Spheronization of ESC spheroids was carried out with the rotating frictional base plate achieving a peripheral tip speed of 10.1 cms^{-1} (Table 3). The process and formulation parameters chosen for ESC batches were intended to produce spheroids within the pharmaceutically useful size range and with narrow size distribution (Table 6). The average D_{wmed} and $Span_w$ of ESC spheroids of 0.877 mm and 0.283 respectively, adequately demonstrated the intention. These batches could be considered as a fair representation of good quality spheroids. This preliminary establishment of desirable attributes of spheroids was important as it formed the basis for comparison if the spheroid formation process or the spheroid formulae for spheronization were to be different.

Table 6. Size, size distribution, roundness, moisture content and crushing strength of ESC, EST and RT spheroids.

Batch	Dwmed (mm)	Spanw	AR	ϵ_R	Moisture content (%w/w)	Crushing strength (N)
ESC	0.877 (0.057)	0.283 (0.0374)	1.085 (0.0042)	0.620 (0.0091)	37.71 (0.360)	6.06 (1.429)
EST793	0.767 (0.040)	0.305 (0.0441)	1.106 (0.0048)	0.599 (0.0090)	29.57 (0.375)	4.17 (1.368)
EST862	0.777 (0.006)	0.352 (0.0385)	1.089 (0.0048)	0.631 (0.0117)	28.89 (0.411)	3.95 (1.624)
EST931	0.880 (0.066)	0.267 (0.0362)	1.079 (0.0026)	0.638 (0.0029)	29.00 (0.262)	5.65 (2.720)
EST1000	0.923 (0.067)	0.253 (0.0715)	1.068 (0.0022)	0.654 (0.0054)	28.36 (0.308)	6.24 (2.717)
RT36%	0.940 (0.106)	0.369 (0.0527)	1.135 (0.0250)	0.570 (0.0249)	28.79 (0.476)	11.19 (2.679)
RT37%	1.103 (0.133)	0.302 (0.0130)	1.102 (0.0193)	0.590 (0.0023)	29.85 (0.291)	12.67 (1.803)
RT38%	1.390 (0.210)	0.287 (0.0298)	1.097 (0.0026)	0.609 (0.0015)	31.09 (0.337)	-

Values are mean with standard deviations in parentheses.

1.1. Equivalency in spheronization conditions between different frictional surfaces

Preliminary EST batches were carried out at equivalent tip speed of 10.1cms^{-1} (698 rpm) for 20 min with the intention of producing spheroids of similar size and roundness to those of the ESC batches. However, the spheroids produced were smaller and less spherical than those produced by ESC. A possible cause could be the dissimilar surface textures of the rotating frictional plates of ESC and EST processes. Therefore, the differences in surface texture were examined in greater detail.

The amount of frictional forces exerted by the rotating frictional plate onto extrudates could be related to the geometry and the density of protuberances per unit surface area on the frictional plate. Surface protuberances of the cross-hatch textured plate were sharp-edged and relatively smaller than the teardrop studs found on the frictional plate of the rotary processor (Figure 2). Visual examination and calculation revealed that that per 10 cm^2 , there were about 111 cross-hatch studs and 6 teardrop studs on the respective plates. The lower density of studs per unit area and the design of the teardrop studs with rounded edges were indicative of lower amount of frictional forces exerted by the teardrop studded frictional plate than that of cross-hatch textured frictional plate at equivalent peripheral tip speed of 10.1 cms^{-1} . Therefore, at identical peripheral tip speeds, processes such as size enlargement by coalescence, densification and rounding of EST extrudates occurred at a comparatively slower rate, resulting in smaller and less spherical spheroids in a similar time frame. Wan et al. (1993) demonstrated that increased spheronization speed and duration resulted in bigger and rounder spheroids. For that reason, EST had to be carried out at a higher peripheral tip speed in order for the teardrop studded frictional surface to exert comparable frictional forces matching those exerted by the cross-hatch textured surface.

EST was thus carried out with a 20 min spheronization duration using a series of higher peripheral tip speeds to empirically elucidate equivalency in the effect of the rotating frictional plate (Table 2). The average D_{wmed} of EST spheroids were

0.767-0.923 mm, with higher spheronization speed predictably producing larger spheroids (Wan et al., 1993) (Table 6). At 931 rpm, EST produced spheroids of average D_{wmed} 0.880 mm, which in terms of size, was the closest to ESC. Spanw of EST931 and ESC were also similar (Table 6). The similarities in terms of size and size distribution of ESC and EST931 spheroids strongly indicated that the spheronization processes of ESC and EST931 were equivalent, implying that spheroids were experiencing equivalent amount of frictional forces.

Upon elucidating spheronization process equivalency between ESC and EST, spheroids were produced by RP with the peripheral tip speed of the rotating frictional plate set at 13.4 cms^{-1} .

1.2. Producing RP spheroids of equivalent size and size distribution to ES spheroids

With equivalent spheronization process conditions and the addition of same amount of granulation liquid, RT38% spheroids were markedly larger than those of ESC and EST931 (Table 6). Conditions have to be adjusted in order to produce RP spheroids with size similar to those produced by ESC. Of the many methods to produce smaller sized RP spheroids, reducing the amount of granulating liquid during RP had been applied (Heng et al., 1996). In this present study, 360 ml of water was the lowest amount of granulating liquid used for the production of spheroids by RP. RP carried out with 350 ml of water produced very small spheroid with large amount of fines and

it was concluded that the spheroid batch obtained was unsuitable for use in this study due to consistency issues.

ESC, EST931 and RT36% products could be considered as batches of spheroids with similar size in terms of average D_{wmed} (Table 6). As important process and formulation parameters were kept constant or equivalent, ESC, EST931 and RT36% spheroids could be compared objectively according to the following aspects: size distribution of spheroids, roundness and crushing strength.

1.3. Effect of processes on size and size distribution of spheroids

ESC, EST931 and RT36% spheroids had narrow size distributions and they were similar in this aspect. The average Spanw for ESC was 0.283 and for EST at the peripheral tip speed investigated, 0.253-0.352. In comparison to ESC and EST931, the average Spanw for RT36% at 0.369 was slightly larger (Table 6). Using one way ANOVA, Spanw of ESC, EST931 and RT36% spheroids were shown not to have significant difference between themselves despite the visually observable small differences which suggested that ESC and EST spheroids were more narrowly distributed than those of RT36% (Tables 6 and 7).

Table 7. One way ANOVA and post hoc LSD test for variables of ESC, EST, and RT batches.

Variable tested	Batch	P value for One-Way ANOVA	Batches compared	P value for post hoc LSD test
Moisture content	EST793	0.000*	EST793 vs EST862	0.036*
	EST862		EST793 vs EST931	0.069
	EST931		EST793 vs EST1000	0.001*
	EST1000		EST793 vs RT36%	0.019*
	RT36%		EST793 vs RT37%	0.362
	RT37%		EST793 vs RT38%	0.000*
	RT38%		EST862 vs EST931	0.724
			EST862 vs EST1000	0.091
			EST862 vs RT36%	0.745
			EST862 vs RT37%	0.006*
			EST862 vs RT38%	0.000*
			EST931 vs EST1000	0.047*
			EST931 vs RT36%	0.501
			EST931 vs RT37%	0.011*
			EST931 vs RT38%	0.000*
			EST1000 vs RT36%	0.160
			EST1000 vs RT37%	0.000*
	EST1000 vs RT38%	0.000*		
	RT36% vs RT37%	0.003*		
	RT36% vs RT38%	0.000*		
	RT37% vs RT38%	0.001*		
Spanw	ESC	0.714	ESC vs EST931	0.666
	EST931		ESC vs RT36%	0.048*
	RT36%		EST931 vs RT36%	0.026*
DI	ESC	0.275	ESC vs EST931	0.719
	EST931		ESC vs RT36%	0.138
	RT36%		EST931 vs RT36%	0.231
SDI	ESC	0.023*	ESC vs EST931	0.733
	EST931		ESC vs RT36%	0.013*
	RT36%		EST931 vs RT36%	0.020*

*denotes statistical significance at 0.05 level

Table 7 (Continued). One way ANOVA and post hoc LSD test for variables of ESC, EST, and RT batches.

Variable tested	Batch	P value for One-Way ANOVA	Batches compared	P value for post hoc LSD test
Skewness	ESC	0.000*	ESC vs EST931	0.337
	EST931		ESC vs RT36%	0.000*
	RT36%		EST931 vs RT36%	0.001*
Kurtosis	ESC	0.005*	ESC vs EST931	0.838
	EST931		ESC vs RT36%	0.003*
	RT36%		EST931 vs RT36%	0.003*
Aspect ratio	ESC	0.000*	ESC vs EST793	0.035*
	EST793		ESC vs EST862	0.697
	EST862		ESC vs EST931	0.483
	EST931		ESC vs EST1000	0.080
	EST1000		ESC vs RT36%	0.000*
	RT36%		EST793 vs EST862	0.070
			EST793 vs EST931	0.009*
			EST793 vs EST1000	0.001*
			EST793 vs RT36%	0.035*
			EST862 vs EST931	0.284
			EST862 vs EST1000	0.040*
			EST862 vs RT36%	0.000*
			EST931 vs EST1000	0.258
	EST931 vs RT36%	0.000*		
	EST1000 vs RT36%	0.000*		

*denotes statistical significance at 0.05 level

Table 7 (Continued). One way ANOVA and post hoc LSD test for variables of ESC, EST, and RT batches.

Variable tested	Batch	P value for One-Way ANOVA	Batches compared	P value for post hoc LSD test
e _R	ESC	0.000*	ESC vs EST793	0.066
	EST793		ESC vs EST862	0.309
	EST862		ESC vs EST931	0.104
	EST931		ESC vs EST1000	0.006*
	EST1000		ESC vs RT36%	0.000*
	RT36%		EST793 vs EST862	0.009*
			EST793 vs EST931	0.003*
			EST793 vs EST1000	0.000*
			EST793 vs RT36%	0.016*
			EST862 vs EST931	0.500
			EST862 vs EST1000	0.044*
			EST862 vs RT36%	0.000*
			EST931 vs EST1000	0.145
	EST931 vs RT36%		0.000*	
EST1000 vs RT36%	0.000*			

*denotes statistical significance at 0.05 level

Table 7 (Continued). One way ANOVA and post hoc LSD test for variables of ESC, EST, and RT batches.

Variable tested	Batch	P value for One-Way ANOVA	Batches compared	P value for post hoc LSD test
Crushing strength	ESC	0.000*	ESC vs EST793	0.000*
	EST793		ESC vs EST862	0.000*
	EST862		ESC vs EST931	0.240
	EST931		ESC vs EST1000	0.600
	EST1000		ESC vs RT36%	0.000*
	RT36%		ESC vs RT37%	0.000*
	RT37%		EST793 vs EST862	0.527
			EST793 vs EST931	0.000*
			EST793 vs EST1000	0.000*
			EST793 vs RT36%	0.000*
			EST793 vs RT37%	0.000*
			EST862 vs EST931	0.000*
			EST862 vs EST1000	0.000*
			EST862 vs RT36%	0.000*
			EST862 vs RT37%	0.000*
			EST931 vs EST1000	0.089
			EST931 vs RT36%	0.000*
			EST931 vs RT37%	0.000*
			EST1000 vs RT36%	0.000*
	EST1000 vs RT37%	0.000*		
	RT36% vs RT37%	0.000*		

*denotes statistical significance at 0.05 level

The size distributions of spheroids were analyzed using another approach. Size and shape data of spheroids obtained from image analysis could be used to compute statistical descriptors such as DI, SDI, skewness and kurtosis. These statistical descriptors were computed to evaluate differences in the size distribution of spheroids produced by ESC, EST931 and RT36% (Table 6). By using data from image analysis instead of sieving, one way ANOVA and post hoc Least Square Difference (LSD) test

indicated that RT36% spheroids had significantly wider size distribution, greater positive skewness and kurtosis than ESC or EST931 spheroids (Tables 7 and 8).

Table 8. Statistical descriptors for size distribution of ESC, EST931 and RT36% spheroids.

Statistical descriptors	Batch		
	ESC	EST931	RT36%
DI	993.1	1086	1193
	1079	951.1	986.5
	940.5	1065	1241
SDI	107.0	87.8	189.4
	89.4	161.8	169.3
	124.2	94.3	191.1
Skewness	0.567	1.135	2.807
	0.860	1.022	3.518
	0.580	1.007	4.333
Kurtosis	-0.131	2.766	14.68
	1.753	0.527	27.46
	-0.473	1.285	37.00

The differences in size distribution between ESC and EST931, and RT36% could have been caused by the extrusion process or the teardrop studded rotating frictional plate. Since the size distributions of ESC and EST931 were not significantly different (Table 7), it would be reasonable to postulate that the teardrop studded rotating frictional plate was unlikely to have caused RT36% spheroids' differing size distribution. When the rotating frictional surface was in motion, both the cross-hatch textured or teardrop studded surfaces would provide the necessary frictional forces to move and remodel the aggregated contents. The resultant spheroid size would be a result of a balance of coalescence and breakdown during spheronization (Wan et al.,

1993). Spheroids could be broken down by some of these methods: excessive force exerted by frictional surface, intense collision between spheroids, or intense collision between spheroid and container wall. When the sharp edged cross-hatch textured surface was compared to the teardrop studs with round edges, the latter most likely exerted lower breakdown forces. By having a higher peripheral tip compared to ESC, EST931 spheroids have similar size and size distribution. This apparent similarity in size distributions between ESC and EST931 spheroids indicated that the process of spheroid agglomeration and breakdown was determined by collisions encountered by the spheroids and not the nature of the rotating frictional plate surface.

Upon demonstrating that different rotating frictional plate surfaces could produce spheroids with similar size and size distribution, it could therefore be reasonably postulated that different spheroid formation mechanisms caused the differences in the shape of size distributions of spheroids produced by ESC and RT.

Certain shape of size distribution could be represented by mathematical models.

Wanibe and Itoh (1998) had fitted the size distributions of crushed materials with the Rosin-Rammler equation. Using a similar approach, it was postulated that by model fitting and analysis of the size distributions of multiparticulate systems obtained by sampling as pelletization runs progressed, the underlying formative processes could be comprehended and understood.

1.4. Shape of size distribution between ES and RP spheroids

Between ES and RP, size distributions of ESC and EST931 spheroids were significantly more symmetrical and more narrowly distributed than those of RT36% (Tables 7 and 8). Sieving data indicated that 3.36% by weight of RT36% spheroids were larger than 1.7 mm. In contrast, the proportions of ESC and EST931 spheroids larger than 1.7 mm were negligible ($\leq 0.06\%$). The oversized spheroids present in RT36% caused the size distribution to be positively skewed and with greater degree of kurtosis. Hence, the concomitant process of wet massing, agglomeration and spheronization during RP could have provided the opportunity for the formation of oversized spheroids. Alternatively, the extrusion step in ES by pre-forming the wet mass into extrudates before the spheronization step could have prevented the formation of such oversized spheroids. Hence, ES and RP spheroid formation mechanisms have to be further investigated.

1.5. Effect of processes on spheroid roundness

ESC did not produce rounder spheroids compared to EST ($p > 0.05$) (Tables 6 and 7) indicating that the choice of appropriate peripheral tip speed, duration and protuberance on the rotating frictional plate did not significantly affect the roundness of spheroids. The similarity in roundness and size between ESC and EST spheroids further reinforced the possibility that spheroid formation relied mainly on collision between spheroids and less on collision between spheroids and the well-defined textured surface of rotating frictional plate. In this study, AR and e_R indicated

increasing roundness with higher peripheral tip speed for EST spheroids, which were similarly observed by Wan et al. (1993) and Newton et al. (1995b).

RT36% spheroids were significantly less spherical when compared to ESC or EST spheroids (Tables 6 and 7). Aggregates have to possess a balance of rigidity and plasticity during spheronization in order to be rounded into spheroids of desired size. RT36% spheroids, having comparatively less water than those of ESC and EST, would be more rigid, less deformable and consequently less round. Roundness of RT spheroids was improved with higher amount of water added. However, the consequential increase in plasticity due to higher amount of water added also yielded larger spheroids which made them unsuitable for equivalent size comparison with those of the ESC spheroids.

1.6. Role of moisture in spheroid formation

The amount of water added during ES and RP is important as it would influence the eventual size of the spheroids. However, the amount of water remaining in spheroids after spheronization need not always correlate with the final spheroid size. In this study, RP used less water to produce spheroids of equivalent size to those of ESC and EST931. However, in another study (Pisek et al, 2001), it was reported that RP required more water than ES to produce spheroids of similar size. In their RP studies, Vertommen et al. (1998) attributed the differences in spheroid size to the amount of water remaining after accounting for moisture loss due to the gap and atomizing air.

The difference in moisture content of spheroids upon spheronization between RT38%, RT37% and RT36% batches were approximately 1.1 %w/w (Table 6). Different amount of moisture content would be expected due to the different amounts of water added for granulation. Although equal amounts of granulating liquid were used for EST and RT38%, moisture content upon spheronization for RT38% spheroids (at 31.1 %w/w) was higher than that of EST spheroids. The better air flow through the extrudates than powder mass could have aided the higher moisture loss rate. Another possibility would be that during extrusion, water might have migrated to the extrudate surface, facilitating moisture loss from the surface during spheronization. These factors might have caused extrudates to lose moisture at a higher rate when exposed to the gap air. Moisture content of spheroids upon spheronization was similar for RT36%, EST862, EST931 and EST1000 batches. The final spheroid size of the RT36%, EST862, EST931 and EST1000 batches were also similar. This coincidental similarity suggested that amount of moisture remaining in spheroids upon spheronization may be indicative of the final spheroid size. However, this “moisture content of spheroids upon spheronization” and “final spheroid size” relationship could not be established as the size of RT37% and EST793 spheroids differed widely despite having similar amounts of moisture. This demonstrated that the final amount of water remaining in the spheroids could not be a reliable predictor of the final size of spheroids if spheroids were produced using different processes. Compared to ESC spheroids, EST spheroids experienced significant moisture loss to the gap air.

Average moisture content of EST spheroids were 28.4- 29.6 %w/w and higher speed of rotation of the rotating frictional plate would contribute to greater moisture loss. Despite the differences in moisture remaining in spheroids, ESC and EST spheroids had similar sizes. This demonstrated that quantity of moisture lost during spheronization did not have a major consequence to the eventual spheroid size for multi-step ESC and EST as the process of spheroid formation almost reached the final size within a minute into the spheronization run. Subsequent moisture loss would have minimal effect unless the integrity of spheroids was compromised.

1.7. Crushing strength of ES and RP spheroids

The quality of spheroids produced could also be measured by the crushing strength of spheroids. Spheroids with high crushing strength would be desirable. Moreover, crushing strength of spheroids could be used to represent and distinguish spheroid structural differences which in turn resulted from differing spheroid formation processes. For that reason, crushing strength could be an indirect indicator for detecting differences in spheroid formation mechanism.

At equivalent spheronizing conditions, ESC, EST931 and EST1000 spheroids had similar crushing strength (Tables 6 and 7). This apparent similarity in crushing strength, size and size distribution between ESC and EST931 spheroids further reinforced the possibility that the spheroid formation process is greatly influenced more by the collisions experienced by the spheroids than by the texture of the rotating

frictional plate. Although EST931 spheroids experienced greater moisture loss during spheronization, spheroid integrity remained similar to that of ESC spheroids, which was reflected by the similar crushing strength measured. Crushing strength of EST spheroids increased with increasing spheronization speed. At higher spheronization speed, spheroids would collide with one another or with the wall of the spheronizer, generating greater densification forces on the spheroids. Kleinebudde et al. (1999) also produced spheroids by ES at different spheronization speeds. Instead of lactose monohydrate and MCC, the spheroid formulation used dicalcium phosphate and MCC. However, Kleinebudde et al. (1999) did not observe the increase crushing strength with higher spheronization speed.

RT37% spheroids had higher crushing strength than those of RT36%. Pore volume was reported to be reduced when higher amount of water was used (Vertommen et al., 1998). The greater amount of water used in RP37% could have increased the percentage of lactose dissolved, thus allowing more extensive solid bridges to be form upon drying, consequently reducing pore volume. In this study, RT36% spheroids had significantly higher crushing strength than those produced by ESC or EST (Tables 6 and 7). While Pisek et al. (2001) reported RP spheroids to be more friable compared to those produced by ES, Robinson and Hollenbeck (1991) could not find significance difference in crushing strength between ES and RP spheroids.

The two possible factors could have caused the difference in spheroid crushing strength: the difference in formulation which in this study was different amount of water used, and the differences in the spheroid formation mechanism. Although ESC, EST and RT38% spheroids should be compared as these batches used the same amount of water for granulation, RT38% spheroids being significantly larger would not provide a fair comparison as crushing strength is largely influenced by size. As aforementioned, higher amount of water could have reduced pore volume of the spheroid matrix due to more extensive formation of solid bridges from dissolved lactose. It would therefore be unlikely that ESC or EST produced weaker spheroids compared to RT36% spheroids. This eliminated the possibility that the amount of water in the spheroid formulation might have contributed to the higher crushing strength of RT36% spheroids. Therefore, the difference in spheroid formation mechanism between ES and RP had to be analyzed in greater detail in order to explain the difference in spheroid crushing strength.

1.8. Visual examination of spheroid formation

Visual examination of time-sampled spheroids revealed differences in spheroid formation between ES and RP. Generally, the morphological changes of ESC and EST931 spheroids during spheronization were similar (Figure 4). The cylindrically shaped extrudates were visually examined to be approximately 5 to 10 mm in length. The spheronization process began with rapid breakdown of extrudates by attrition around the edges and fractures across the extrudates caused by the impact on the

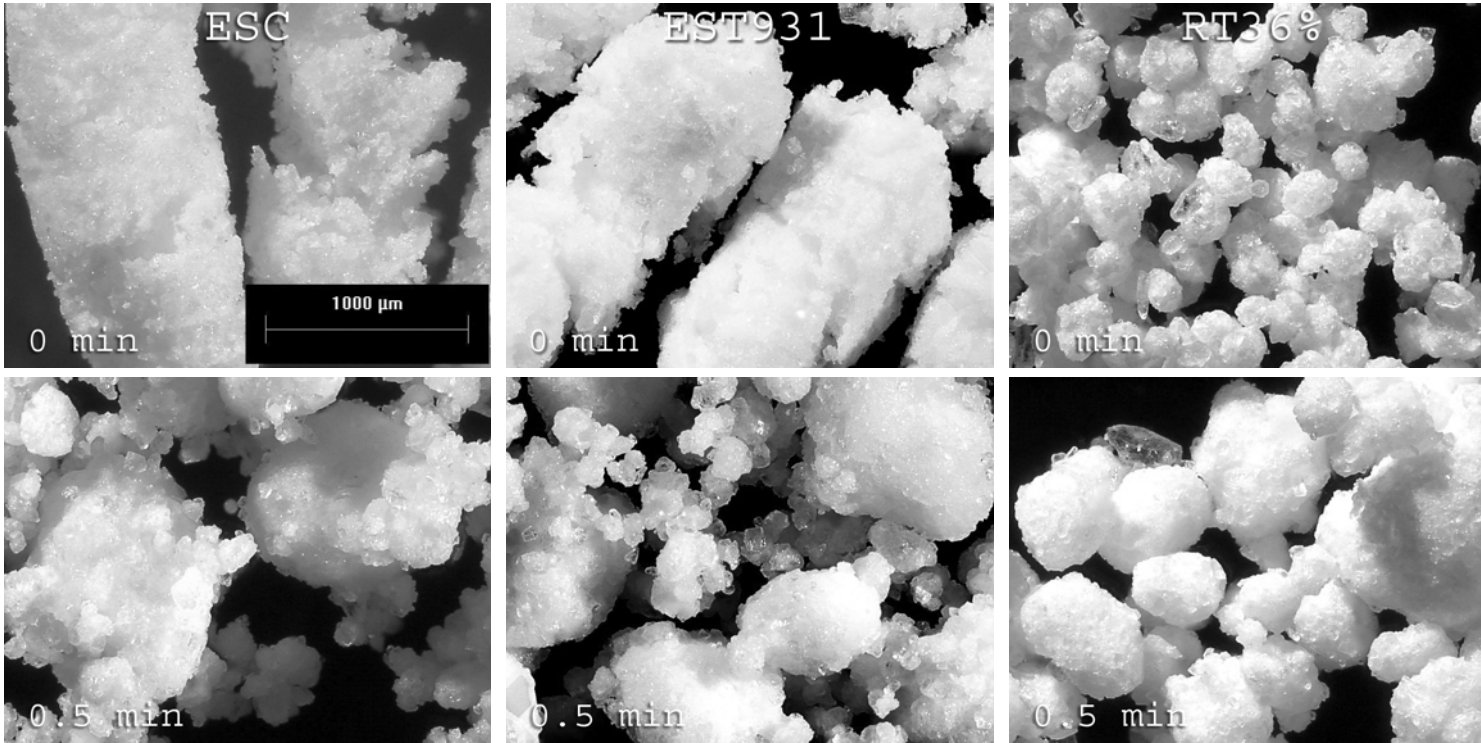


Figure 4. Photographs of time-sampled spheroids depicting stages of spheroid formation in ESC, EST931 and RT36%. For ESC and EST931, time annotations indicate time lapsed during spheronization. For RT36%, time annotations indicate time lapsed after completion of water addition.

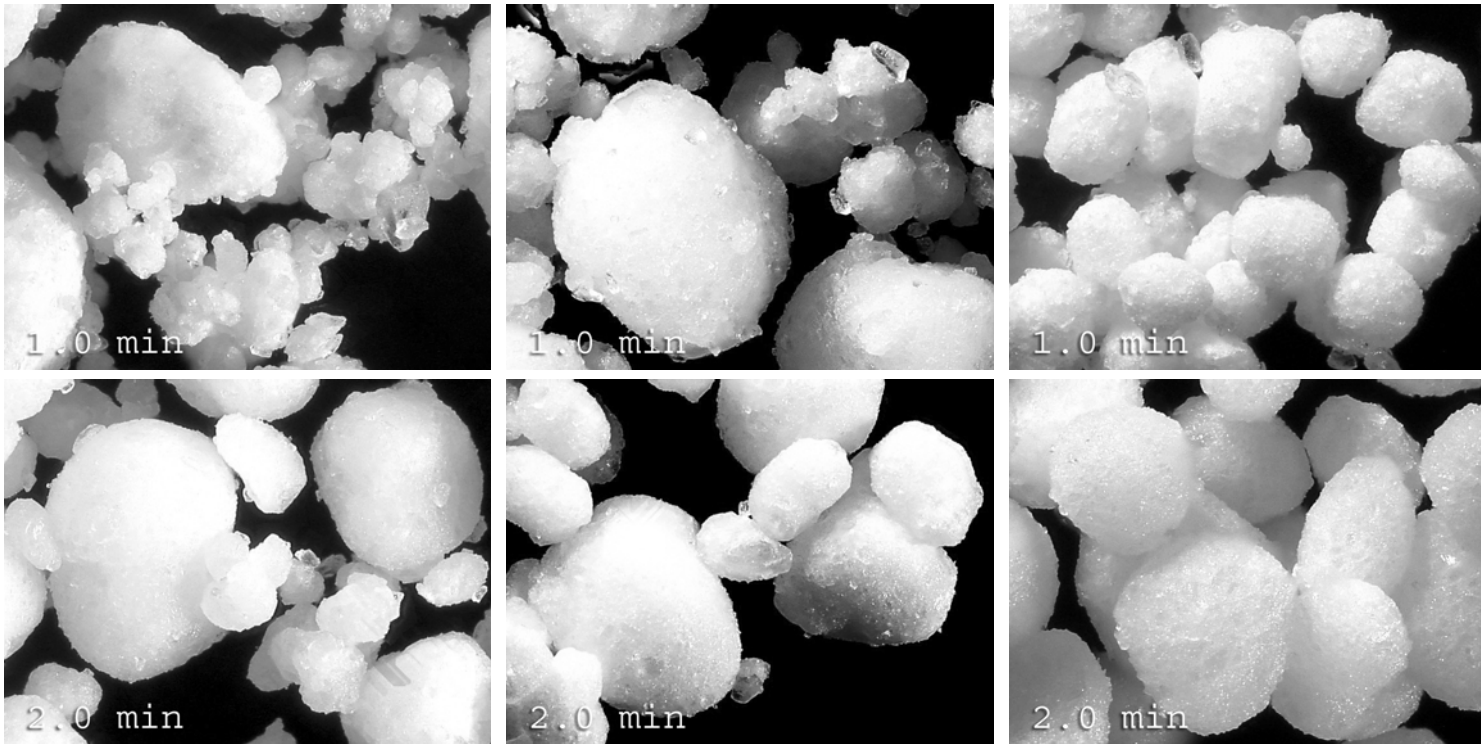


Figure 4 (Continued). Photographs of time-sampled spheroids depicting stages of spheroid formation in ESC, EST931 and RT36%. For ESC and EST931, time annotations indicate time lapsed during spheronization. For RT36%, time annotations indicate time lapsed after completion of water addition.

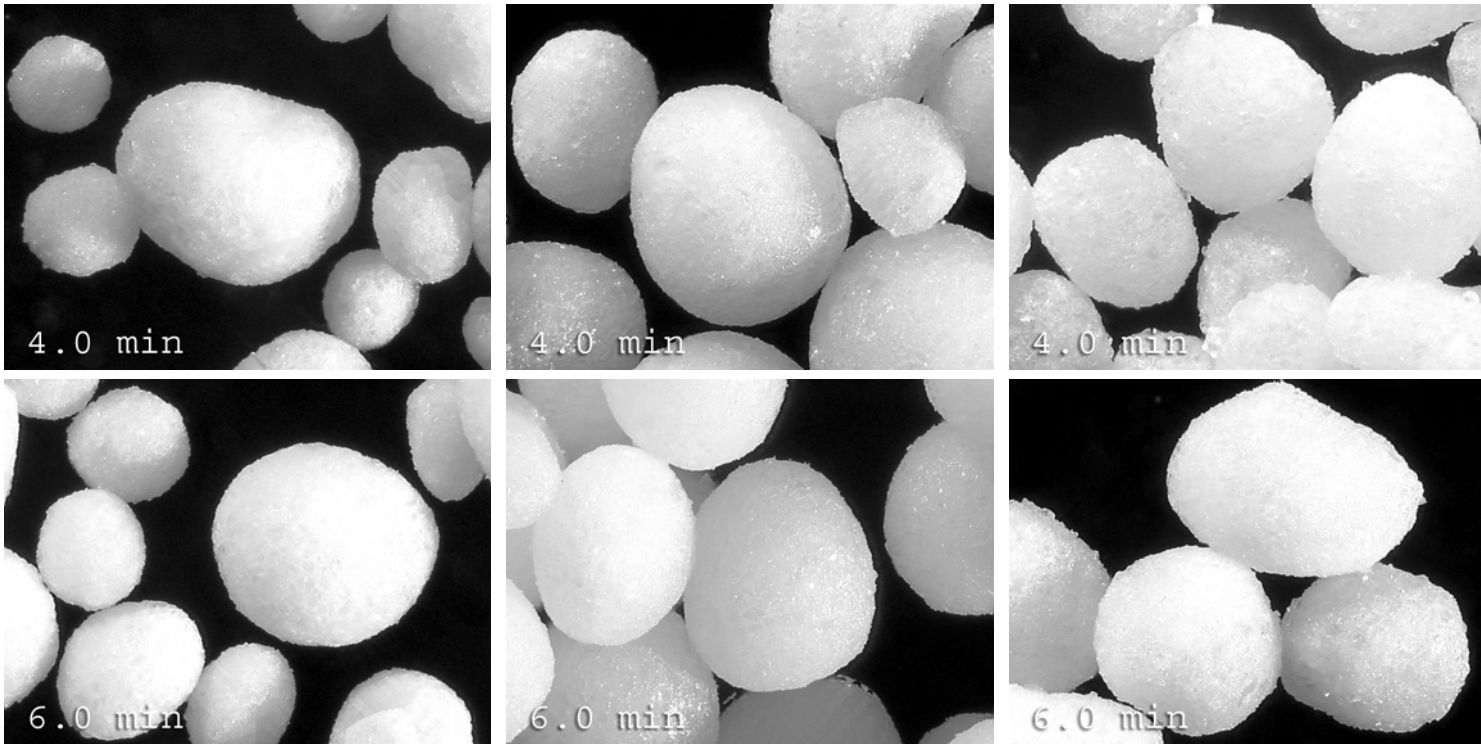


Figure 4 (Continued). Photographs of time-sampled spheroids depicting stages of spheroid formation in ESC, EST931 and RT36%. For ESC and EST931, time annotations indicate time lapsed during spheronization. For RT36%, time annotations indicate time lapsed after completion of water addition.

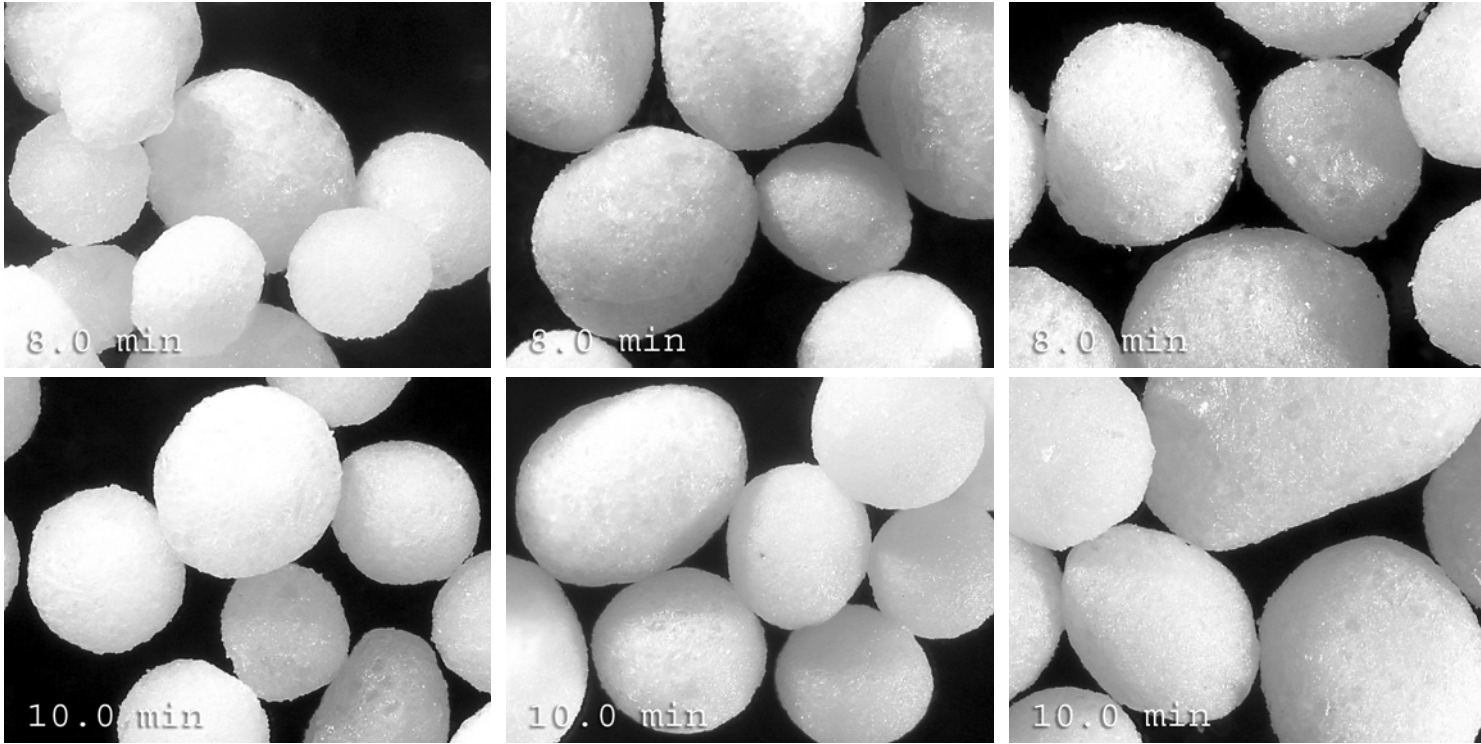


Figure 4 (Continued). Photographs of time-sampled spheroids depicting stages of spheroid formation in ESC, EST931 and RT36%. For ESC and EST931, time annotations indicate time lapsed during spheronization. For RT36%, time annotations indicate time lapsed after completion of water addition.

textured rotating frictional plate and collisions between extrudates as well as with the container wall. Extrudates broke down within 0.5 min seemingly into two populations distinguished by size: aggregates of size approximately 1 mm, and 0.2 mm in length. In this study, the larger aggregates were termed core aggregates and those of approximately 0.2 mm lengths were termed fines. Upon spheronization for 1 min, fines which initially appeared irregularly shaped became rounder and slightly larger. These fines increased in size by coalescence between themselves. Materials that were larger than fines but smaller than core aggregates were termed nucleated aggregates. As spheronization proceeded into the 2nd min, nucleated aggregates became increasingly rounder and larger, concurrently with the core aggregates. Beyond the 2nd min, the proportion of unagglomerated individual particles reduced considerably and the remaining population consisted only of nucleated aggregates and core aggregates. These were also usually rounder. The disparity in size between nucleated and core aggregates was small, in comparison to that of fines and core aggregates. The nucleated aggregates became progressively larger with time whilst size of core aggregates remained relatively unchanged. From the 4th min onwards, both core and nucleated aggregates were indistinguishable from one another as aggregates were approaching uniformity in size.

Video footage of spheronization for ESC captured *in situ* using high speed photography revealed images which were in agreement with observations made on time-sampled ESC spheroids (Figure 5). Upon 0.5 min of spheronization, the

population consisted of less spherical core aggregates which distinctively had much fines adhered onto their surfaces. At 1 min into spheronization, these core aggregates were observed to be more spherical. Nucleated aggregates were also observed to be rounder. Core aggregates consolidated as they were being spheronized. They resisted size enlargement but became progressively rounder. In contrast, nucleated aggregates continued to grow bigger and rounder as spheronization proceeded (Figure 5).

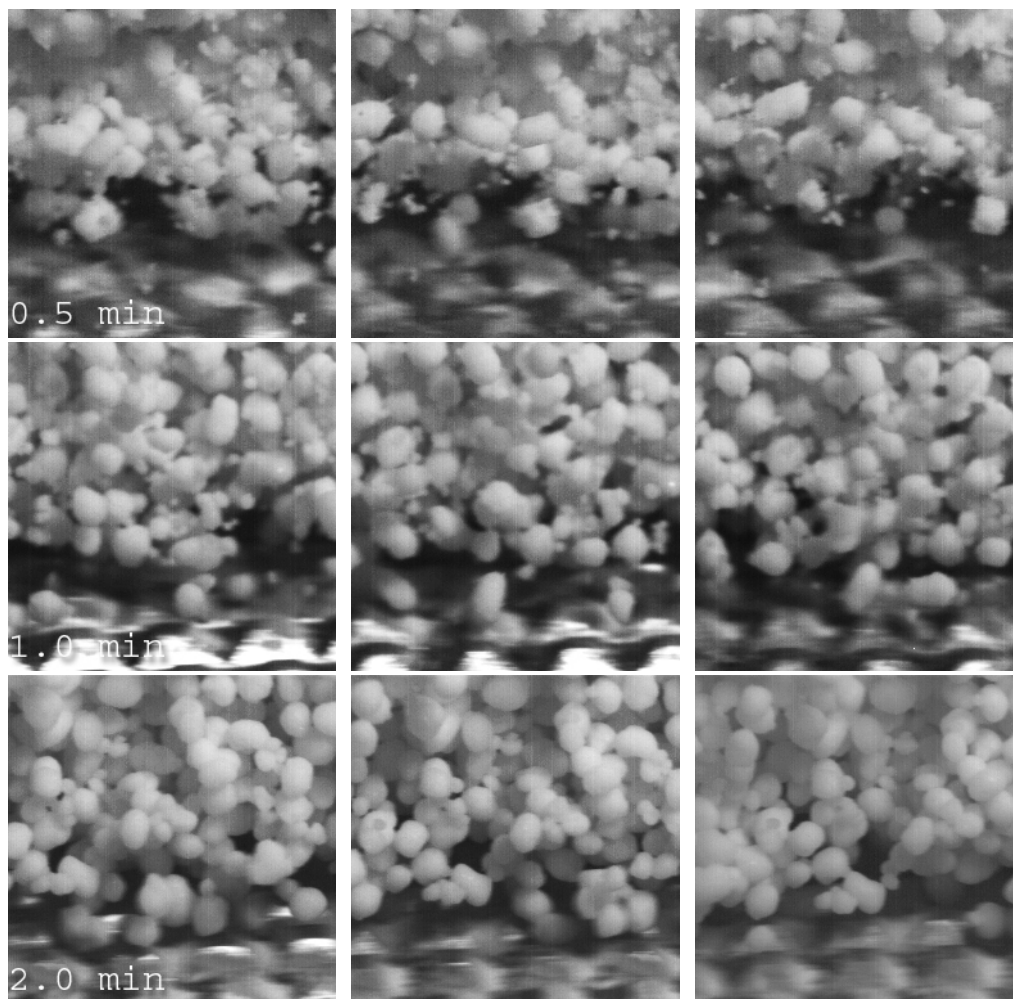


Figure 5. Sequential frames of ESC spheroid formation captured *in situ* using high speed video camera.

Time annotations indicate time lapsed during spheronization.

In general, spheroid production could be considered as a specialized form of granulation. The classic granulation model depicts 3 stages: wetting and nucleation,

consolidation and growth, and attrition and breakdown (Iveson et al., 2001). ES began with the moistening of powder mixture, causing nucleation of particles to form aggregates. Agglomerates formed experienced compressive forces during transit through the extrusion screen, resulting in consolidation and formation of extrudates. In RP, nucleation occurred when water was sprayed onto the powder mixture. Unlike the process of extrusion, consolidation of aggregates during RP was brought about by the shearing forces of the rotating frictional plate. Although shearing forces could cause consolidation, excessive shearing forces would cause agglomerates to be broken down.

1.9. Comparison of observed spheroid formation with existing theories

Extrudates could be fractured across their lengths: by shear forces from the rotating frictional plate surface of the spheronizer, collision among extrudates, or collision between extrudates and container wall. Fractured extrudates yielded core aggregates. Edges and surface irregularities of extrudates underwent attrition, producing fines. Visual observation of core aggregates and fines in the 0.5 min and 1 min samples of ESC and EST931 might suggest that size distribution could assume a bimodal characteristic (Figure 4). The initial phase of extrudate breakdown was followed by these size enlargement mechanisms: coalescence of fines forming aggregates, coalescence of aggregates with core aggregates, and layering of fines onto core aggregates. One of the spheroid formation models (Vervaet et al., 1995) suggested

that extrudates were rounded at the edges, followed by the formation of dumbbell shaped aggregates. These dumbbell shaped aggregates were intermediates which proceeded to become elliptical spheres, eventually rounding to yield spheroids. This model hypothesized that extrudates were relatively plastic and non-brittle, able to deform during spheronization to form dumbbells. The alternative model proposed by Baert and Remon (1993) also hypothesized the formation of dumbbell shaped aggregates as intermediates. However, the main difference between the two models was that in the latter model, the dumbbell shaped aggregates would break into two in the middle. Folding would occur at the point of breakage before spheroids eventually formed. These intermediates which were dumbbell shaped aggregates should exist at the beginning of spheronization (0-2 min). However, visual observation of time-sampled spheroids of ESC and EST931 (0.5-2 min) indicated that existence of dumbbell shaped aggregates as intermediates were unlikely unless they occurred within the first 30 s of spheronization (Figure 4). The video footage of the spheronization of ESC spheroids, captured by the high speed camera, showed the existence of elongated core aggregates (Figure 5). However, these elongated core aggregates did not resemble precursors that were dumbbell shaped aggregates but rather, they were short rod-like core aggregates. These core aggregates progressively became rounder. A distinct decrease in size in the mid-section of core aggregates could suggest a dumbbell breakage. However, this decrease in size was not observed in this present study.

It has been hypothesized that the dumbbell breakage and folding was the reason for the presence of cavity found within spheroids (Baert and Remon, 1993 and Pisek et al., 2001). However, Pisek et al. (2001) used ES and RP to produce spheroids with different amount of lactose and noticed that spheroids with higher percentage of lactose in the formulation also correlated with larger cavities within the spheroids. This would indicate the possibility that the cavities were present if the spheroid formulation contained soluble excipients. Remodelling also tended to be more of a surface phenomena with the cohesive but plastic aggregate surfaces remodelled or realigned along the circumferential direction, away from the ends of the longer axes, to the mid-sections as the impact forces were regular but of low magnitudes. Entrapped cavities would likely remain unaffected as the impact forces were dissipated along the agglomerate surfaces as they remodelled. In fact, the remodelling process itself could have contributed to the existence or enlargement of entrapped cavities. As the rod-like aggregate ends were pressured inwards by impact forces, the mid-section may be forced outwards by inward moving water liberated by the sponge-like microcrystalline particles (Heng and Koo, 2001), contributing to a high water pressure within. Subsequently, these water-rich regions, upon drying became cavities in the spheroids. This observation provided an alternative explanation for the existence of the cavity, complementing the observations by other investigators as discussed earlier. Although the spheroid formation mechanism could be different using different formulation or process parameters, within the limits of this study where the formulation used was able to produce typically good quality spheroids of

suitable size and narrow size distribution, the ES spheroid formation mechanism could be described as follows,

- (a) breakdown of extrudates to length approximately equal to their diameter,
- (b) attrition of corners and edges of extrudates, producing core aggregates and fines,
- (c) layering of fines onto core aggregates, coalescence between fines, small aggregates to form larger core aggregates, and
- (d) remodelling of rod-like aggregates by gradual and consistent impacts on the circumferential edges to form spheroids of high sphericity (Figure 6a)

In comparison, the RP spheroid formation mechanism followed this pattern:

- (a) nuclei formation from agglomeration of wetted particles,
- (b) agglomeration of nuclei, forming small agglomerates,
- (c) layering of fines onto larger agglomerates, and
- (d) coalescence of agglomerates and rounding to form spheroids (Figure 6b).

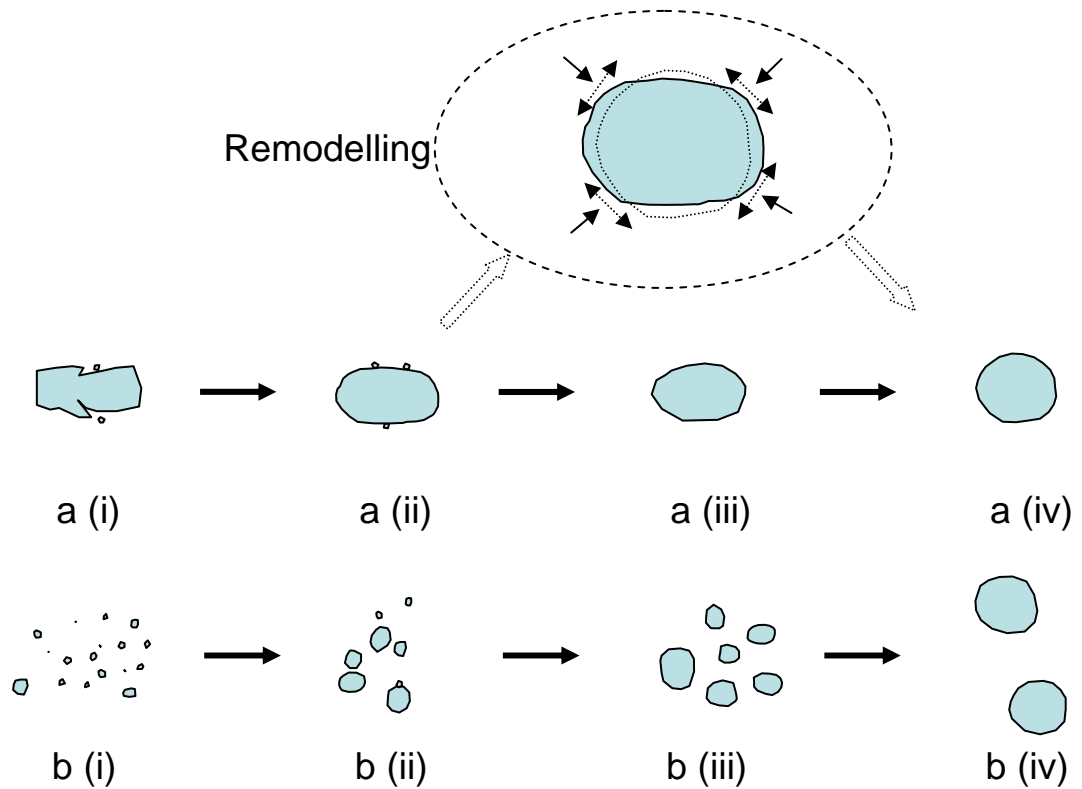


Figure 6. Model of spheroid formation by (a) ES and (b) RP.

The visually observed differences in spheroid formation (Figure 4) and presence of oversized spheroids for RT36% (3.36% by weight larger than 1.7 mm) emphasized the importance of uniform water distribution in RP. A homogenous distribution of water throughout the powder mixture depended on factors such as flow pattern of the powder mixture and spray rate. Flow pattern of powder mixture would be related to its rheology and the speed of the rotating frictional plate. When the powder mixture did not flow uniformly or consistently, its transit time and movement across the spray zone became irregular, resulting in localized overwetting. In a high shear mixer granulator, an increase in amount of granulating liquid increased the rate of granule

growth and also the final size of the granules (Hoornaert et al., 1998). Examining the process similarities between high shear granulation and RP, localized overwetting would cause rapid agglomerate growth, bringing about disparity in sizes of formed agglomerates in the processor. According to the granulation model concerning coalescence of non-deformable granules, the opportunity to coalesce upon impact is higher between granules of dissimilar sizes during coalescence of non-deformable granules (Iveson et al., 2001). This model postulated the existence of a maximum size which granules could achieve by coalescence. During spheronization, large aggregates increased in size by a “snowball effect”, continuously coalescing smaller aggregates onto its surfaces. When the amount of moisture on the surface was insufficient to facilitate subsequent successful coalescence, aggregates would have reached their maximum size. Excessively large aggregates would also be broken down by the impact forces exerted by the textured surface of the rotating frictional plate. During spheronization, there was concurrent loss of moisture by evaporation. This also acted as an additional barrier to agglomerate growth with time. Moreover, if spheronization run was continued beyond the usual run time for making good spheroids, breakdown of formed spheroids would have occurred for both ES and RP.

The extrusion step caused ES spheroids to be formed differently compared to RP. The occurrence of core aggregates and layering of fines during the initial stage of spheronization could have produced aggregates of non homogenous matrix, in terms of particle to particle interaction. In RP, nuclei formation, agglomeration of nuclei and

coalescence of agglomerates with the possibility of minimal layering of fines could have produced aggregates with a more homogenous matrix, resulting in higher crushing strength.

Inevitably, as both ES and RP are different spheroid production methods, it would be expected that spheroids produced would have different attributes. However, up to this point, the aim of the study is to establish equivalent process and formulation parameters for comparison between ES and RP. The common parameters established are:

- a) identical excipients used with slight variation in amount of water used,
and
- b) equivalent spheronization conditions.

These common parameters allowed the production of spheroids of similar size, which were within the pharmaceutically useful size range. Using these common parameters, spheroid size distribution and morphology were studied in greater detail in order to characterize the spheroid formation mechanism and at the same time investigate whether there is any common spheroid mechanism that would be present in ES and RP.

2. Mathematical quantification of spheroid formation process

2.1. Conventional size and shape characterization methods

2.1.1. Sieving

Regardless of the mathematical formula used for calculation, the mean size of spheroids, as analyzed by sieving, was approximately 0.85 mm (Table 9). As expected, D_{wmed} and $Span_w$ of ESC and ESC(TS) batches were similar. All the descriptors in Table 9 consistently indicated that ESC(TS) batches were of optimum mean size and narrow size distribution, representing a typical good formulation with suitable process parameters. Numerically, the descriptors represented mean size values with slight differences. The manner in which the descriptors vary with one another would depend on the shape of the size distribution. D_{warith} was marginally larger than D_{wgeo} and both were consistently larger than D_{wmed} (Table 9). The size distribution of spheroids was positively skewed, possibly resembling a log normal distribution as D_{wmed} was consistently smaller than D_{warith} . D_{wmed} is an empirical and distribution-free method of finding the size at the 50th %. If the underlying size distribution of spheroids is a log normal distribution, the values of D_{wmed} and D_{wgeo} should be approximately the same. However, as values of D_{wmed} and D_{wgeo} were not comparable, spheroid size distribution might not be log normal. In this study, spheroids were sized using sieves and typically, a maximum of 5-7 sieve fractions were obtained. This would also result in only 5-7 data points to plot a size distribution curve. From the mismatch of D_{wmed} and D_{wgeo} , and the limited data

points obtainable from sieving of spheroids to plot a size distribution curve, there was insufficient evidence to deduce or validate whether size distribution of spheroids could be represented by a log normal distribution. Conventional method of sizing spheroids using sieves could not provide enough data points to accurately show the size distribution of spheroids. In order to observe the size distribution of spheroids, sizing with image analysis and analyzing hundreds of spheroids per spheroid batch must be carried out. For this reason, size distributions of spheroids were plotted using image analysis data points from at least 625 spheroids per batch.

Table 9. Mean size and size distribution of ESC(TS) spheroids derived from size analysis using sieves.

Batch	Dwgeo (mm)	SDwgeo	Dwarith (mm)	SDwarith	Dwmed (mm)	Spanw
1ESC(TS)	0.891	1.135	0.898	0.116	0.815	0.350
2ESC(TS)	0.884	1.138	0.891	0.118	0.805	0.348
3ESC(TS)	0.844	1.171	0.854	0.142	0.780	0.404

2.1.2. Image analysis

The typical endpoint for spheronization could be taken when spheroid size achieves a constant stable value, concurrent with a sufficiently good degree of roundness. As shown by data in Table 10 and Figure 7, the spheronization process for ESC(TS) batches was sufficiently completed within 10 min. Size of ESC(TS) spheroids increased during spheronization, with the greatest increase between the 2nd and 4th min. This trend was similar to that observed by Wan et al. (1993). From 6th to 10th min, spheroid size reached a plateau. Spheroid size distribution narrowed with increased residence time during spheronization (Figure 8). Mean AR and e_R of

spheroids indicated increasing roundness with increasing residence time during spheronization (Figure 7).

Table 10. Mean size and size distribution of ESC(TS) spheroids derived from image analysis.

Batch	DI (μm)	SDI	DIgeo (μm)	SDIgeo	DImed (μm)	SpanI
1ESC(TS)2	753.0	266.5	707.9	1.422	688.4	1.029
1ESC(TS)4	908.5	217.3	882.3	1.277	905.5	0.628
1ESC(TS)6	908.6	170.5	893.0	1.204	879.8	0.499
1ESC(TS)8	926.1	142.1	915.5	1.164	907.4	0.413
1ESC(TS)10	935.5	125.4	927.4	1.140	910.7	0.355
2ESC(TS)2	690.3	312.2	626.7	1.546	574.0	1.423
2ESC(TS)4	889.5	212.3	864.5	1.271	847.5	0.664
2ESC(TS)6	921.8	167.7	906.9	1.197	895.8	0.501
2ESC(TS)8	925.1	144.2	914.2	1.166	888.9	0.425
2ESC(TS)10	924.9	123.5	917.0	1.139	885.5	0.355
3ESC(TS)2	676.1	322.2	602.7	1.622	565.4	1.489
3ESC(TS)4	800.9	238.9	766.7	1.344	752.6	0.817
3ESC(TS)6	847.8	193.7	826.8	1.248	798.7	0.630
3ESC(TS)8	872.4	169.8	856.5	1.210	819.2	0.531
3ESC(TS)10	862.2	149.0	850.2	1.179	802.6	0.479

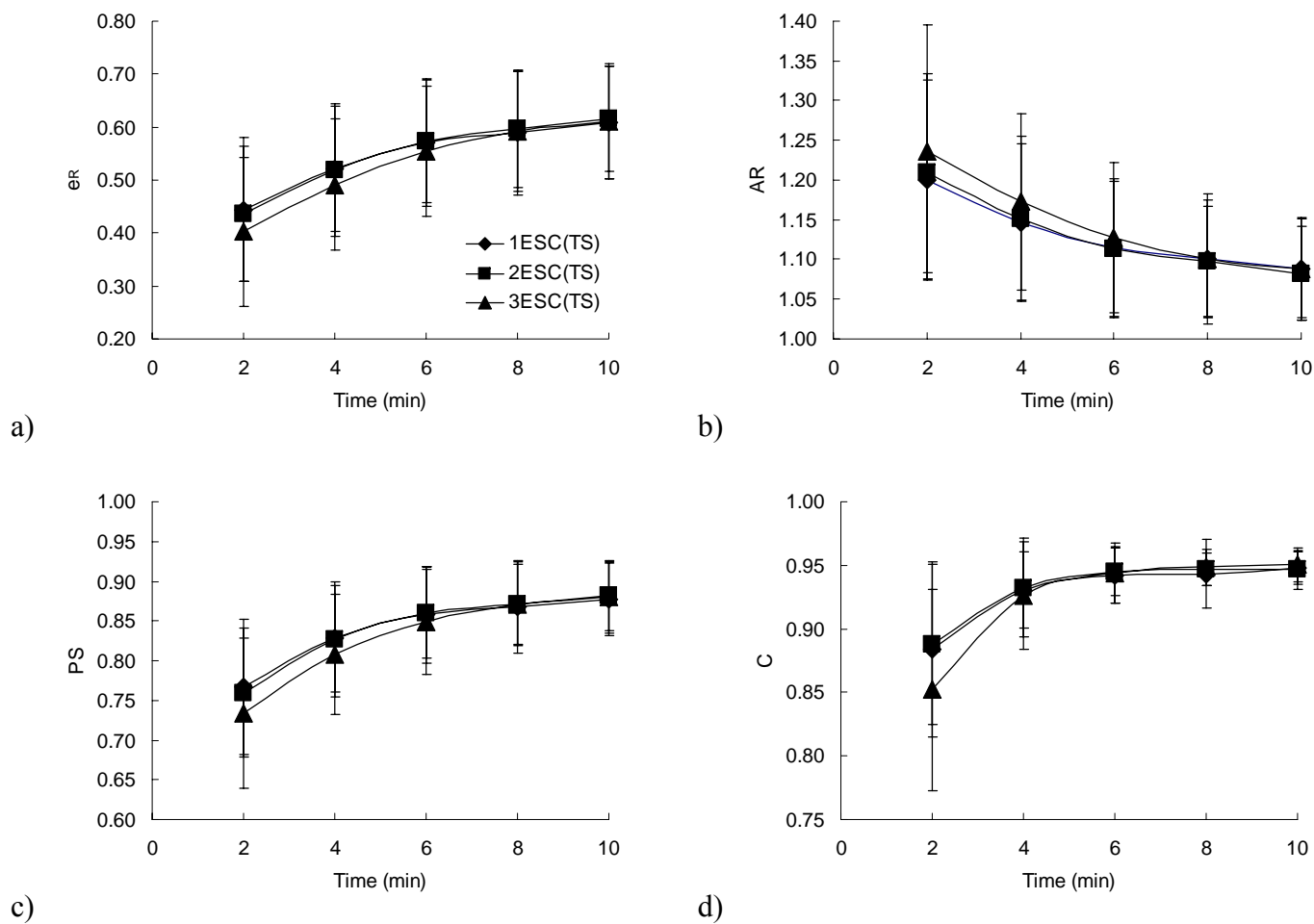


Figure 7. Effect of spheronization duration on (a) e_R , (b) AR, (c) PS and (d) C of ESC(TS) spheroids. Error bars represent \pm standard deviations.

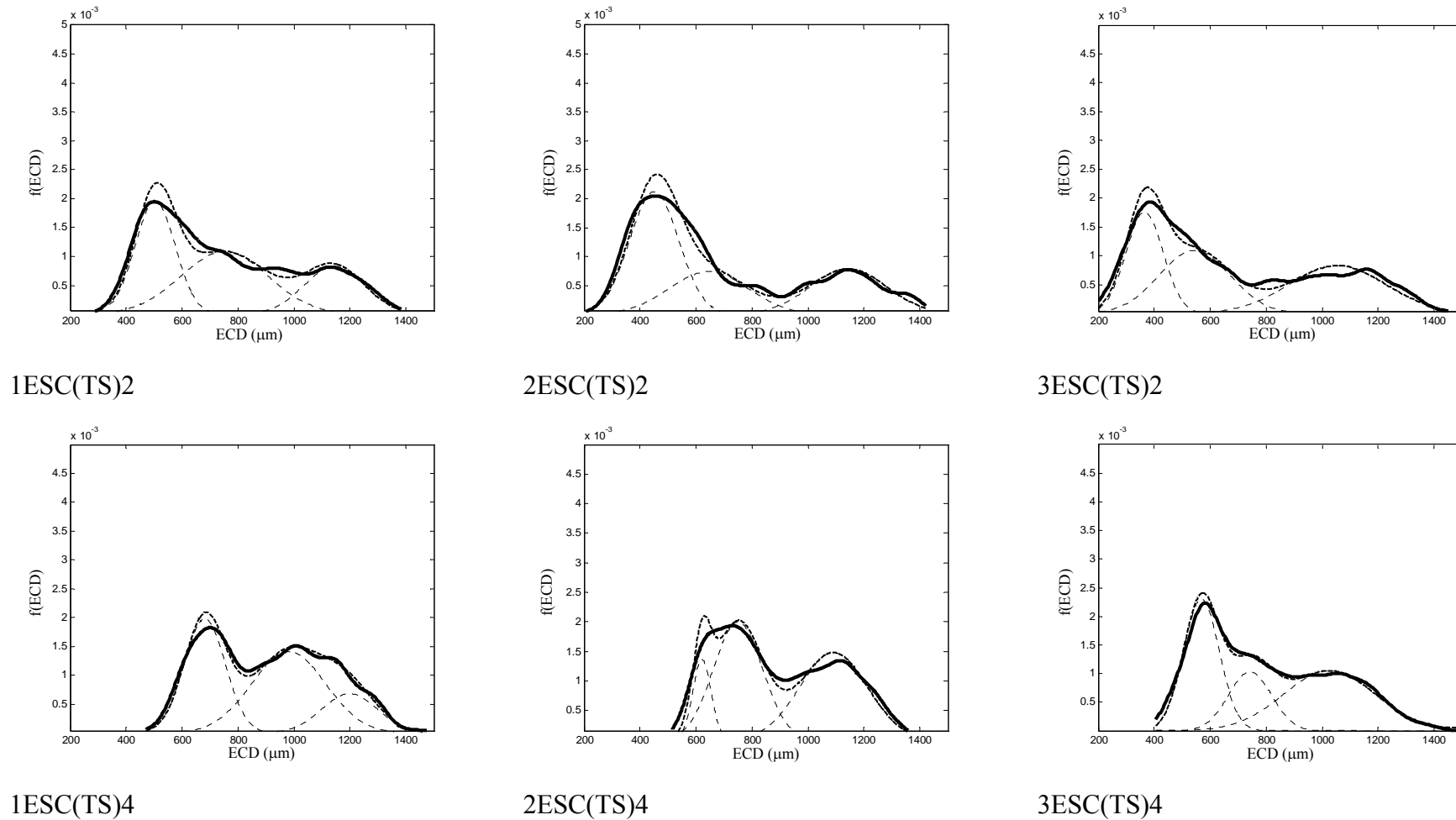


Figure 8. Population density function of ESC(TS) spheroids.

(Solid line - empirical PDF, light dashes - 3 individual component of MG, bold dashes - PDF of fitted 3 components MG).

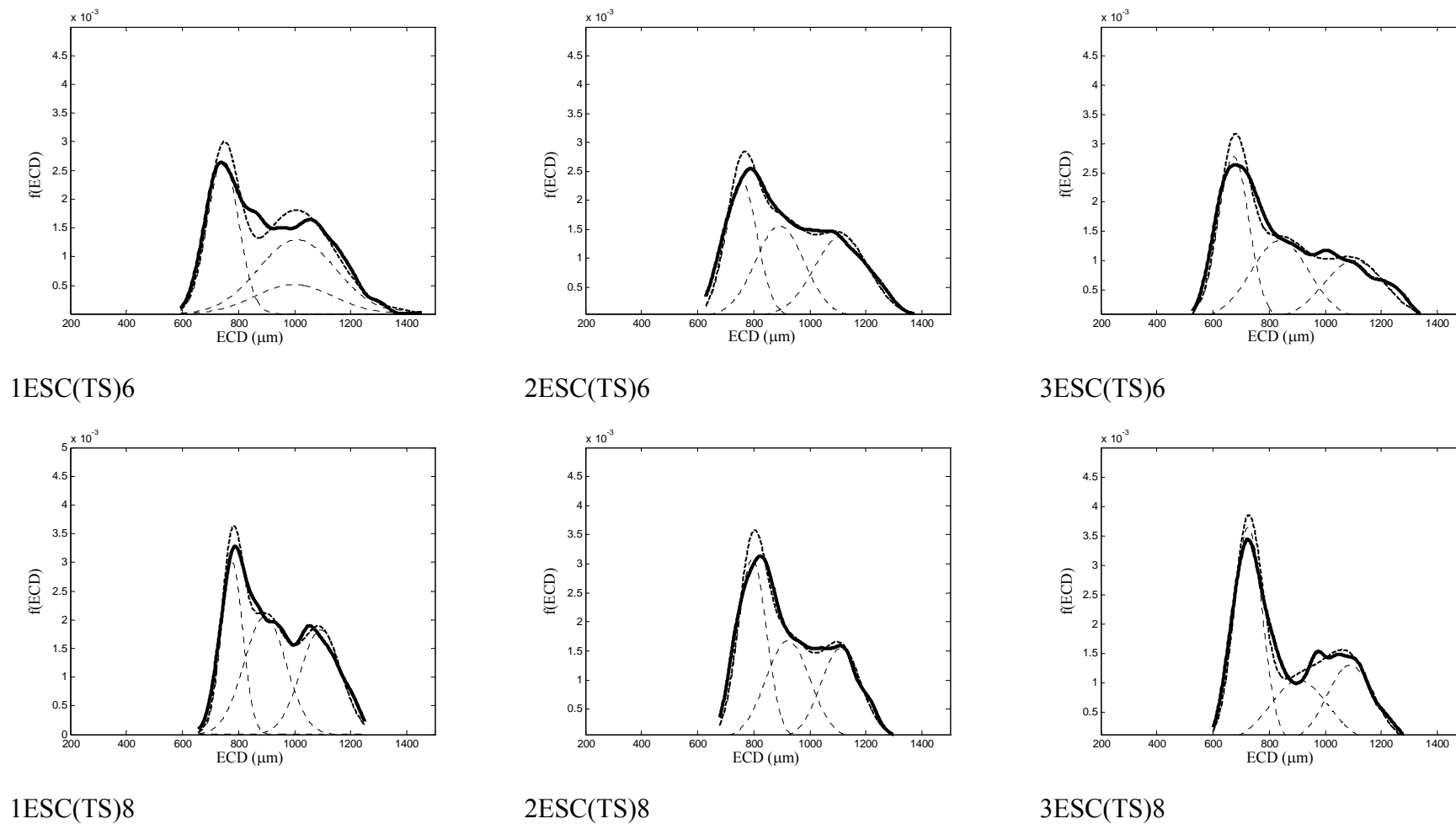
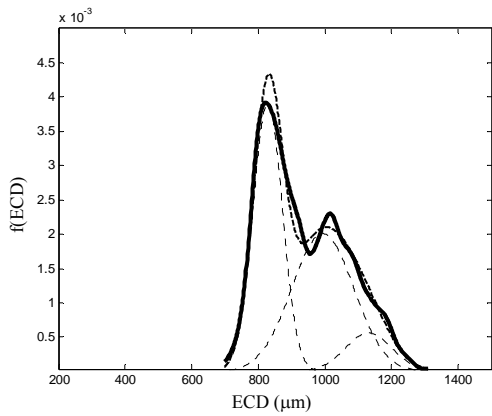
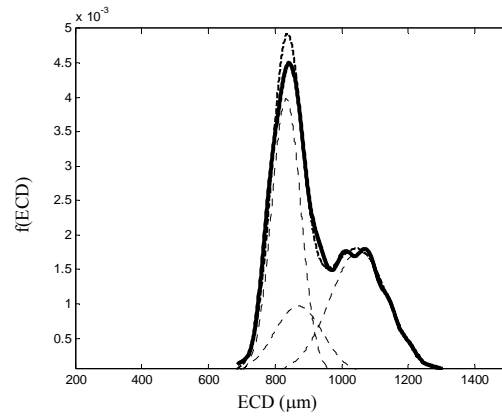


Figure 8 (Continued). Population density function of ESC(TS) spheroids.

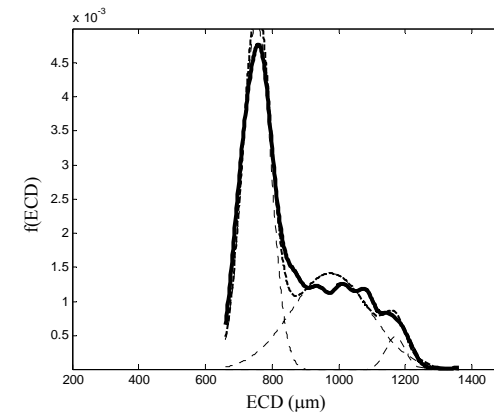
(Solid line - empirical PDF, light dashes - 3 individual component of MG, bold dashes - PDF of fitted 3 components MG).



1ESC(TS)10



2ESC(TS)10



3ESC(TS)10

Figure 8 (Continued). Population density function of ESC(TS) spheroids.

(Solid line - empirical PDF, light dashes - 3 individual component of MG, bold dashes - PDF of fitted 3 components MG).

One way ANOVA (Table 11) and post hoc test verified that the increase in spheroid roundness was significant throughout the 10 mins of spheronization. DI of ESC(TS) spheroids increased significantly during the initial stage of spheronization from 2nd to 4th min, after which (from 6th to 10th min) no significant increase was observed (Table 11). During spheronization, mass transfer between spheroids can be reflected by size changes. Concurrently, spheroids also underwent plastic deformation upon collision with one another and with surfaces, resulting in greater roundness. As verified statistically, there was significant mass transfer between ESC(TS) spheroids during the first 4 min of spheronization. Subsequently, any collision between spheroids did not appear to result in mass transfer. The conclusion arrived upon analysis of DI and spheroid roundness was that while plastic deformation of spheroids occurred throughout spheronization, mass transfer between spheroids occurred during the first 4 min of spheronization. While DI of spheroids was able to show mass transfer between spheroids for the first 4 min of spheronization, it was unable to detect any considerable mass transfer after 4 min of spheronization.

Table 11. One way ANOVA and post hoc test for size and roundness of ESC(TS) spheroids.

Batches compared		P value for LSD post hoc test					
		DI	μ_1, σ_1	e_R	AR	PS	C
1ESC(TS)2 vs.	1ESC(TS)4	0.000*(0.000*)	0.000*(0.000*)	0.000*(0.000*)	0.000*(0.000*)	0.000(0.000*)	0.000(0.000*)
	1ESC(TS)6	0.000*	0.000*	0.000*	0.000*	0.000*	0.000*
	1ESC(TS)8	0.000*	0.000*	0.000*	0.000*	0.000*	0.000*
	1ESC(TS)10	0.000*	0.000*	0.000*	0.000*	0.000*	0.000*
1ESC(TS)4 vs.	1ESC(TS)6	0.993	0.000*	0.000*	0.000*	0.000*	0.000*
	1ESC(TS)8	0.104	0.000*	0.000*	0.000*	0.000*	0.000*
	1ESC(TS)10	0.013*	0.000*	0.000*	0.000*	0.000*	0.000*
1ESC(TS)6 vs.	1ESC(TS)8	0.106	0.000*	0.010*	0.003*	0.004*	0.653
	1ESC(TS)10	0.013*	0.000*	0.000*	0.000*	0.000*	0.011*
1ESC(TS)8 vs.	1ESC(TS)10	0.387	0.000*	0.016*	0.008*	0.008*	0.037*
2ESC(TS)2 vs.	2ESC(TS)4	0.000*(0.000*)	0.000*(0.000*)	0.000*(0.000*)	0.000*(0.000*)	0.000*	0.000*
	2ESC(TS)6	0.000*	0.000*	0.000*	0.000*	0.000*	0.000*
	2ESC(TS)8	0.000*	0.000*	0.000*	0.000*	0.000*	0.000*
	2ESC(TS)10	0.000*	0.000*	0.000*	0.000*	0.000*	0.000*
2ESC(TS)4 vs.	2ESC(TS)6	0.005*	0.000*	0.000*	0.000*	0.000*	0.000*
	2ESC(TS)8	0.002*	0.000*	0.000*	0.000*	0.000*	0.000*
	2ESC(TS)10	0.002*	0.000*	0.000*	0.000*	0.000*	0.000*
2ESC(TS)6 vs.	2ESC(TS)8	0.773	0.000*	0.003*	0.001*	0.002*	0.198
	2ESC(TS)10	0.789	0.000*	0.000*	0.000*	0.000*	0.342
2ESC(TS)8 vs.	2ESC(TS)10	0.984	0.000*	0.005*	0.002*	0.002*	0.736

Values in parenthesis are P values for one way ANOVA. * indicates statistical significance at $P \leq 0.05$.

Table 11 (Continued). One way ANOVA and post hoc test for size and roundness of ESC(TS) spheroids.

Batches compared	P value for LSD post hoc test						
	DI	μ_1, σ_1	e_R	AR	PS	C	
3ESC(TS)2 vs. 3ESC(TS)4	3ESC(TS)4	0.000*(0.000*)	0.000*(0.000*)	0.000*(0.000*)	0.000*(0.000*)	0.000*	0.000*
	3ESC(TS)6	0.000*	0.000*	0.000*	0.000*	0.000*	0.000*
	3ESC(TS)8	0.000*	0.000*	0.000*	0.000*	0.000*	0.000*
	3ESC(TS)10	0.000*	0.000*	0.000*	0.000*	0.000*	0.000*
3ESC(TS)4 vs. 3ESC(TS)6	3ESC(TS)6	0.000*	0.000*	0.000*	0.000*	0.000*	0.000*
	3ESC(TS)8	0.000*	0.000*	0.000*	0.000*	0.000*	0.000*
	3ESC(TS)10	0.000*	0.000*	0.000*	0.000*	0.000*	0.000*
3ESC(TS)6 vs. 3ESC(TS)8	3ESC(TS)8	0.051	0.000*	0.000*	0.000*	0.000*	0.047*
	3ESC(TS)10	0.420	0.000*	0.000*	0.000*	0.000*	0.003*
3ESC(TS)8 vs. 3ESC(TS)10	3ESC(TS)10	0.420	0.000*	0.039*	0.005*	0.024	0.310

Values in parenthesis are P values for one way ANOVA. * indicates statistical significance at $P \leq 0.05$.

2.2. Representing ES spheroid size with MG distribution

The shape of the size distribution of ESC(TS) spheroids changed characteristically as spheronization progressed, from 2nd -10th min (Figure 8). Qualitatively, size distribution of ESC(TS)2 spheroids showed multimodal characteristics. These multiple peaks merged with one another with continued spheronization, reducing the observed multimodal characteristics as size distribution narrowed. Eventually, size distribution of ESC(TS)10 spheroids developed into a shape which resembled a log normal distribution. However, statistical curve fitting revealed that ESC(TS) spheroid size distributions did not significantly follow normal or log normal distribution (Table 12).

Shape of the size distribution for all the 3 batches of ESC(TS) spheroids changed throughout the 10 min of spheronization period in a consistently similar manner, suggesting that mass transfer between spheroids occurred during the entire duration of spheronization. It was discussed previously on page 82 that the analysis of DI and spheroid roundness would only provide evidence of spheroid mass transfer during the first 4 min of spheronization. This inability to detect spheroid property changes during spheronization prompted the need for an alternative approach to spheroid size analysis. This alternative approach should have the ability to detect any mass transfer between spheroids during the entire spheronization process. Attempts were therefore made to quantify and mathematically describe the shape of size distribution of spheroids throughout the entire spheronization process.

Table 12. P values from Chi square curve fitting of size distribution of ESC(TS) spheroids to various distributions.

Batch	Distribution				
	Normal	Log normal	2cMG	3cMG	4cMG
1ESC(TS)2	0.000*	0.000*	0.296	0.936	0.975
1ESC(TS)4	0.000*	0.000*	0.265	0.291	0.430
1ESC(TS)6	0.000*	0.000*	0.002*	0.002*	0.002*
1ESC(TS)8	0.000*	0.000*	0.042*	0.340	0.420
1ESC(TS)10	0.000*	0.000*	0.328	0.321	0.328
2ESC(TS)2	0.000*	0.000*	0.000*	0.026*	0.243
2ESC(TS)4	0.000*	0.000*	0.052	0.505	0.607
2ESC(TS)6	0.000*	0.000*	0.624	0.763	0.817
2ESC(TS)8	0.000*	0.000*	0.347	0.617	0.874
2ESC(TS)10	0.000*	0.000*	0.237	0.356	0.426
3ESC(TS)2	0.000*	0.000*	0.000*	0.078	0.239
3ESC(TS)4	0.000*	0.000*	0.000*	0.000*	0.194
3ESC(TS)6	0.000*	0.000*	0.000*	0.459	0.654
3ESC(TS)8	0.000*	0.000*	0.220	0.265	0.266
3ESC(TS)10	0.000*	0.000*	0.544	0.452	0.046*

* denotes statistical significance at $P \leq 0.05$.

2.2.1. Verifying size distribution of ES spheroids statistically

Contrary to Souto et al.'s (2005) assumption that size distribution of spheroids followed a normal or log normal distribution, most of the ESC(TS) spheroid size distributions could be represented by and followed 2, 3, and 4 components (c) MG distributions.

Among the multi components MG distributions, the size distributions best fitted to 3 or 4 components. The number of equation variables defining MG distribution increases with increasing number of components. With more components, the ability

of MG distribution to assume the observed empirical distribution would increase. However, the usefulness of having more variables to define a distribution would be questionable if these variables could not be used to explain or provide additional insight to the spheronization process. In order to achieve a balance between best fit to the curve fitting and simplicity in mathematical equation, a 3cMG distribution was used to quantify the size distribution of spheroids and with the attempt to model the spheronization process.

3cMG distribution can be used to characterize spheroid population and information obtained be used to supplement knowledge drawn from conventional methods by illustrating the characteristics of each size distribution. The findings obtained by fitting to the 3cMG distribution model can help to reveal evidence of heterogeneity in spheroid sizes within the spheroid population. The heterogeneity could be regarded as the coexistence of spheroids in various states or phases of growth. Fines, core aggregates, nucleated aggregates and spheroids could be observed at different phases during spheronization (Figure 8). Fines, core aggregates, nucleated aggregates and spheroids distinguished from one another mainly by their size distributions.

Heterogeneity could be understood as subpopulations of spheroids within a population of spheroids, distinguished from one another by size. By analyzing the proportions of the subpopulations, the size of spheroids within those subpopulations and the relative spheroid size between subpopulations, spheroid growth processes during spheronization could be better understood.

2.2.2. Quantifying spheroid formation with MG distribution

The 3cMG distribution could be hypothesized to represent 3 subpopulations of spheroids. Each of these 3 subpopulations of spheroids would be defined by a normal distribution of mean μ_i and standard deviation σ_i (Table 13). The relative proportion of each subpopulation with respect to the composite of the 3 subpopulations would be indicated by α_i .

Table 13. Size distribution of ESC(TS) spheroids as defined by 3cMG distribution.

Batch	α_1	μ_1 (μm)	σ_1	α_2	μ_2 (μm)	σ_2	α_3	μ_3 (μm)	σ_3
1ESC(TS)2	0.3511	503.8	71.56	0.4245	752.4	156.2	0.2245	1144	107.9
1ESC(TS)4	0.3643	681.4	73.27	0.4665	980.7	131.4	0.1692	1199	98.85
1ESC(TS)6	0.3717	744.8	55.17	0.1788	998.1	138.3	0.4495	1009	138.3
1ESC(TS)8	0.2853	777.0	37.97	0.3860	894.4	74.97	0.3287	1093	71.97
1ESC(TS)10	0.4335	828.3	44.22	0.4682	993.5	92.84	0.0984	1132	69.89
2ESC(TS)2	0.4659	450.7	87.55	0.2630	646.0	141.6	0.2711	1145	137.2
2ESC(TS)4	0.1115	621.2	32.53	0.4382	750.2	87.53	0.4503	1092	121.3
2ESC(TS)6	0.3254	756.1	55.59	0.3396	892.7	87.08	0.3350	1112	96.79
2ESC(TS)8	0.3901	794.9	50.47	0.3309	921.8	78.75	0.2791	1111	71.92
2ESC(TS)10	0.4359	833.5	43.73	0.1753	870.0	71.95	0.3888	1052	88.02
3ESC(TS)2	0.2928	365.4	66.33	0.3470	544.6	126.1	0.3603	1055	173.0
3ESC(TS)4	0.3696	568.6	64.00	0.1978	742.3	76.53	0.4326	1026	164.5
3ESC(TS)6	0.3814	673.5	54.75	0.3475	838.8	103.1	0.2711	1104	107.7
3ESC(TS)8	0.4612	725.2	50.51	0.2677	906.9	101.6	0.2711	1089	82.77
3ESC(TS)10	0.5421	753.8	42.48	0.4213	974.9	118.9	0.03654	1171	30.14

Consistently throughout spheronization for all batches, μ_1 increased as σ_1 decreased (Table 13). In comparison, μ_2 increased less and σ_2 did not consistently decrease.

Throughout the spheronization process from 2nd -10th min, μ_3 remained relatively unchanged while σ_3 decreased as spheronization progressed. Therefore, μ_3 could be an indicator for the maximum size achievable by spheroids during spheronization. At

the 2nd min into spheronization, α_1 represented a considerable segment of the spheroid population, ranging from 0.292 to 0.466. μ_1 ranged from 365.4 – 503.8 μm and represented the population of nucleated aggregates, pending coalescence with core aggregates. Fines which were produced from the breakage and attrition of extrudates at the start of spheronization could coalesce with each another to yield the nucleated aggregates that constituted the proportion, α_1 . Cylindrical extrudates produced in this study would be about 1 mm diameter. As μ_3 for all batches were about 1 mm, it suggested that the cylindrical extrudates were surface attrited and broke down to form core aggregates which were represented by α_3 of the population at the 2nd min of the spheronization run.

μ_1 and DI of ESC(TS) had a significant logarithmic increase, as verified using regression analysis, during spheronization (Table 14). Although the increase in μ_1 and DI could also be represented linearly, the Pearson correlation (R) values for logarithmic trend were higher. When one way ANOVA and LSD post hoc test were carried out on μ_1 and σ_1 of ESC(TS) spheroids, it indicated that this subpopulation of ESC(TS) spheroids had significant spheroid growth throughout the spheronization run (Table 14). DI, which represented mean size of the entire spheroid population, generally did not show significant increase in size after 6 min of spheronization. μ_1 and σ_1 as size descriptors were more sensitive in detecting spheroid size increase during the entire duration of spheronization. By representing the entire spheroid population as a heterogeneous population consisting of subpopulations, the changes in subpopulations during the entire process of spheronization provided evidences of

mass transfer between spheroids during the entire duration of spheronization. μ_1 and σ_1 showed the potential to be size descriptors critical in demonstrating any possible spheroid size changes within the spheroid population during the entire spheronization process.

Table 14. Regression analysis for logarithmic trend of spheroid size against duration of spheronization.

Batch	μ_1		μ_2		μ_3		DI	
	R	P value	R	P value	R	P value	R	P value
1ESC(TS)	0.990	0.001*	0.723	0.168	-0.353	0.560	0.908	0.033*
2ESC(TS)	0.993	0.001*	0.926	0.024*	-0.762	0.135	0.903	0.036*
3ESC(TS)	0.992	0.001*	0.999	0.000*	0.750	0.144	0.959	0.010*

* denotes statistical significance at $P \leq 0.05$.

μ_2 and μ_3 were statistically analyzed in the same manner as μ_1 to investigate if μ_2 and μ_3 had increased logarithmically during spheronization run. Two out of 3 μ_2 values of ESC(TS) have significant logarithmic increase throughout the spheronization run (Table 14). Low R values and insignificant P values for μ_3 indicated that μ_3 did not change significantly throughout the spheronization process (Table 14). The subpopulation of spheroids which was smaller in size, as represented by μ_1 , showed significant size changes and therefore, displayed evidence of mass transfer. In contrast, the subpopulations of bigger spheroids, as represented by μ_2 and μ_3 , due to inconclusive or insignificant size changes during spheronization, were not able to show evidence of mass transfer between spheroids during spheronization. The 3 subpopulations of spheroids represented by MG distributions showed different

tendencies to increase in size. μ_3 showed a clear indication that large spheroids within the population did not increase in size during spheronization. These large spheroids also did not show any reduction in size which could be construed as mass transfer to smaller spheroids, promoting the enlargement of smaller spheroids. The μ_1 logarithmic increase during spheronization suggested that mass transfer or coalescence occurred exclusively between smaller spheroids to yield larger spheroids. μ_2 , being a subpopulation between μ_1 and μ_3 , represented a region of intermediates which existed transiently and had unclear size trends during spheronization.

3. Relationship between size and roundness of ES spheroids

Within a single population of spheroids, the relationship between size and roundness was not constant during spheronization. The R value for ECD against roundness and its significance varied during spheronization (Table 15). When ECD was correlated against e_R , PS or C, a negative R value indicated that smaller spheroids were rounder. Likewise, when ECD was correlated against AR, a positive R value showed that smaller spheroids were rounder.

Table 15. Correlation coefficient (R) of roundness against ECD of ESC(TS) spheroids.

Batch	Sampling time (min)	Correlation coefficient (R)							
		e_R	P value	AR	P value	PS	P value	C	P value
1ESC(TS)2	2	-0.033	0.406	0.035	0.382	0.013	0.748	-0.068	0.088
1ESC(TS)4	4	-0.170*	0.000	0.173*	0.000	-0.121*	0.002	-0.189*	0.000
1ESC(TS)6	6	-0.298*	0.000	0.290*	0.000	-0.265*	0.000	-0.234*	0.000
1ESC(TS)8	8	-0.352*	0.000	0.324*	0.000	-0.249*	0.000	-0.123*	0.002
1ESC(TS)10	10	-0.261*	0.000	0.281*	0.000	-0.206*	0.000	-0.137*	0.001
2ESC(TS)2	2	-0.097	0.016	0.093	0.019	-0.043	0.285	-0.172*	0.000
2ESC(TS)4	4	-0.138*	0.001	0.152*	0.000	-0.068	0.088	-0.125*	0.002
2ESC(TS)6	6	-0.205*	0.000	0.195*	0.000	-0.133*	0.001	-0.129*	0.001
2ESC(TS)8	8	-0.317*	0.000	0.313*	0.000	-0.242*	0.000	-0.108*	0.007
2ESC(TS)10	10	-0.267*	0.000	0.303*	0.000	-0.254*	0.000	-0.068	0.090
3ESC(TS)2	2	0.040	0.317	-0.034	0.401	0.109	0.006	-0.033	0.417
3ESC(TS)4	4	-0.053	0.184	0.045	0.258	-0.037*	0.355	-0.137*	0.001
3ESC(TS)6	6	-0.261*	0.000	0.254*	0.000	-0.203*	0.000	-0.186*	0.000
3ESC(TS)8	8	-0.382*	0.000	0.402*	0.000	-0.309*	0.000	-0.228*	0.000
3ESC(TS)10	10	-0.361*	0.000	0.368*	0.000	-0.261*	0.000	-0.175*	0.000

* denotes statistical significances at $P \leq 0.05$.

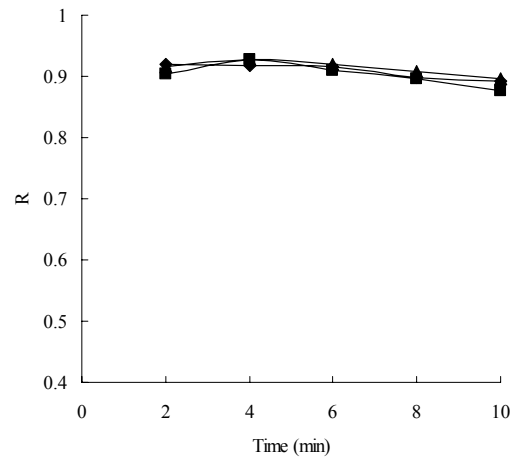
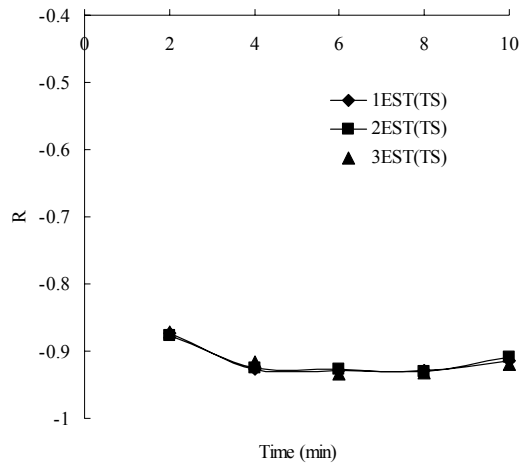
R values of ESC(TS)₂ spheroids were generally small and statistically insignificant, indicating that at the start of spheronization run, spheroid size was not related to its degree of sphericity. With increasing spheronization duration, the R values generally increased in magnitude, indicating that smaller spheroids were rounder within the population. For spheroids to be rounded, spheroid surface should be plastic, allowing remodelling of the circumferential shape during spheronization. These forces which remodelled spheroid shape could be from: collision between spheroids, collision between spheroids and spheronizer wall or collision between spheroid and both spheronizer wall and spheronizer base frictional plate. The degree of spheroid remodelling would also depend on the mass and velocity of spheroids during spheronization. Therefore, the combination of highly plastic surfaces, large mass and high velocity would favor the occurrence of highly spherical spheroids. On the other hand, smaller spheroids were rounder as mentioned above. Smaller spheroids with their lower mass would not be expected to be rounder unless they had higher velocities or greater surface plasticity. Tendency for spheroids to coalesce with one another would be higher with greater surface plasticity (Wan et al., 1993). μ_3 spheroids, being the subpopulation which did not increase in size during spheronization, were of lower roundness, suggested that μ_3 spheroids were less plastic and resisted coalescence and roundening. There may even be attritive breakdown of the outer surfaces. In contrast, the μ_1 spheroids increased in size as spheronization progressed, along with higher degree roundness due to their greater surface plasticity.

3.1. Sensitivity of roundness descriptors in characterizing spheronization

As mentioned earlier, all roundness descriptors, namely e_R , PS, AR and C, showed significance in LSD post hoc test, demonstrating that spheroids were indeed significantly rounder after 10 min of spheronization (Table 11). Qualitatively, roundness descriptors had also shown trends of increasing spheroid roundness with increasing residence time during spheronization. However, the practical usefulness of these roundness descriptors should be to quantify any change in spheroid roundness throughout the spheronization process. In this study, the ability of roundness descriptors to quantify changes in roundness for every 2 min of spheronization was tested. Using statistical analysis, e_R , PS and AR showed significant improvement in roundness at every 2 min interval during spheronization. C indicated that spheroids were rounder up to 6 min into spheronization. After the 6th min, C generally could not significantly represent improvement in roundness (Table 11). e_R , AR and PS appeared as sensitive roundness descriptors which were able to detect and represent improvement in roundness throughout spheronization. In comparison, the inability of C to detect subtle improvement in roundness toward the end of spheronization made C a questionable roundness descriptor for quantifying spheroid shape changes for ES processes.

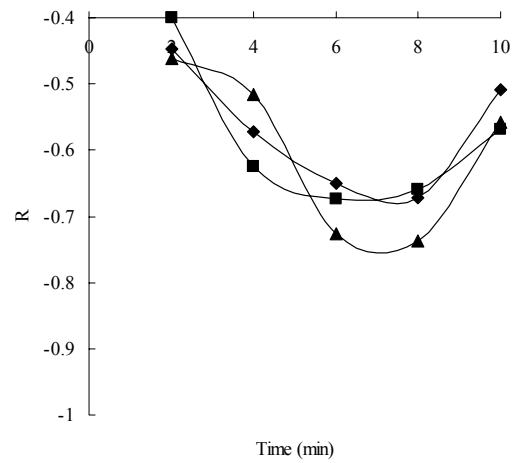
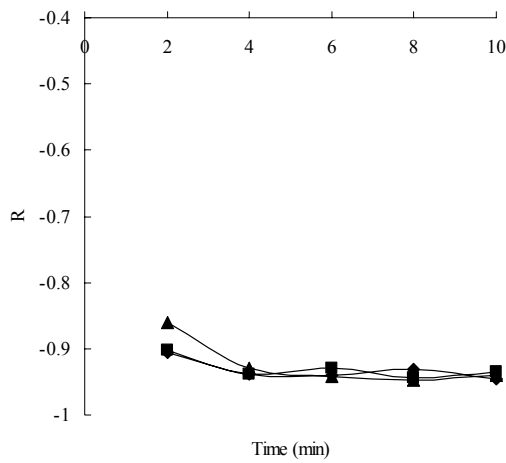
3.2. Correlation between roundness descriptors

Correlation analysis of e_R , PS, AR and C values were carried out for all ESC(TS) spheroids. R values for ESC(TS)'s e_R -PS, e_R -AR, PS-AR correlation were high at approximately 0.9 (Figure 9). From a practical perspective where good quality



a) PS-AR

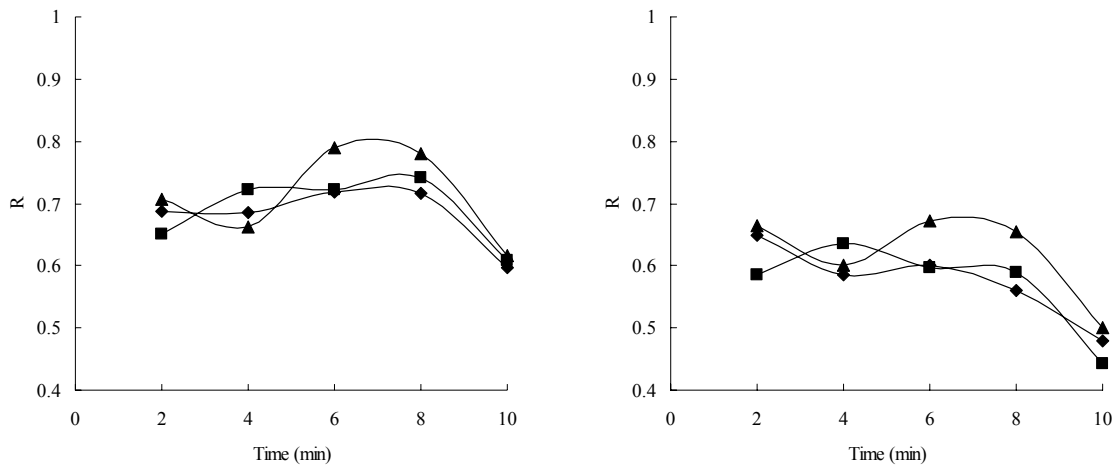
b) e_R -AR



c) e_R -PS

d) C-AR

Figure 9. R values of correlations among roundness descriptors for ESC(TS) spheroids. a) PS-AR, b) e_R -AR, c) e_R -PS, d) C-AR, e) C-PS, and f) C- e_R . All R values are significant at $P \leq 0.05$.



e) C-PS

f) C- e_R

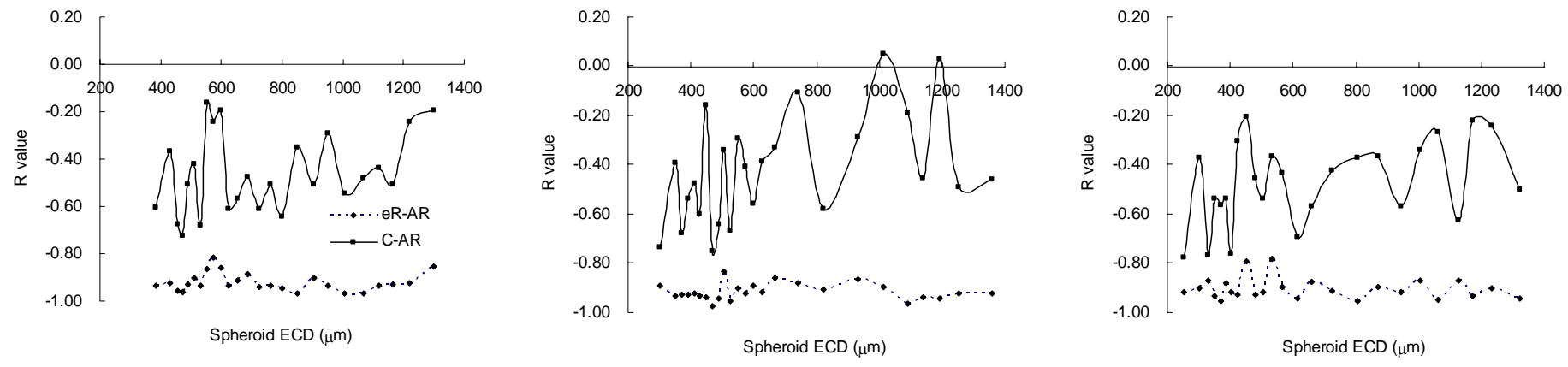
Figure 9 (Continued). R values of correlations among roundness descriptors for ESC(TS) spheroids. a) PS-AR, b) e_R -AR, c) e_R -PS, d) C-AR, e) C-PS, and f) C- e_R . All R values are significant at $P \leq 0.05$.

spheroids were generally produced, e_R , PS and AR could be used interchangeably to chart changes in spheroid shape during spheronization. Interestingly, R values for ESC(TS) C- e_R , C-PS and C-AR correlations ranged approximately from 0.4-0.8. R values of PS-AR, e_R -AR, and e_R -PS correlations in Figure 9 varied linearly with duration of spheronization. In contrast, R values of C-AR, C-PS and C- e_R correlations showed trend containing maxima or minima at the 6th -8th min of spheronization. R values of e_R -AR ranged from -0.85 to -0.95, representing a highly correlated pair. In contrast, R values of C-AR ranged from -0.4 to -0.78, representing a variably correlated pair, depending on duration of spheronization. e_R -AR and C-AR represented extreme values and therefore the relationship of the R values of e_R -AR and C-AR correlations were examined in greater detail.

3.3. Shape heterogeneity within ES spheroid population during spheroid formation

Using data from image analysis, 625 spheroids from every ESC(TS) sample were divided into 25 equal intervals according to their individual ECD. Within each interval, R values for e_R -AR and C-AR correlations were computed and plotted accordingly as shown in Figure 10.

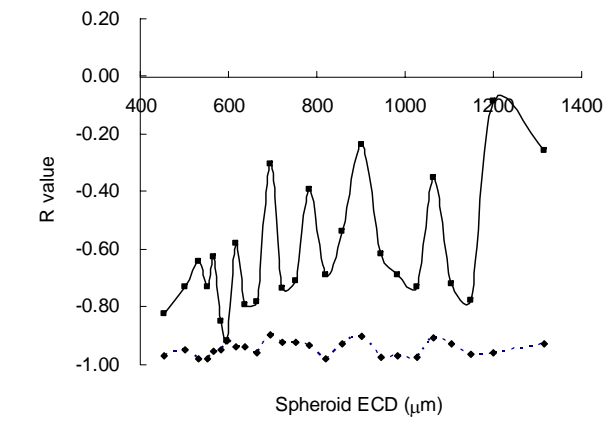
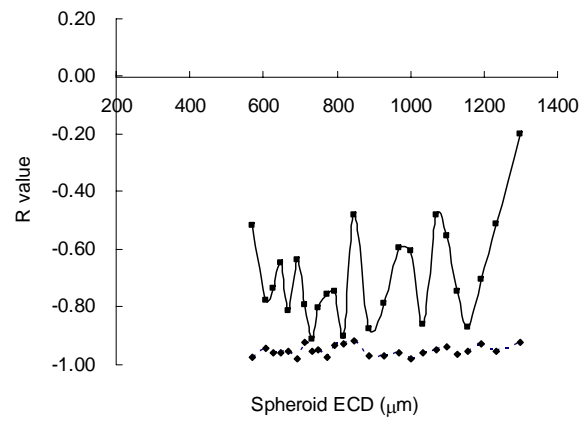
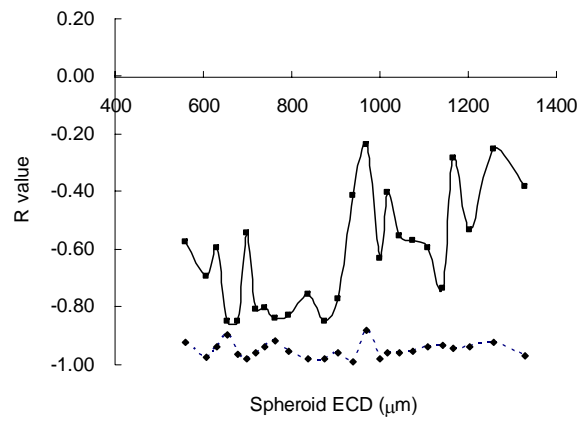
All ESC(TS) batches showed that intra lot R values of e_R -AR correlations were similar. The intra lot R values of e_R -AR correlations did not vary with spheroid size within any ESC(TS) batch. In contrast, the intra lot R values of C-AR correlations were related to spheroid size. The intra lot R values of C-AR correlations fluctuated greatly with increasing spheroid size and there was an observable trend of bigger spheroid having larger (less negative) R values. As spheronization progressed, ESC(TS)6-10 spheroids showed distinctly that smaller spheroids had larger intra lot R values of C-AR correlations. The intra lot R values of C-AR correlations of ESC(TS)6-10 spheroids did not vary proportionally with increasing spheroid diameter. The intra lot R values generally took 2 extremes; R values at below 900 μm fluctuated greatly but were generally larger, whereas R values above 900 μm were more consistent and generally smaller. Comparing the MG distribution representation for spheroid size distribution (Figure 8) and Figure 10 of ESC(TS)6-10, the region where the intra lot R values of C-AR correlations fluctuated coincided with spheroids which belonged to α_1 of respective MG distributions. Apart from showing heterogeneity in



1ESC(TS)2

2ESC(TS)2

3ESC(TS)2



1ESC(TS)4

2ESC(TS)4

3ESC(TS)4

Figure 10. Intra lot R values of AR-e_R and C-AR correlations against ECD of spheroids (μm).

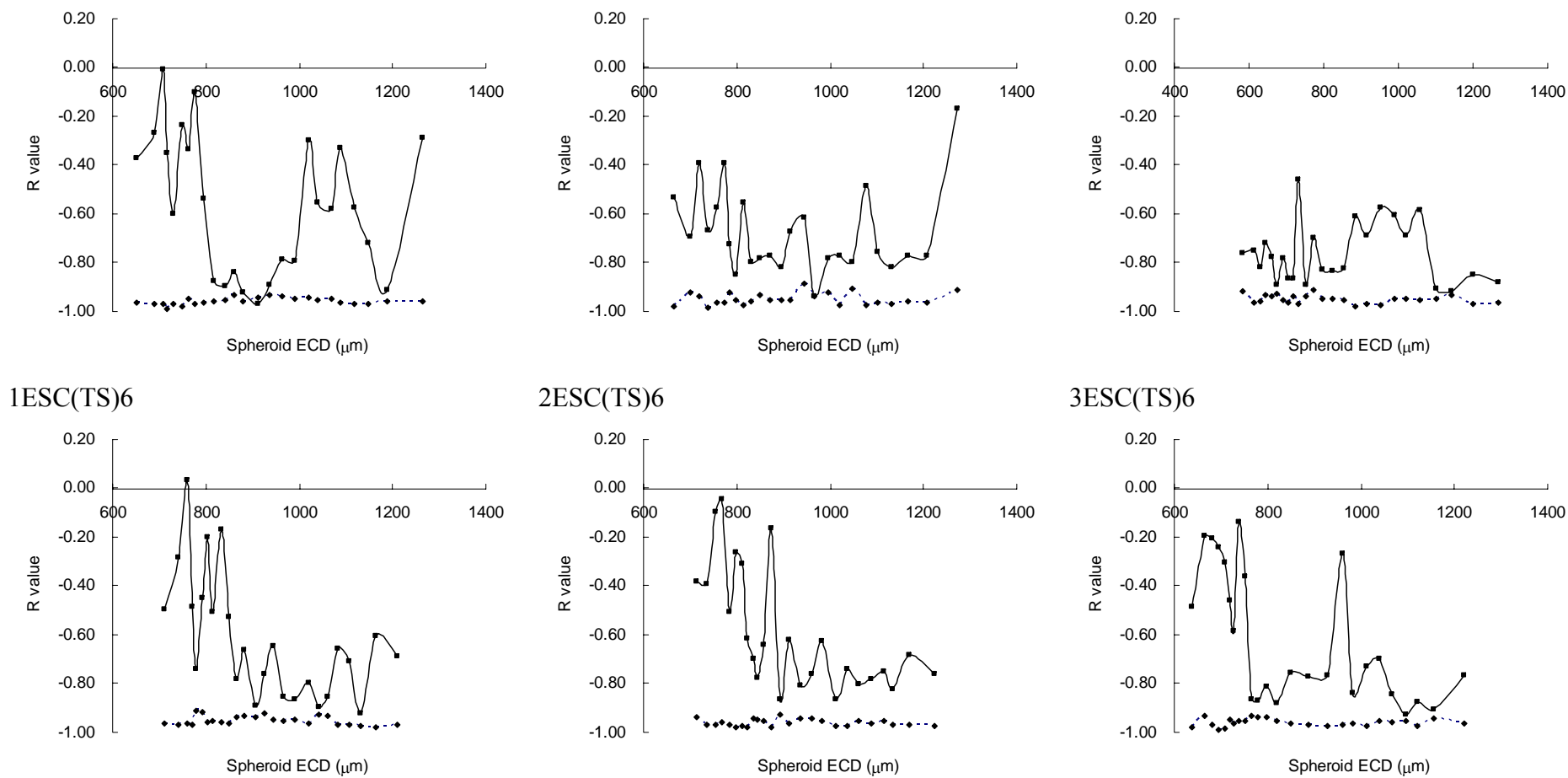
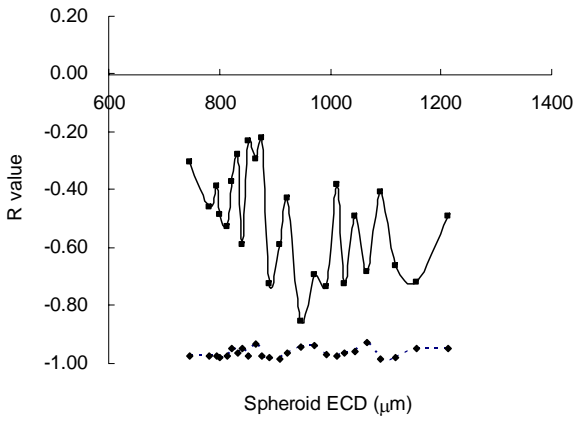
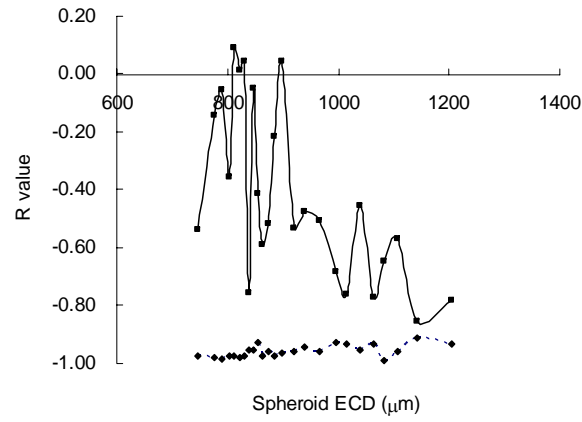


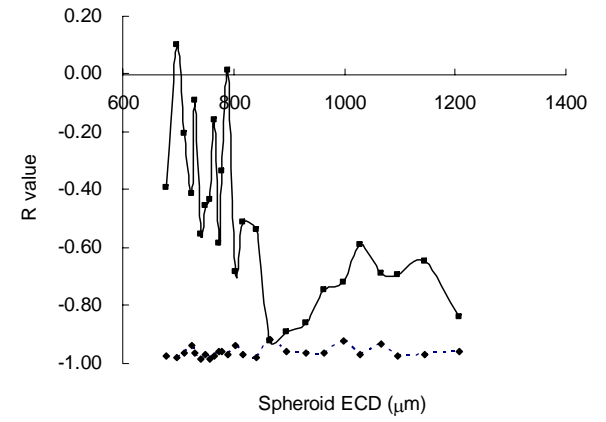
Figure 10 (Continued). Intra lot R values of AR- e_R and C-AR correlations against ECD of spheroids (μm).



1ESC(TS)10



2ESC(TS)10



3ESC(TS)10

Figure 10 (Continued). Intra lot R values of AR- e_R and C-AR correlations against ECD of spheroids (μm).

size within a batch of spheroid population, MG distribution could suggest heterogeneity in shape of spheroids within a spheroid population if evaluated with intra lot R values of C-AR correlations.

3.4. Novel method in spheroid shape analysis

Figures 4 and theories on spheroid formation (Rowe, 1985, Baert and Remon, 1993) suggested that spheroids could possibly assume the following 2 dimensional shapes after 2-10 min of spheronization:

1. Circle - An ideal spheroid shape for comparison.
2. Ellipse - A distorted circle which could assume perfect circularity with sufficient roundening.
3. Oval – A possible resultant shape if 2 round spheroids collided and resulted in abrasion transfer of material.
4. Rectangle with rounded corners (RRC) - A fragmented extrudate with edges rounded.
5. Rectangle with rounded ends (RRE) – RRC could be further attrited at both ends to yield RRE. A dumbbell could become a RRE if its bi-concave surfaces were flattened.
6. Dumbbell - Spheroid formation theory (Baert and Remon, 1993) suggested that stretching of extrudates would occur during spheronization, forming dumbbell shaped aggregates.

In consideration of the likely spheroids shapes proposed by the theories, these shapes should be artificially simulated and compared with empirical observations to verify the validity of the theories. Therefore the possible shapes of spheroids were drawn, image analyzed and results tabulated in Table 16.

In order to generate a series of simulated images, ellipse, oval and RRE were stretched along their length with AR of respective shape increasing in a predictable manner, from 1.05 to 2. Altogether 20 images were generated and analyzed for each of the shape (ellipse, oval and RRE). Only circle and selected images of ellipse, oval and RRE are included in Table 16.

e_R , C and PS decreased when the length of ellipse, oval and rectangle were increased. However, among the 3 descriptors, e_R decreased with greatest magnitude as the shapes were increasingly distorted while C decreased with the smallest magnitude. This supported the early findings when concluded that shape data obtained from ESC(TS) spheroids (Figure 7) demonstrated that e_R , AR and PS, unlike C, were able to show significant improvement in spheroid roundness with increasing spheronization duration. The minimal numerical change in C in Table 11 suggested that C was less sensitive and less critical as roundness descriptor for spheroids.

Table 16. Roundness values for different shapes.























Shape		e_R	AR	PS	C
Circle		0.990	1.000	1.002	1.010
Ellipse		0.693	1.051	0.962	1.012
		0.440	1.250	0.810	0.991
		0.301	1.500	0.673	0.950
		0.218	1.750	0.576	0.899
		0.148	2.000	0.504	0.847
Oval		0.694	1.050	0.961	1.009
		1.252	0.802	0.990	0.429
		0.287	1.504	0.678	0.935
		0.198	1.748	0.575	0.883
		0.131	2.000	0.505	0.823

Table 16 (Continued). Roundness values for different shapes.

Shape		e_R	AR	PS	C
RRE		0.694	1.050	0.977	1.009
		0.423	1.252	0.858	0.990
		0.298	1.496	0.737	0.951
		0.218	1.741	0.648	0.904
		2.000	0.572	0.854	0.143
RRC		0.080	2.000	0.550	0.750
		0.109	2.000	0.577	0.794
		0.124	2.000	0.586	0.829
Dumbbell		0.127	1.985	0.537	0.787
		0.120	1.985	0.525	0.753
		0.080	1.985	0.517	0.717

Roundness values of the 20 images each of ellipse, oval and RRE were correlated with one another and tabulated in Table 17. Using the same data, a plot was also

obtained (Figure 11). All roundness descriptors were highly correlated ($|R| \geq 0.9$) with one another for the three shapes (Table 17). If the roundness descriptors of spheroids were correlated in the same manner and $|R| \geq 0.9$, it indicated that all spheroids would have similar shapes, either ellipse, oval or RRE. However, the observed R values from the simulated images were not exactly similar to the R values obtained from actual spheroid images (Figure 9 and Table 17).

Table 17. Correlation between roundness descriptors for ellipse, oval and RRE.

Correlated roundness descriptors	Correlation coefficient (R)		
	Ellipse	Oval	RRE
PS-AR	-0.985	-0.985	-0.990
e_R -AR	-0.956	-0.953	-0.948
e_R -PS	0.990	0.989	0.980
C-AR	-0.994	-0.995	-0.994
C-PS	0.961	0.966	0.971
C- e_R	0.920	0.922	0.911

All R values are statistical significant at $P \leq 0.05$.

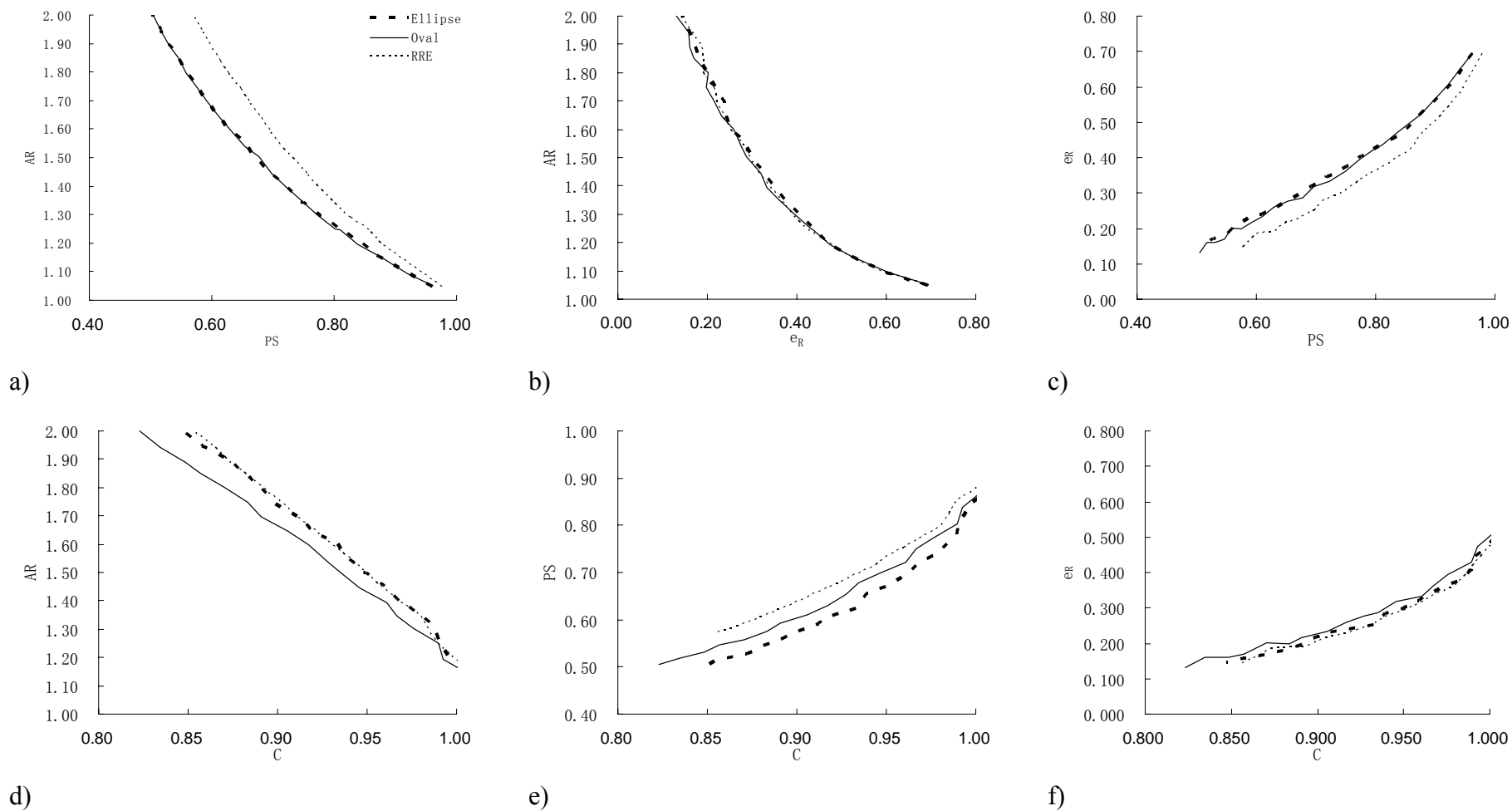


Figure 11. e_R , AR, PS, C of simulated images plotted against one another.

Figure 11 shows the relationship between the different roundness descriptors obtained for the different shapes. In an ideal scenario, a spheroid which is elliptical would have a coordinate along the line representing an ellipse as in Figure 11. Likewise, a spheroid assuming an oval shape would be represented by a coordinate along the “oval” line. An area would be bounded by the “oval” and “ellipse” lines. This area constitutes a region where the shape would be irregular and possesses characteristics of both oval and ellipse. Similarly, an area could also be bound by “RRE”, “oval” or “ellipse” lines. In Figure 11, the 2 features to observe for each plot would be the overlap of lines and the size of the area bound by the lines. In figures where the lines overlap, if a coordinate lies on the lines, the graph would be unable to distinguish which shape the coordinate represents. If lines were far apart, the area bound by the lines would be bigger, indicating that the graphs would be more definitive in distinguishing between shapes. In Figures 11a and 11c, the plots show that oval and ellipse lines overlapped each other. Figure 11b shows that all 3 shape lines overlapped with one another. In contrast, all 3 shape lines in Figure 11e do not cross over one another. In Figure 11f, ellipse and RRE lines overlapped, with the oval line running nearby but not overlapping. Figure 11a shows that the ellipse and RRE lines overlapped each other. On the sizes of areas bounded by the lines, Figures 11a, 11c, 11d and 11e show that areas enclosed were relatively similar. The bound area in Figure 11f, in comparison, was distinctly smaller. Due to the overlap of all the shape lines with minimal bound area for Figure 11b, shapes of the spheroids present were either ellipse, oval or RRE. AR and e_R of spheroids would be expected to be highly

correlated. This is shown in Figure 9b with R values approximately 0.9. Figures 11a and 11c could differentiate ellipse and oval from RRE but not between ellipse and oval. In contrast, Figure 11d could differentiate ellipse and RRE from oval but not between ellipse and RRE. Figure 11e plot could differentiate all three shapes.

3.4.1. Predominant spheroid shape during spheronization

Spheroids with roundness coordinates scattered within the area bound by the shape lines would result in low R values when these coordinates were correlated. ESC(TS)

R values of AR-PS, AR- e_R , and e_R -PS correlations were high (≈ 0.9) in Figure 9.

When Figures 11a and 11c were evaluated together with high R values in Figure 9a-c,

it indicated that throughout spheronization, the likely spheroid shape was either

ellipse or oval, not RRE. The smaller R values in Figure 9d, in relation to the

observation with Figure 11d suggested that spheroid shape would be (i) ellipse or

RRE and (ii) oval. If Figures 9a-d were to be evaluated together with Figure 11, it

indicated that during spheronization, the predominant spheroid shapes was not RRE.

Instead, the shape was likely to have characteristics of oval and ellipse. The maxima

or minima in R values of Figures 9d-f suggested that at 6-8 min, ESC(TS) spheroids

were of similar shape, possibly RRE or ellipse. Since the presence of RRE was ruled

out, the likely predominant spheroid shape would be ellipse for ESC(TS)6 and

ESC(TS)8 batches.

Figure 11 does not include lines representing RRC and dumbbells. However, from the C and e_R values shown in Table 16, effects of RRC and dumbbells on RRE line in C-AR and AR- e_R plots could be estimated. RRC with increasing sharp corners and increasing biconcave dumbbells would cause RRE line in Figure 11d to shift towards the left. With AR- e_R plot, RRC would cause the RRE line in Figure 11b to deviate away from the oval and ellipse lines. The presence of RRC or dumbbells in the spheroid population would therefore have mixed effects on the R values of AR-C correlation. However, presence of RRC or dumbbells in spheroid population would cause the R values of AR- e_R correlation to decrease.

The concept of spheroid shape analysis using R values of C-AR plot was applied again in Figure 10 to demonstrate intra batch spheroid shape variations during spheronization. Apart from the heterogeneity suggested by variations in intra batch R values and MG distribution, the R values demonstrated that changes in spheroid shape depended on the spheroid size and duration of spheronization. R values of ESC(TS)2 batches were generally less negative, with high variability across different spheroid sizes, indicating that at any size, spheroids did not exist with a consistent or predominant shape (Figure 10). The consistency in shape versus size for spheroids changed with the increasing duration of spheronization. ESC(TS)8 and ESC(TS)10 batches showed that spheroids were generally larger than 900 μm and had average R values which were more negative but with less variability, indicating that larger spheroids were similar in shape with one another (Figure 10). In comparison,

ESC(TS)8 and ESC(TS)10 spheroids with ECD smaller than 900 μm had average R values which were less negative but with higher variability. This indicated that with increasing spheronization duration, smaller spheroids maintained less negative and more variable R values while larger spheroids assumed more negative but consistent R values. With indication that smaller spheroids had greater shape variation, it would be likely that mass transfer and remodelling were predominantly active among smaller spheroids toward the end of spheronization.

4. Controlled spheroid agglomeration in rotary processor

Upon completion of spheroid formation in the rotary processor, the spheroids were rotated in the processor for an extended period. During that period, additional amount of water termed “AGL” was sprayed onto spheroids with the intention of inducing physical changes on spheroid surfaces and controlling spheroid agglomeration. The size, size distribution, surface roughness, roundness of spheroids during agglomeration and yield were evaluated.

During RP, spheroids were expected to lose moisture with increasing processing duration. After RP, all RT(SR)20 batches had about 31 %w/w moisture remaining in the spheroids (Figure 12). As expected, RT(SR)50 spheroids had the least amount moisture left in the spheroids. Higher AGL spray rate increased the remaining amount of moisture in the spheroids. When AGL was added at 4 ml/min, the amount of

moisture remaining in spheroids at the end of the process run was approximately 31 %w/w, indicating that amount of moisture gained and lost by spheroids had reached equilibrium (Figure 12). RT(SR6)50 spheroids had a net gain in moisture content with AGL spray rate at 6 ml/min.

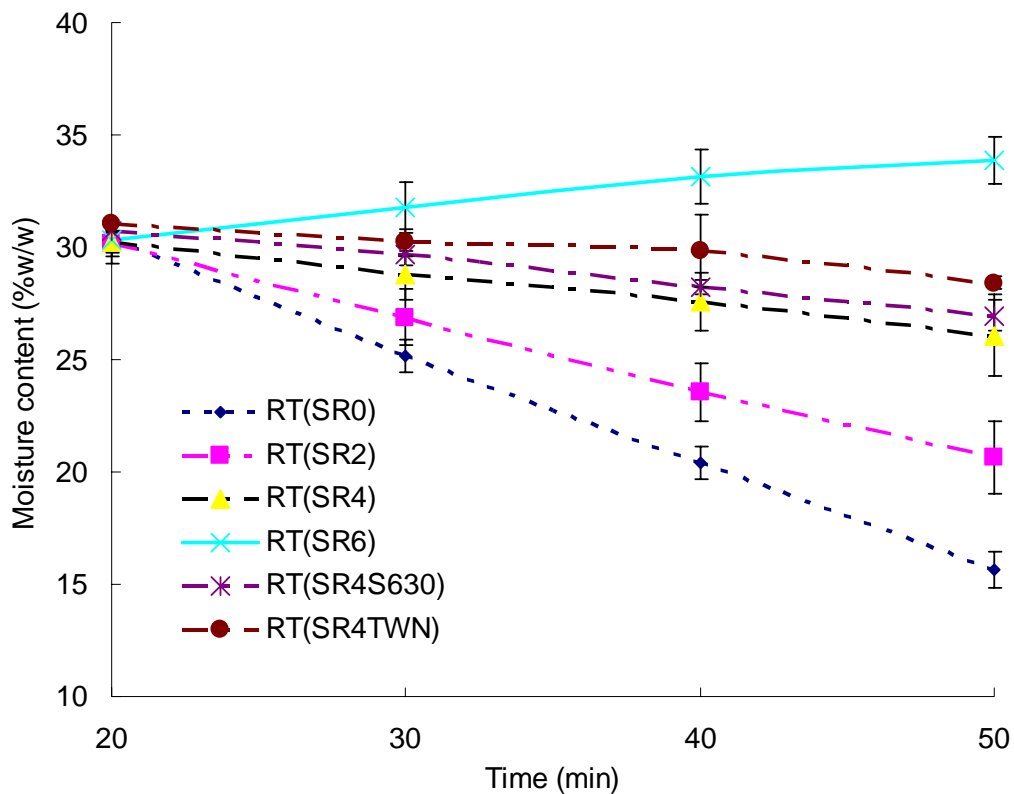


Figure 12. Moisture content of RT(SR) spheroids during RP. Error bars represent standard deviations.

Addition of AGL was expected to affect the plasticity and rigidity of the spheroid surface, if not that of entire spheroid. The interrelated nature of plasticity and rigidity with roundness and agglomeration suggested that the addition of AGL would affect the roundness and size of the resultant spheroids. Size and size distribution of

spheroids with the least amount of moisture remaining (RT(SR50)) were analyzed by sieving and results presented in Table 18.

Table 18. Size and size distribution of RT(SR) spheroids as characterized by sieving.

Batch	Dwgeo (mm)	SDwgeo	Dwarith (mm)	SDwarith	Dwmed (mm)	Spanw
RT(SR0)50	1.006 (0.081)	1.189 (0.019)	1.024 (0.080)	1.051 (0.078)	0.898 (0.088)	0.244 (0.017)
RT(SR2)50	0.933 (0.117)	1.200 (0.029)	0.951 (0.116)	0.980 (0.113)	0.828 (0.100)	0.294 (0.035)
RT(SR4)50	0.955 (0.200)	1.197 (0.027)	0.974 (0.201)	1.004 (0.200)	0.847 (0.185)	0.314 (0.011)
RT(SR6)50	1.013 (0.164)	1.181 (0.011)	1.029 (0.167)	1.051 (0.170)	0.925 (0.151)	0.294 (0.018)
RT(SR4S630)50	1.097 (0.065)	1.185 (0.021)	1.114 (0.061)	1.140 (0.052)	0.985 (0.057)	0.300 (0.003)
RT(SR4TWN)50	1.076 (0.128)	1.182 (0.007)	1.095 (0.130)	1.121 (0.132)	0.960 (0.120)	0.301 (0.014)

Values are mean with standard deviations in parentheses.

Size analysis of RT(SR) spheroids using sieves did not demonstrate any significant changes in the size and size distribution of spheroids with increasing rate of AGL addition nor with the inclusion of S630 or Tween 80 in AGL (Table 19). One exception was that Spanw of RT(SR0)50 was significantly smaller, as indicated by the LSD post hoc test (Table 19). Since SDwgeo and SDwarith of RT(SR0)50 were not significantly different from the rest of the RT(SR)50 batches, the presence of AGL could not be attributed to cause a widening in the size distribution of spheroids.

Table 19 One way ANOVA of size and size distribution of RT(SR) spheroids.

Size and size distribution descriptors	P value for one way ANOVA
Dwgeo (mm)	0.756
SDwgeo	0.847
Dwarith (mm)	0.765
SDwarith	0.781
Dwmed (mm)	0.724
Spanw	0.027*

* denotes statistical significance at $P \leq 0.05$.

4.1. Representation of RP spheroids with MG distribution

Size distribution of RT(SR) spheroids did not significantly fit a normal or log normal distribution (Table 20). Instead, the size distribution of RT(SR) spheroids fitted significantly to MG distribution (Table 20). This finding was similar to that found for ESC(TS) spheroids. Size distribution of the majority of the RT(SR) batches could be best fitted to 4cMG or 3cMG, followed by 2cMG distribution. Although RT(SR) batches best fitted a 4cMG distribution with 56 out of 64 batches having P value greater than 0.05, RT(SR) batches would instead be approximated to a 3cMG for reasons similar to those of ESC(TS) batches; i.e. to achieve a balance between absolute closest in fitting and simplicity in mathematical equation for practical understanding.

Table 20. P values for Chi square curves fitting of size distribution of RT(SR) spheroids to statistical distributions.

Batch	Distribution				
	Normal	Log normal	2cMG	3cMG	4cMG
1RT(SR0)20	0.000*	0.000*	0.648	0.882	0.981
1RT(SR0)30	0.000*	0.000*	0.919	0.943	0.990
1RT(SR0)40	0.000*	0.000*	0.872	0.906	0.907
1RT(SR0)50	0.000*	0.000*	0.436	0.677	0.679
2RT(SR0)20	0.000*	0.000*	0.180	0.702	0.726
2RT(SR0)30	0.000*	0.000*	0.182	0.377	0.472
2RT(SR0)40	0.000*	0.000*	0.872	0.917	0.923
2RT(SR0)50	0.000*	0.000*	0.379	0.327	0.267
3RT(SR0)20	0.000*	0.000*	0.029*	0.735	0.843
3RT(SR0)30	0.000*	0.000*	0.249	0.474	0.485
3RT(SR0)40	0.000*	0.000*	0.212	0.240	0.358
3RT(SR0)50	0.000*	0.000*	0.000*	0.000*	0.000*
1RT(SR2)20	0.000*	0.000*	0.570	0.755	0.769
1RT(SR2)30	0.000*	0.000*	0.276	0.566	0.568
1RT(SR2)40	0.000*	0.000*	0.407	0.424	0.891
1RT(SR2)50	0.000*	0.000*	0.570	0.527	0.557
2RT(SR2)20	0.000*	0.000*	0.242	0.539	0.849
2RT(SR2)30	0.000*	0.000*	0.457	0.800	0.926
2RT(SR2)40	0.000*	0.000*	0.010*	0.038*	0.051
2RT(SR2)50	0.000*	0.000*	0.003*	0.001*	0.002*
3RT(SR2)20	0.000*	0.000*	0.793	0.860	0.925
3RT(SR2)30	0.000*	0.000*	0.000*	0.000*	0.000*
3RT(SR2)40	0.000*	0.000*	0.985	0.994	0.995
3RT(SR2)50	0.000*	0.000*	0.074	0.138	0.125

* denotes statistical significance at $P \leq 0.05$.

Table 20 (Continued). P values for Chi square curves fitting of size distribution of RT(SR) spheroids to statistical distributions.

Batch	Distribution				
	Normal	Log normal	2cMG	3cMG	4cMG
1RT(SR4)20	0.000*	0.000*	0.038*	0.770	0.895
1RT(SR4)30	0.000*	0.000*	0.183	0.452	0.444
1RT(SR4)40	0.000*	0.000*	0.354	0.521	0.610
1RT(SR4)50	0.000*	0.000*	0.045*	0.063	0.040*
2RT(SR4)20	0.000*	0.000*	0.040*	0.310	0.580
2RT(SR4)30	0.000*	0.000*	0.129	0.277	0.517
2RT(SR4)40	0.000*	0.000*	0.003*	0.024*	0.139
2RT(SR4)50	0.000*	0.000*	0.183	0.468	0.698
3RT(SR4)20	0.000*	0.000*	0.331	0.834	0.821
3RT(SR4)30	0.000*	0.000*	0.096	0.104	0.126
3RT(SR4)40	0.000*	0.000*	0.378	0.650	0.614
3RT(SR4)50	0.000*	0.000*	0.105	0.173	0.162
1RT(SR6)20	0.000*	0.000*	0.351	0.946	0.991
1RT(SR6)30	0.000*	0.000*	0.294	0.721	0.840
1RT(SR6)40	0.000*	0.000*	0.152	0.655	0.708
1RT(SR6)50	0.000*	0.000*	0.062	0.671	0.740
2RT(SR6)20	0.000*	0.000*	0.003*	0.029*	0.047*
2RT(SR6)30	0.000*	0.000*	0.894	0.957	0.957
2RT(SR6)40	0.000*	0.000*	0.000*	0.074	0.082
2RT(SR6)50	0.000*	0.000*	0.006*	0.127	0.188
3RT(SR6)20	0.000*	0.000*	0.000*	0.000*	0.000*
3RT(SR6)30	0.000*	0.000*	0.077	0.225	0.223
3RT(SR6)40	0.000*	0.000*	0.027*	0.027*	0.053
3RT(SR6)50	0.003*	0.012*	0.021*	0.748	0.991

* denotes statistical significance at $P \leq 0.05$.

Table 20 (Continued). P values for Chi square curves fitting of size distribution of RT(SR) spheroids to statistical distributions.

Batch	Distribution				
	Normal	Log normal	2cMG	3cMG	4cMG
1RT(SR4S630)20	0.000*	0.000*	0.005*	0.213	0.465
1RT(SR4S630)30	0.000*	0.000*	0.056	0.126	0.226
1RT(SR4S630)40	0.000*	0.000*	0.052	0.143	0.264
1RT(SR4S630)50	0.000*	0.000*	0.130	0.334	0.328
2RT(SR4S630)20	0.000*	0.000*	0.335	0.390	0.651
2RT(SR4S630)30	0.000*	0.000*	0.002*	0.069	0.105
2RT(SR4S630)40	0.000*	0.000*	0.643	0.751	0.749
2RT(SR4S630)50	0.000*	0.000*	0.373	0.407	0.414
1RT(SR4TWN)20	0.000*	0.000*	0.054	0.179	0.543
1RT(SR4TWN)30	0.000*	0.000*	0.000*	0.000*	0.000*
1RT(SR4TWN)40	0.000*	0.000*	0.058	0.456	0.449
1RT(SR4TWN)50	0.000*	0.000*	0.000*	0.000*	0.000*
2RT(SR4TWN)20	0.000*	0.000*	0.269	0.308	0.330
2RT(SR4TWN)30	0.000*	0.000*	0.018*	0.042*	0.057
2RT(SR4TWN)40	0.000*	0.000*	0.030*	0.100	0.113
2RT(SR4TWN)50	0.000*	0.000*	0.626	0.904	0.932

* denotes statistical significance at $P \leq 0.05$.

4.2. Effects of AGL on spheroid size

Paired T test was carried out on DI of RT(SR)20 and RT(SR)50 batches to investigate the effects of AGL. DI of RT(SR) batches demonstrated that with sufficiently high rate of AGL addition, spheroid increased in size (Figure 13). This observation was similar to the reported work in Wan et al.'s (1994) study which related high spray rate to production of larger spheroids. As a control, DI of RT(SR0) did not significantly increase with prolonged spherization. RT(SR6) demonstrated that with sufficiently high rate of AGL addition and prolonged spherization, spheroids continued to

increase in size. At moderate rate of AGL addition, the results were not conclusive to prove any size changes for RT(SR2) or RT(SR4) batches.

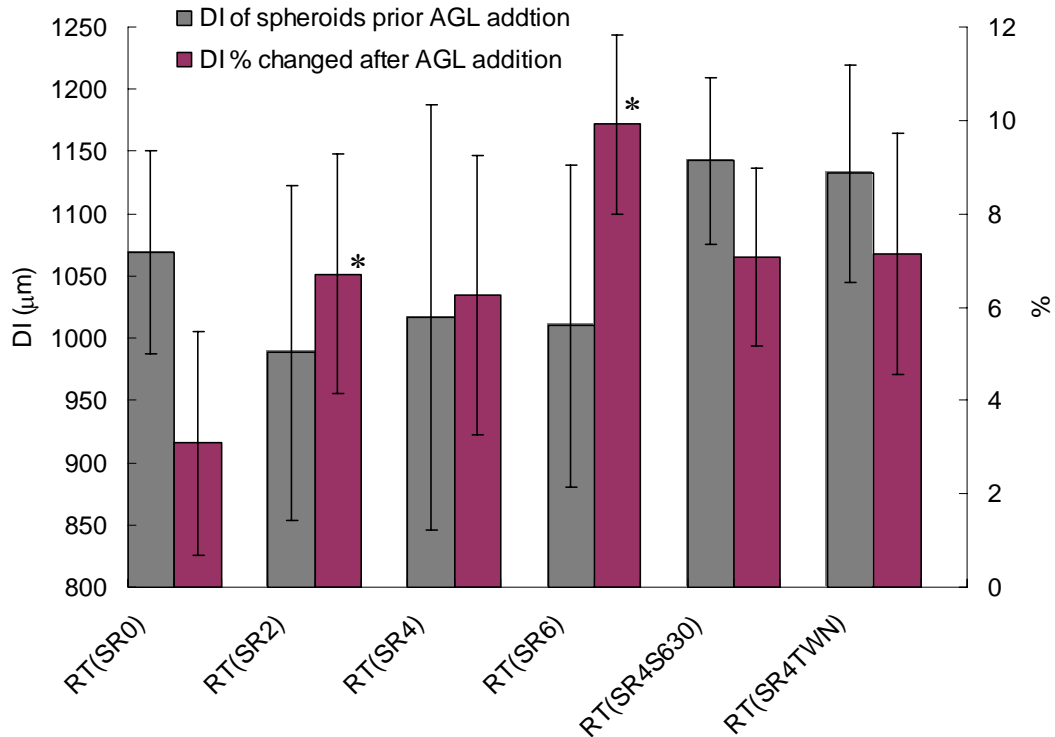


Figure 13. Average DI of RT(SR)20 batches and respective DI % changed after AGL addition.

Error bars represent standard deviation. * denotes statistical significant increase in DI after processing.

Low AGL spray rates were used to examine the possibility of inducing changes in spheroid morphology without causing spheroid growth or agglomeration, and consequently size increase. Apart from performing paired T test on DI, paired T test was also carried out on μ_1 to validate any spheroid size increase with the addition of AGL. Without AGL, μ_1 of RT(SR0) had significant increase with prolonged spherization (Table 21).

Table 21. Size distribution of RT(SR) spheroids as defined by 3cMG distribution.

Batch	α_1	μ_1 (μm)	σ_1	α_2	μ_2 (μm)	σ_2	α_3	μ_3 (μm)	σ_3
1RT(SR0)20*	0.229	956.6	26.60	0.527	968.5	60.51	0.245	1154.2	112.55
1RT(SR0)30	0.395	986.7	31.21	0.283	1016.6	40.14	0.323	1181.9	116.42
1RT(SR0)40	0.428	995.2	28.42	0.306	1001.6	46.23	0.266	1141.3	117.40
1RT(SR0)50	0.483	1003.0	29.19	0.272	1030.4	67.73	0.245	1240.5	113.37
2RT(SR0)20	0.558	1091.1	48.77	0.393	1221.1	99.85	0.049	1495.7	58.96
2RT(SR0)30	0.096	1113.3	14.79	0.527	1152.1	38.53	0.377	1243.8	125.39
2RT(SR0)40	0.260	1128.7	42.76	0.443	1160.3	35.48	0.297	1306.7	115.04
2RT(SR0)50	0.167	1139.3	44.65	0.453	1161.3	35.63	0.381	1253.1	139.18
3RT(SR0)20	0.389	933.4	33.67	0.461	1046.8	69.60	0.151	1249.6	65.62
3RT(SR0)30	0.066	986.7	8.36	0.576	983.8	45.40	0.358	1140.4	111.42
3RT(SR0)40	0.395	984.7	31.96	0.197	1001.0	58.92	0.408	1113.8	133.54
3RT(SR0)50	0.193	987.7	26.44	0.428	998.8	41.61	0.379	1121.5	167.53
1RT(SR2)20*	0.223	763.1	29.58	0.564	818.3	42.62	0.213	949.7	79.73
1RT(SR2)30	0.698	832.1	35.57	0.051	928.2	17.87	0.251	1028.2	93.96
1RT(SR2)40	0.395	826.1	24.08	0.239	864.8	24.81	0.366	961.9	100.69
1RT(SR2)50	0.299	846.1	25.26	0.327	857.8	43.70	0.374	1019.0	137.75

* denotes paired T test statistical significance at $P \leq 0.05$.

Table 21 (Continued). Size distribution of RT(SR) spheroids as defined by 3cMG distribution.

Batch	α_1	μ_1 (μm)	σ_1	α_2	μ_2 (μm)	σ_2	α_3	μ_3 (μm)	σ_3
2RT(SR2)20	0.252	948.9	33.02	0.470	1017.5	53.74	0.278	1200.6	101.50
2RT(SR2)30	0.554	1018.7	30.77	0.303	1073.4	76.20	0.143	1243.0	98.55
2RT(SR2)40	0.269	1029.5	42.92	0.426	1052.2	29.27	0.306	1189.4	115.60
2RT(SR2)50	0.263	1053.6	29.01	0.452	1057.4	44.21	0.285	1226.7	143.21
3RT(SR2)20	0.331	993.6	40.85	0.375	1048.8	50.31	0.294	1217.4	100.01
3RT(SR2)30	0.525	1063.2	40.33	0.206	1146.4	72.87	0.269	1233.5	161.06
3RT(SR2)40	0.261	1097.2	60.68	0.476	1099.0	37.26	0.263	1306.4	112.15
3RT(SR2)50	0.568	1102.9	47.33	0.091	1092.9	9.79	0.341	1208.8	158.95
1RT(SR4)20*	0.475	827.1	35.74	0.461	975.3	91.77	0.064	1226.4	58.38
1RT(SR4)30	0.437	867.6	28.73	0.339	900.6	55.17	0.225	1044.6	127.22
1RT(SR4)40	0.517	902.2	27.85	0.2968	937.4	72.89	0.186	1126.6	80.31
1RT(SR4)50	0.388	924.9	85.77	0.4752	924.1	28.18	0.137	1109.1	67.98
2RT(SR4)20	0.597	855.6	42.09	0.347	977.1	77.86	0.056	1174.6	68.00
2RT(SR4)30	0.476	893.0	29.59	0.380	955.9	69.80	0.143	1112.7	78.30
2RT(SR4)40	0.531	913.4	40.16	0.202	929.7	18.62	0.266	1077.8	107.92
2RT(SR4)50	0.304	939.5	51.59	0.436	934.4	23.06	0.259	1087.0	104.45

* denotes paired T test statistical significance at $P \leq 0.05$.

Table 21 (Continued). Size distribution of RT(SR) spheroids as defined by 3cMG distribution.

Batch	α_1	μ_1 (μm)	σ_1	α_2	μ_2 (μm)	σ_2	α_3	μ_3 (μm)	σ_3
3RT(SR4)20	0.572	1140.9	54.98	0.404	1296.4	112.53	0.024	1562.2	16.25
3RT(SR4)30	0.420	1186.2	45.31	0.352	1238.8	38.88	0.228	1395.3	93.36
3RT(SR4)40	0.361	1284.8	90.03	0.588	1264.4	48.91	0.051	1508.9	45.94
3RT(SR4)50	0.808	1299.6	72.10	0.109	1361.5	22.09	0.083	1511.3	76.73
1RT(SR6)20*	0.537	898.6	46.05	0.381	1054.6	93.52	0.082	1267.6	39.37
1RT(SR6)30	0.632	950.7	35.07	0.320	1055.1	92.97	0.048	1276.7	43.44
1RT(SR6)40	0.370	1011.1	65.25	0.478	1010.8	29.24	0.152	1233.4	78.68
1RT(SR6)50	0.255	971.4	43.59	0.622	1072.6	40.39	0.123	1235.5	62.01
2RT(SR6)20	0.596	829.9	41.77	0.323	950.0	74.70	0.081	1122.2	39.70
2RT(SR6)30	0.565	889.1	33.42	0.369	988.0	80.23	0.066	1154.5	50.79
2RT(SR6)40	0.118	861.4	33.69	0.588	934.4	31.73	0.294	1074.2	80.95
2RT(SR6)50	0.593	940.5	67.19	0.2132	987.6	25.90	0.194	1100.1	91.38
3RT(SR6)20	0.385	1050.2	36.38	0.279	1143.4	67.47	0.336	1265.0	154.44
3RT(SR6)30	0.552	1164.5	60.10	0.275	1168.3	31.64	0.174	1378.1	101.59
3RT(SR6)40	0.220	1160.0	56.19	0.698	1240.7	55.22	0.083	1430.6	72.23
3RT(SR6)50	0.314	1178.5	59.17	0.655	1323.1	60.63	0.031	1530.4	37.17

* denotes paired T test statistical significance at $P \leq 0.05$.

Table 21 (Continued). Size distribution of RT(SR) spheroids as defined by 3cMG distribution.

Batch	α_1	μ_1 (μm)	σ_1	α_2	μ_2 (μm)	σ_2	α_3	μ_3 (μm)	σ_3
1RT(SR4S630)20	0.547	1014.1	46.09	0.371	1151.9	97.80	0.082	1379.9	37.93
1RT(SR4S630)30	0.411	1082.5	35.03	0.362	1102.0	59.67	0.226	1281.0	117.93
1RT(SR4S630)40	0.087	1059.6	23.97	0.648	1135.2	34.21	0.265	1275.9	130.63
1RT(SR4S630)50	0.250	1107.1	44.33	0.596	1174.7	40.05	0.155	1366.3	89.02
2RT(SR4S630)20	0.083	1048.6	32.83	0.596	1131.0	47.86	0.321	1336.2	138.36
2RT(SR4S630)30	0.358	1254.7	99.30	0.626	1180.5	39.79	0.016	1523.8	18.28
2RT(SR4S630)40	0.229	1249.1	92.27	0.706	1215.8	49.14	0.065	1501.1	80.56
2RT(SR4S630)50	0.395	1211.3	47.67	0.304	1275.6	40.99	0.301	1301.7	118.17
1RT(SR4TWN)20	0.255	952.4	33.11	0.352	1013.0	47.66	0.393	1197.7	151.75
1RT(SR4TWN)30	0.273	1019.5	28.17	0.406	1054.8	35.57	0.321	1176.9	134.46
1RT(SR4TWN)40	0.107	1002.2	27.66	0.594	1075.0	30.83	0.298	1198.9	118.27
1RT(SR4TWN)50	0.503	1097.0	50.03	0.216	1118.0	22.80	0.282	1187.1	124.70
2RT(SR4TWN)20	0.046	1060.6	7.31	0.646	1131.8	59.37	0.306	1346.5	112.53
2RT(SR4TWN)30	0.345	1189.9	35.13	0.509	1206.4	60.42	0.146	1392.1	120.48
2RT(SR4TWN)40	0.023	1156.9	6.01	0.703	1244.9	41.87	0.274	1338.0	141.76
2RT(SR4TWN)50	0.649	1254.4	69.93	0.246	1339.6	35.87	0.105	1502.7	90.90

* denotes paired T test statistical significance at $P \leq 0.05$.

This was contrary to the findings earlier when DI was used instead. With AGL, RT(SR2) RT(SR4) and RT(SR6) also had significant increase in size with prolonged spheronization (Table 21). The extent of size increase would be higher with higher AGL spray rates. When AGL was sprayed onto spheroid surface, the amount of moisture on spheroid surface was instantaneously increased. The increased amount of surface moisture would increase the spheroid surface plasticity while reducing its rigidity. Higher surface plasticity would in turn allow greater tendency for agglomeration during spheroid collisions, resulting in size increase. At 2 and 4 ml/min, the rate of AGL addition did not increase the net moisture content in the spheroids (Figure 12). However, as AGL was sprayed onto the spheroid surface, its immediate effect would be to cause the spheroid surface to be more plastic, promoting spheroid coalescence. It would take considerable amount of time for excessive moisture on the spheroid surface to migrate and distribute itself throughout the spheroid matrix. Hence, compared to amount of surface moisture, the net amount of moisture remaining in spheroids was less important in contributing to agglomeration.

All the 3 methods used to quantify spheroid size, sieving, image analysis and statistical curve fitting into mix Gaussian distribution, highlighted different aspects of RP spheroid agglomeration due to the addition of AGL (Table 18, Figure 13 and Table 21). RP inherently is widely regarded as less robust compared to ES. When experiments were repeated, variability in mean size of RP spheroids was higher than those of ES. This variability would obscure any subtle spheroid size change due to

AGL. Sieving, the less sensitive sizing method also could not detect this subtle spheroid size change caused by the AGL addition. As suggested by the MG distribution representing spheroid size distribution, the whole batch of spheroids could be considered as a heterogeneous population, consisting subpopulations of spheroids. The highest AGL spray rate of 6 ml/min caused all the subpopulations to increase in size (Figure 13). At lower spray rate of 2 and 4 ml/min, only the subpopulation represented by μ_1 had distinct size increase (Table 21). In a situation where granules of different sizes had the same level of surface plasticity, the smaller granules were more likely to coalesce with one another until a maximum size was reached (Iveson et al., 2001). Therefore, at low rate of AGL addition, surface plasticity of the subpopulation of the smaller spheroids were sufficiently increased, allowing agglomeration to take place. However, the low rate of AGL addition did not increase the surface plasticity of larger spheroid sufficiently to promote agglomeration among subpopulations of larger spheroids. The effect of low rate of AGL addition to cause spheroid size increase could only be observed on smaller spheroids. This phenomenon of spheroid size increase for smaller spheroids instead of larger spheroids could be viewed as a step-wise size increase process. Hence, at low rate of AGL addition, smaller spheroids increased in size while larger ones remained unchanged in size. At high AGL spray rate, both small and large spheroids increased in size at the same time.

4.3. Effects of AGL on spheroid roundness

Apart from the increase in spheroid size, introduction of AGL also altered the roundness of spheroids. Paired T test was carried out on roundness of RT(SR)20 and RT(SR)50 batches to investigate the effects of AGL (Figure 14). At zero AGL spray rate, e_R , AR and PS of RT(SR0) spheroids did not show significance changes. However, when AGL was introduced at 2-6 ml/min, spheroids became significantly less round as shown by the e_R , PS, and AR values. Percentage change in e_R , PS and AR reached a maximum with AGL spray rate at 4 ml/min. At 4 ml/min, net moisture content of RT(SR4) spheroids reached an equilibrium, with moisture loss balanced by uptake of AGL into the spheroid matrix. When C was used to quantify the roundness of spheroids during the addition of AGL, the findings appeared to be contrary to those obtained using e_R , PS and AR as roundness descriptors (Figure 14). At zero AGL spray rate, RT(SR0) spheroids were significantly rounder with increased spheronization duration. With the exception of RT(SR4S630), the introduction of AGL did not cause the C of spheroids to change significantly. RT(SR4S630) spheroids had significantly higher C value.

4.3.1. Applicability of roundness correlations with RP spheroids

The contradiction between e_R , PS and AR, and C prompted further examination. e_R , PS, AR and C were correlated with one another using the method which was applied to ESC(TS) spheroids. R values of e_R -AR correlations of RT(SR) spheroids were approximately 0.88 (Figure 15). Addition of AGL did not cause any change in the R

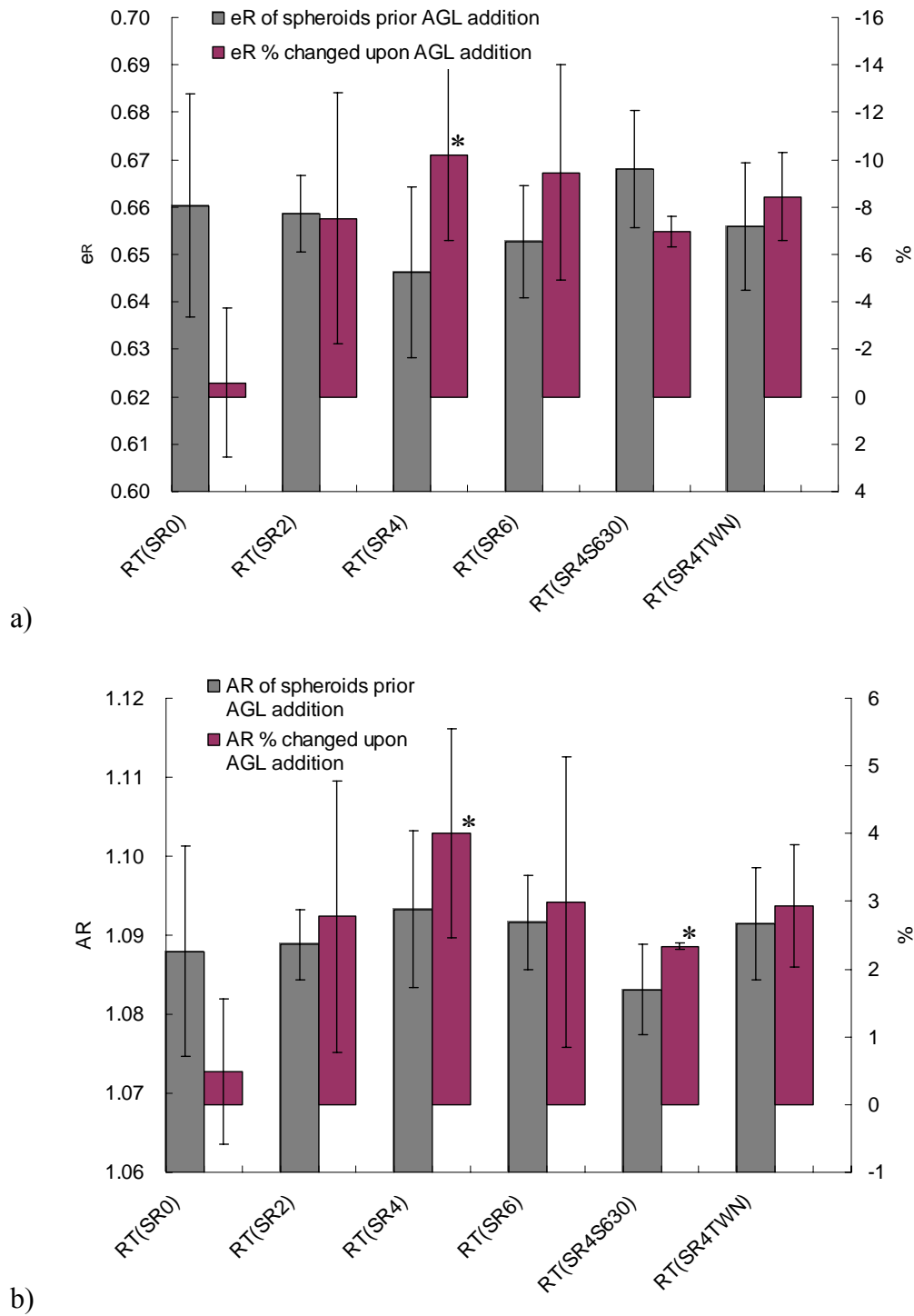
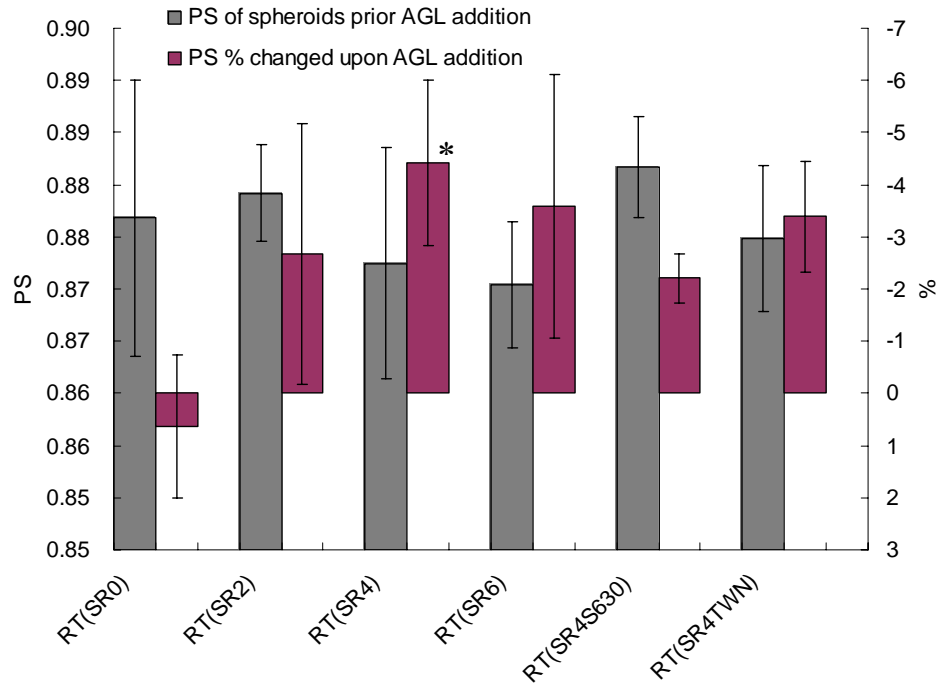
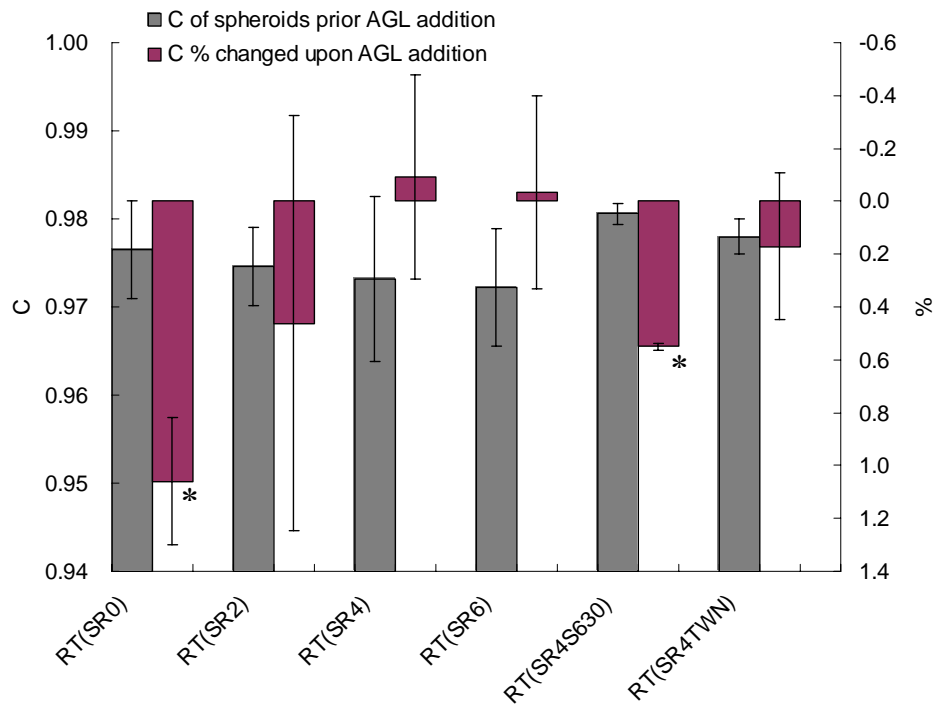


Figure 14. Roundness RT(SR)20 batches and respective roundness % changed upon AGL addition. Error bars represent standard deviation. * denotes statistical significant change in roundness upon AGL addition.



c)



d)

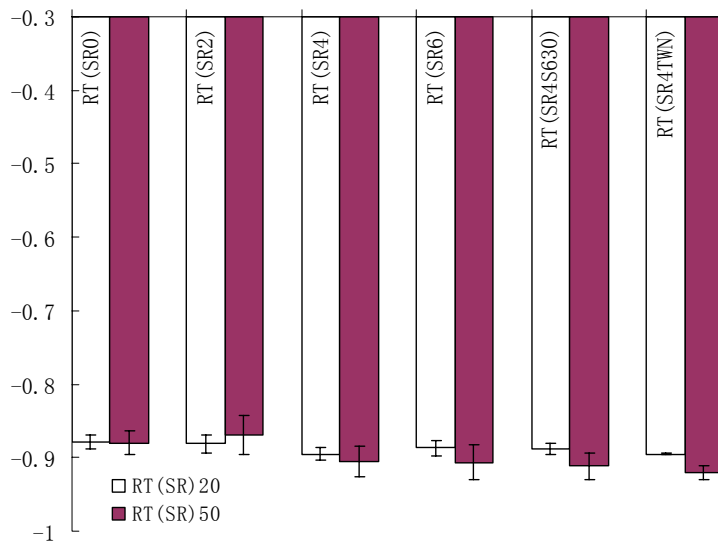
Figure 14 (Continued). Roundness RT(SR)20 batches and respective roundness % changed upon AGL addition.

Error bars represent standard deviation. * denotes statistical significant change in roundness upon AGL addition.

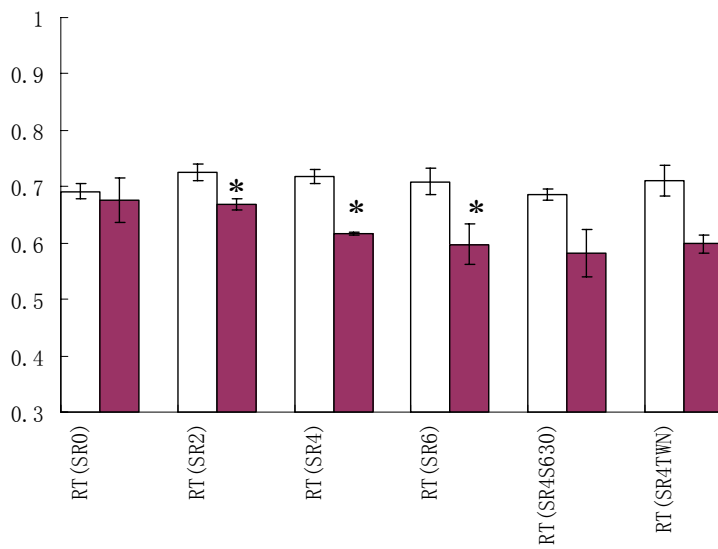
values of e_R -AR correlations (Figure 15). Compared to e_R -AR correlations, addition of AGL caused a significance decrease in the R values of e_R -PS correlations. R values of e_R -PS correlations of RT(SR2)20, RT(SR4)20 and RT(SR6)20 batches were approximately 0.7, which decreased significantly by about 0.1 with the introduction of AGL (Figure 15). R values of e_R -C correlations of RT(SR) spheroids were approximately 0.5 and addition of AGL did not cause significant change in the R values. R values of AR-PS correlations for RT(SR)20 batches averaged about -0.75 and introduction of AGL caused a significant change in the R values (less negative). R values of AR-C and PS-C correlations averaged about -0.6 and 0.8 respectively for RT(SR) batches and presence of AGL did not cause significance change.

4.3.2. Choosing robust spheroid roundness descriptors

The R values of roundness correlations could be evaluated independently among the RT(SR) batches and also in comparison with ESC(TS) batches. Both RT(SR) and ESC(TS) batches have R values of e_R -AR correlations approximately 0.9. This high R value indicated that for ES and RP spheroids, spheroid represented by e_R or AR would yield approximately equivalent results. In consideration of the complexity of the mathematical equation and the extra measurements required from image analysis to calculate e_R , it would be advantageous to use AR as a spheroid roundness descriptor for its simplicity in calculations. Apart from complexity in the calculation, spheroid measurements required by e_R might be obtained differently when different image analysis systems are used. In order to obtain p and r_e , an image analysis system has to



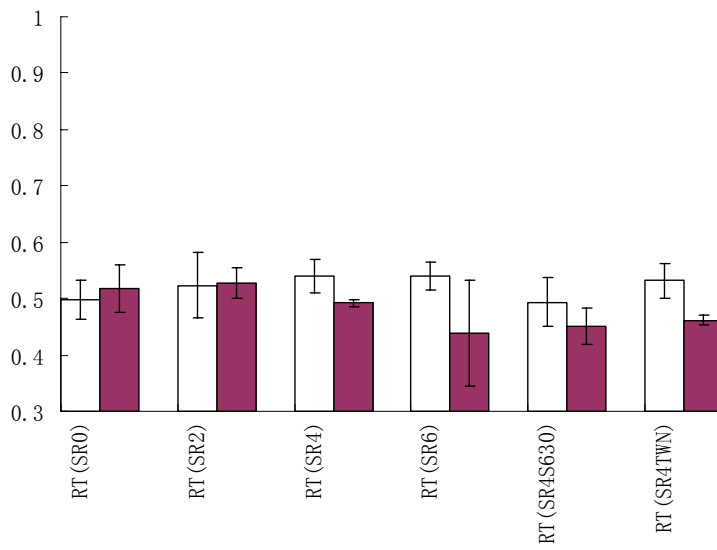
a) e_R -AR



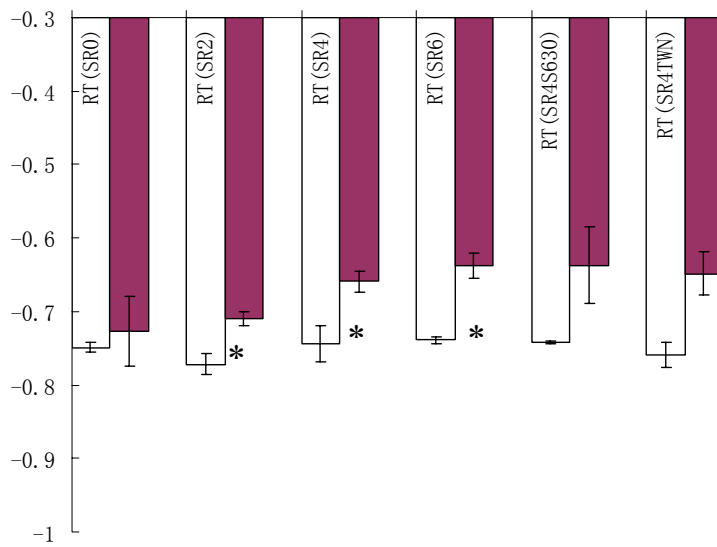
b) e_R -PS

Figure 15. R values of roundness correlations for RT(SR) spheroids.

* denotes statistical significant change upon AGL addition

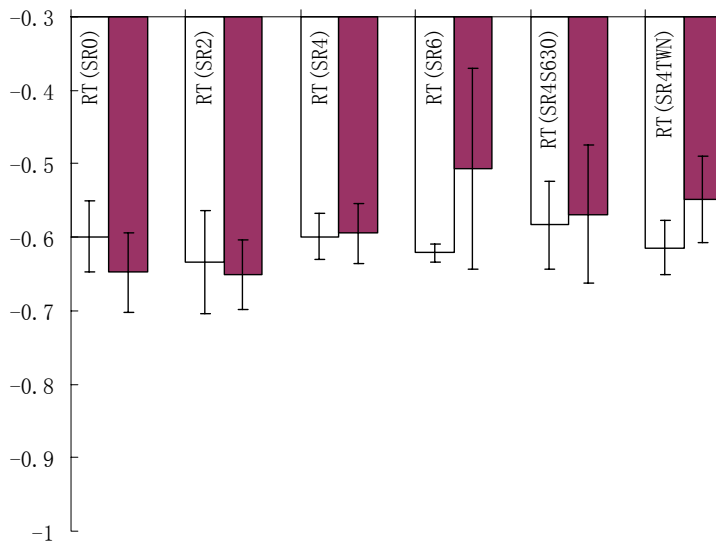


c) e_{R-C}

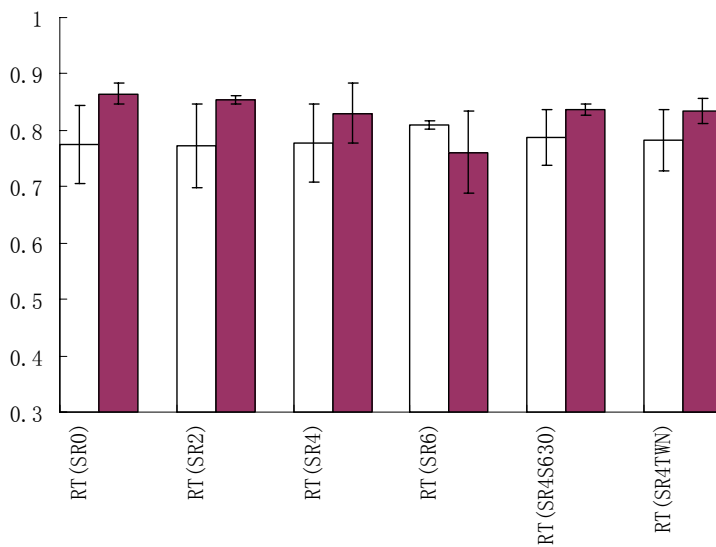


d) AR-PS

Figure 15 (Continued). R values of roundness correlations for RT(SR) spheroids.
 * denotes statistical significant change upon AGL addition.



e) AR-C



f) PS-C

Figure 15 (Continued). R values of roundness correlations for RT(SR) spheroids.

* denotes statistical significant change upon AGL addition.

accurately detect and resolve the 2 dimensional outline of the spheroid. Podczec et al. (1999) ensured consistency in image analysis by standardizing the specimen illumination method and minimum pixel resolution. Although the minimum number of pixels was specified, resolution of image outline would also depend on the quality

of the optical system to competently resolve the outline of the spheroids. Slight differences in image thresholding process and optical resolution would affect the measurements of both the length and breadth of the spheroid image in a similar manner. However, as AR is calculated as a ratio of the length and breadth, having length and breadth of the spheroid image affected in a similar manner would yield the same AR value with different image analysis systems. Taking into consideration the large R values of e_R -AR, the complexity in calculating e_R , the likelihood of higher variability in e_R values when analyzed by different laboratories and research groups, AR could be applied in place of e_R to evaluate spheroids produced by ES and RP.

The R values of e_R -PS and AR-PS correlations between ESC(TS) and RT(SR) batches were distinctively different compared to the rest of the R values (Figures 9 and 15). R values of e_R -PS and AR-PS correlations for RT(SR) were smaller than those of ESC(TS). R values of e_R -PS and AR-PS correlations for ESC(TS) averaged 0.9 and -0.94 respectively versus 0.7 and -0.75 for e_R -PS and AR-PS of RT(SR) respectively (Figures 9 and 15). Out of the 6 R values of roundness correlations of RT(SR), only e_R -Ps and AR-PS r values were significantly different in the presence of AGL. Since e_R -PS and AR-PS plots could distinguish between spheroid shape RRE from oval and ellipse (Figure 11), smaller R values of e_R -PS and less negative R values of AR-PS correlations would indicate that shape of some of RT(SR) spheroids have changed, resulting in a more homogenous mix of RRE, oval and ellipse. The introduction of AGL caused μ_1 and DI of RT(SR) spheroids to increase, pointing to agglomeration

taking place among the spheroids. During the process of agglomeration with the addition of AGL, the resultant spheroids would become less spherical, possibly taking on a shape similar to RRE. The presence of agglomeration, resulting in newly formed enlarged spheroids of different shape would have caused the change in the R values of e_R -PS and AR-PS correlations. The R values of AR- e_R , e_R -C, AR-C and PS-C correlations of RT(SR) spheroids were similar to those of ESC(TS), demonstrating the applicability of roundness correlation plots in evaluating shapes of spheroids produced by ES and RP.

4.4. Surface changes during spheronization with addition of AGL

The introduction of AGL had mixed effects on the surface roughness of spheroids (Figure 16). Paired T test was carried out on Ra values of RT(SR)20 and RT(SR)50 batches to investigate the effects of AGL. Without AGL, surfaces of RT(SR0) spheroids were significantly smoother with the lowest Ra among all RT(SR) batches at the end of the process run (50 min). At AGL spray rate of 2 ml/min, surface roughness values of RT(SR2) spheroids were also significantly lowered. At higher AGL spray rates, with the exception of RT(SR4TWN), higher AGL spray rates did not appear to effect a significant decrease in surface roughness of the resultant spheroids. Spheroids surfaces could be smoothed by attrition and abrasion when spheroids collide between themselves or with the rotating frictional plate. When AGL was sprayed onto spheroid surfaces, surface material may be solvated, possibly

yielding smoother surfaces. Similarly, plasticity of spheroid surfaces may be increased when AGL was sprayed onto spheroid surfaces. With higher surface plasticity, spheroid collision during spheronization may give rise to spheroids with higher sphericity or cause protrusions to be flattened to yield smoother surfaces. Conversely, the higher surface plasticity or surface moisture could promote spheroid enlargement by abrasion transfer, coalescence or layering. Enlarged spheroids would have newly formed surfaces that are rougher than surfaces prior to enlargement.

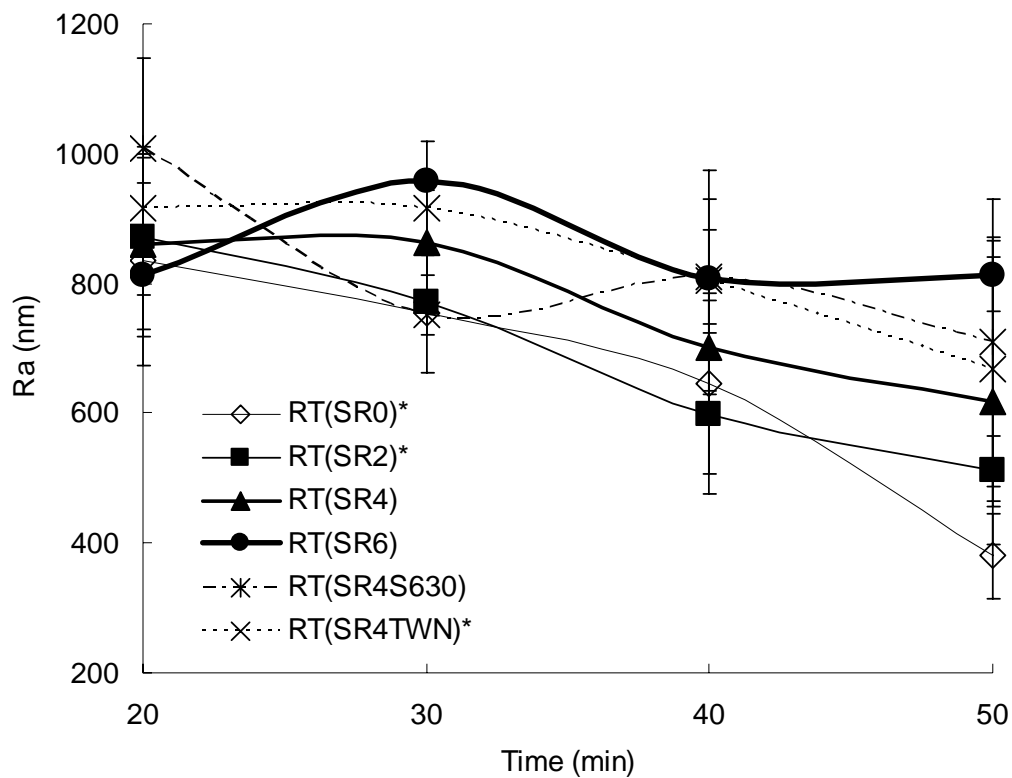
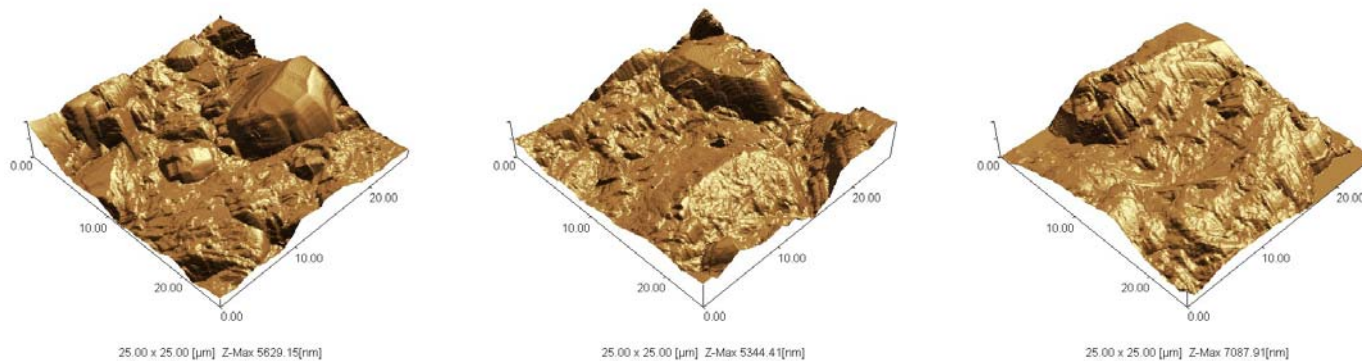


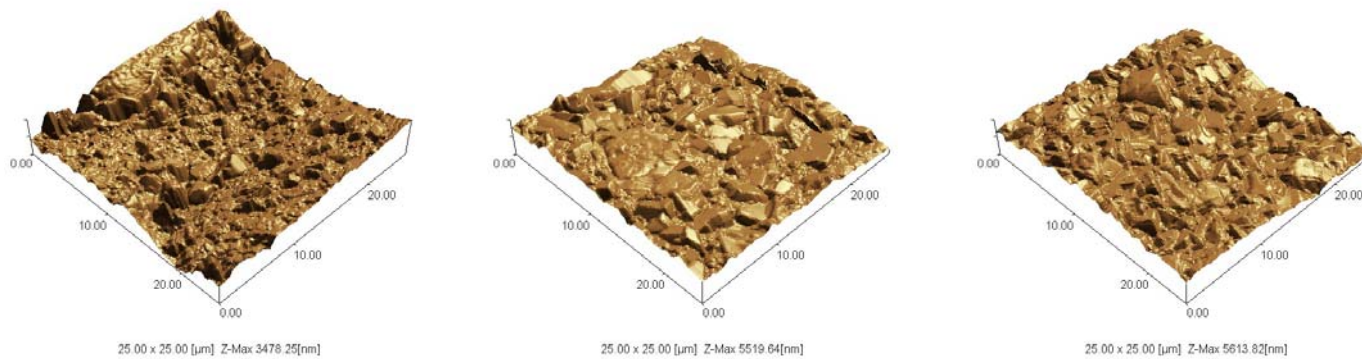
Figure 16. Surface roughness of RT(SR) spheroids.

* denotes statistical significant change in roughness between 20th and 50th min ($P \leq 0.05$).

Qualitative examination of spheroid surfaces by scanning probe microscopy revealed that surfaces of RT(SR0)50 spheroids were distinctively different from the rest of the surfaces as shown in Figure 17. Surfaces of RT(SR0)50 spheroids possessed crystalline features, with surface protrusions having sharp, well-defined edges. There was absence of large protrusions which could account for its lowest Ra value. In general, the surface of RT(SR0)50 spheroids resembled “sand paper”. Prolonged spheronization of RT(SR0) spheroids could have allowed large surface protrusions to be attrited. The continued loss of moisture from the spheroids was also a possible contributing factor leading to crystallization at the surfaces to give the “sand paper” appearance. The rest of the surfaces in Figure 17 appeared similar, with “smooth-muddy” features interspersed with large surface protrusions. Surfaces of RT(SRS630) and RT(SR4TWN) spheroids did not reveal any distinctive features which might suggest the influence of S630 or Tween 80. The solvation of spheroid surface by AGL and the possible exposure of new surfaces after spheroid agglomeration maintained the “smooth muddy” appearance. Therefore, the Ra value of spheroid surface could result from a balance of attrition, surface solvation and new surface exposure upon agglomeration. RT(SR2)50 spheroids which had significantly lower Ra could be due to predominant attrition, surface solvation and minimal exposure of new surfaces due the low AGL spray rate which limited agglomeration.

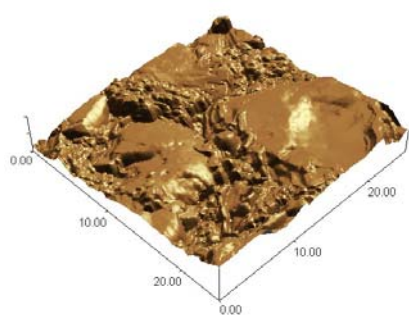
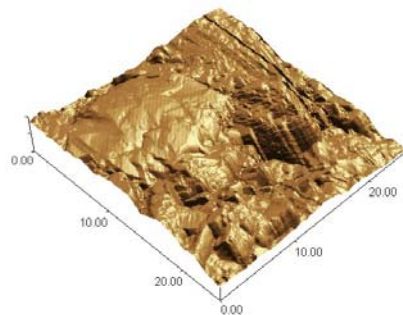
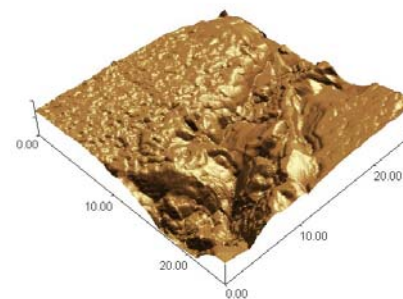


1RT(SR4)20

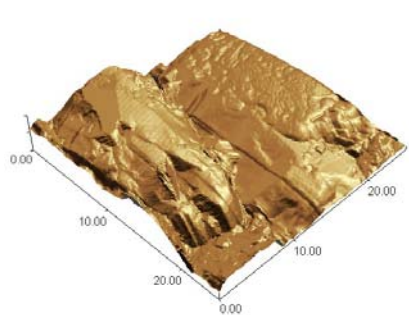
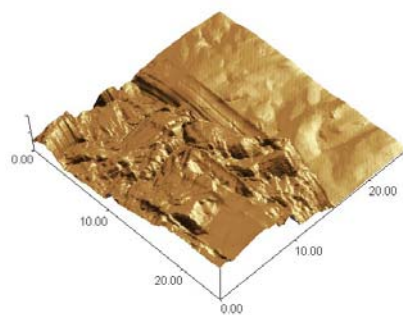
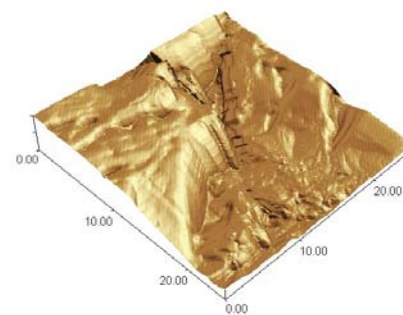


1RT(SR0)50

Figure 17. Surface morphology of RT(SR) spheroids as observed under scanning probe microscopy. Three pictures per batch represent surfaces from 3 different spheroids.

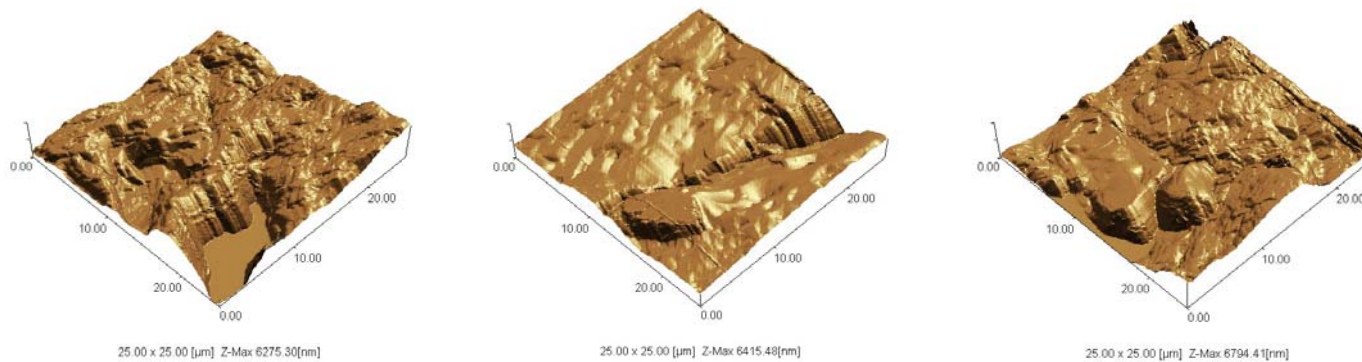
25.00 x 25.00 [μm] Z-Max 4010.50[nm]25.00 x 25.00 [μm] Z-Max 6207.40[nm]25.00 x 25.00 [μm] Z-Max 5410.12[nm]

1RT(SR2)50

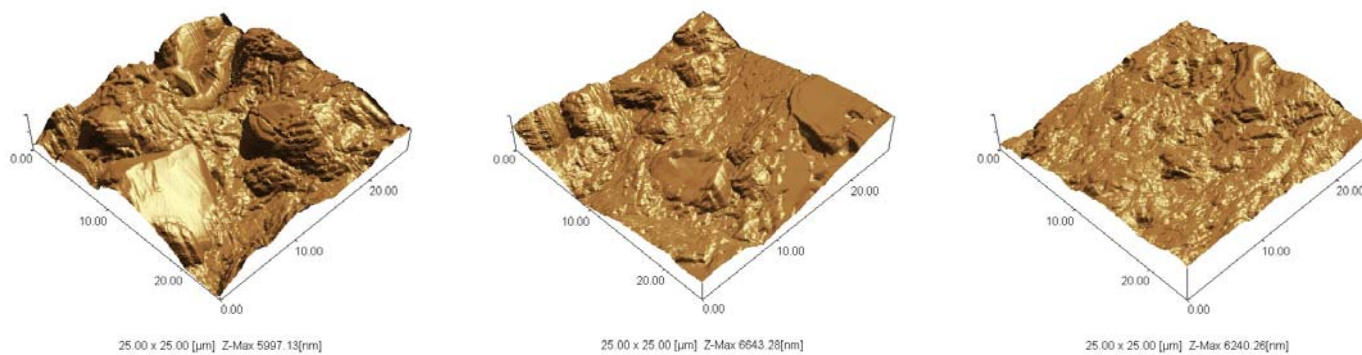
25.00 x 25.00 [μm] Z-Max 6841.09[nm]25.00 x 25.00 [μm] Z-Max 6943.35[nm]25.00 x 25.00 [μm] Z-Max 7674.92[nm]

1RT(SR4)50

Figure 17 (Continued). Surface morphology of RT(SR) spheroids as observed under scanning probe microscopy. Three pictures per batch represent surfaces from 3 different spheroids.

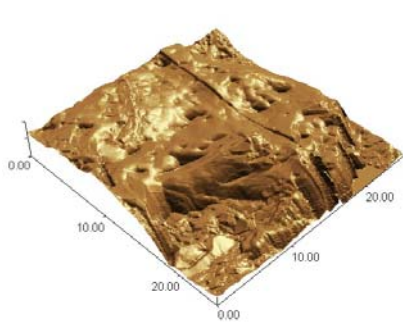


1RT(SR6)50

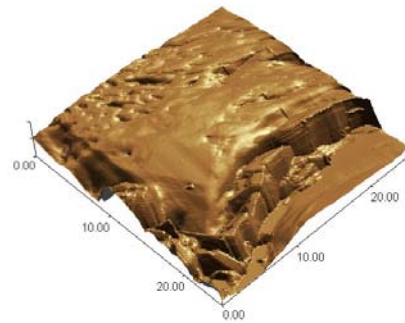


1RT(SR4S630)50

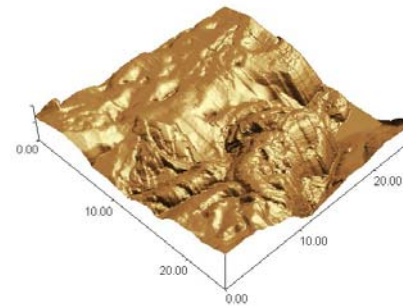
Figure 17 (Continued). Surface morphology of RT(SR) spheroids as observed under scanning probe microscopy. Three pictures per batch represent surfaces from 3 different spheroids.



25.00 x 25.00 [μm] Z-Max 5782.48[nm]



25.00 x 25.00 [μm] Z-Max 4406.95[nm]



25.00 x 25.00 [μm] Z-Max 6135.12[nm]

1RT(SR4TWN)50

Figure 17 (Continued). Surface morphology of RT(SR) spheroids as observed under scanning probe microscopy. Three pictures per batch represent surfaces from 3 different spheroids.

4.5. Yield

Among the RT(SR) batches, RT(SR0) had the lowest yield, averaging approximately 750 g (Figure 18). The remaining RT(SR) batches had relatively the same amount of yield, approximately 850 g. For RT(SR0) batches, towards the end of the 50 min process run, more spheroids were observed to eject or vault out over the wall of the rotary processing chamber, resulting in material loss and lowered yield. Without the addition of AGL, the surfaces of spheroids would be relatively drier than those from batches with AGL. Surface-wetted spheroids, due to water tension between surfaces, could have momentarily attracted spheroids together during collision while undergoing spheronization. The surface could also be more plastic while wetted, resulting in a lower tendency to rebound when spheroids collided with one another or walls of the rotary processor. The lower rebound tendency would reduce the likelihood of spheroids vaulting out of the rotary processing chamber, resulting in increased yield.

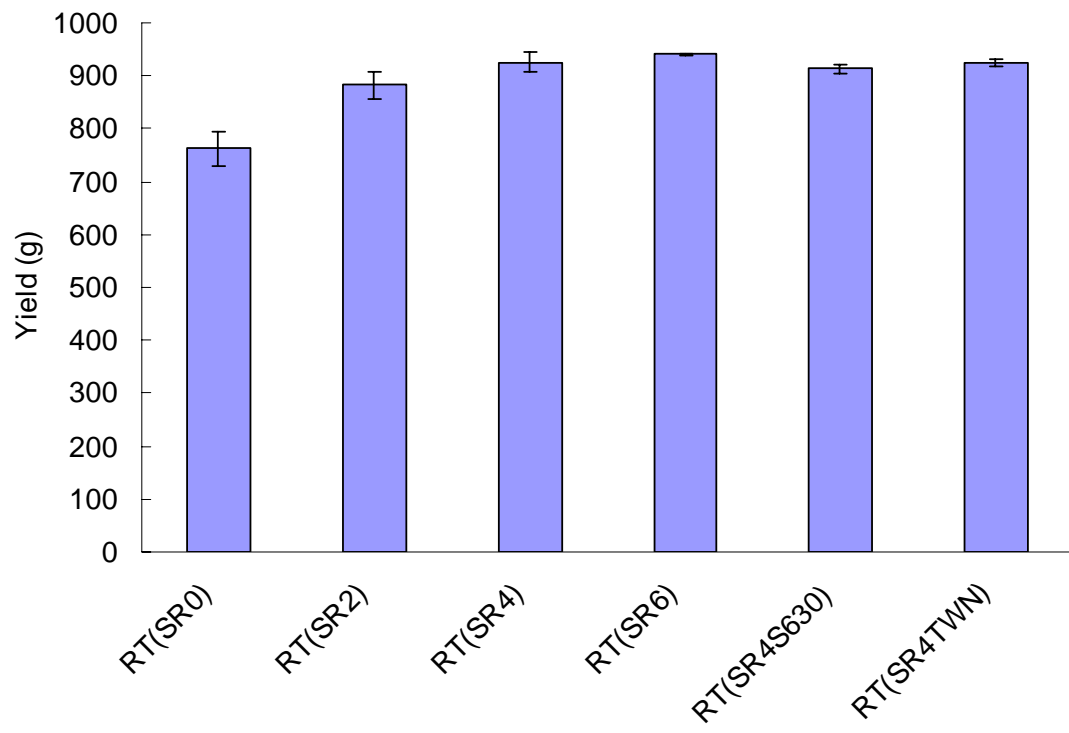


Figure 18. Yield for RT(SR) processes.
Error bars represent standard deviations.

PART 5.
CONCLUSIONS

PART 5. CONCLUSIONS

Extrusion-spheronization spheroids of similar size and quality could be produced by frictional base plates with dissimilar plate design if the spheronization speed and duration are adjusted appropriately to compensate for differences in frictional forces exerted by the plates. With appropriate choice of spheronization speed and amount of granulation liquid, the quality of spheroids produced by RP could approximate that of ES. In this study, RP was found to require less granulation liquid and at the same time produced harder spheroids compared to ES. The amount of moisture present during the initial stage of spheroid formation (and not the amount of moisture remaining after spheronization) determined the eventual size of ES spheroids.

Visual examination of spheroid formation revealed that for ES, extrudates are broken up to lengths approximately equal to their diameters. This would be followed by attrition of the edges of the broken extrudates. During the first 2 min of spheronization, layering was the predominant mechanism for spheroid size enlargement in ES. In contrast, RP spheroid size enlargement was characterized by layering and coalescence. Contrary to existing ES spheroid formation theories, occurrence of dumbbell like intermediates was not observed.

Extrusion spheronization spheroid size changes during spheronization could not be represented by conventional methods of sizing via sieving or image analysis. Size distribution of ES spheroids was found to follow a 3 components MG distribution

instead of normal or log normal distribution. By representing spheroid size distribution using 3 components MG distribution, ES spheroid size changes during spheronization could be quantified. Furthermore, being represented by a MG distribution reinforced the observed heterogeneity in size whereby layering was observed to be a predominant mechanism for ES spheroid size enlargement.

Generally within the spheroid population, smaller ES spheroids were rounder. e_R and e_R were found to be highly correlated with each other, indicating that both descriptors could be used interchangeably. Among the roundness descriptors examined, C was found to be the least critical in quantifying improvement in roundness for ES spheroids as spheronization progressed. However, when C-AR correlations were carried out, it had the ability to detect heterogeneity in spheroid shape within subpopulations of ES spheroids of different sizes.

Correlation analysis of e_R , PS, AR and C values of spheroids could be carried out to identify the possible shapes of spheroids. This novel shape identification method was proposed. By comparing results from simulated spheroids shapes with actual data, the likely ES spheroid shape towards the end of spheronization would be ellipse.

Occurrences of dumbbells and RRC shapes were unlikely. Generally, smaller ES spheroids were rounder. Mass transfer and remodeling were also found to be more active with smaller ES spheroids especially towards the end of spheronization run as smaller spheroids had greater variation in shape.

Size distribution of RP spheroids also fitted the MG distribution. By representing RP spheroids with MG distribution, different subpopulations of spheroids based on size were found to have varying tendencies to agglomerate when AGL was added. This phenomenon would not be observed if size of spheroids were characterized by conventional methods.

PART 6.
REFERENCES

PART 6. REFERENCES

Agrawal, A.M., Howard, M.A., Neau, S.H., 2004. Extruded and spheronized beads containing no microcrystalline cellulose: Influence of formulation and process variables. *Pharm. Dev. Technol.*, 9(2), 197-217

Alderliesten, M., 2004. Mean particle diameter. Part IV: Empirical selection of the proper type of mean particle diameter describing a product or material property. Part. *Syst. Charact.*, 21, 179-196.

Almeida-Prieto, S., Blanco-Mendez, J., Otero-Espinar, F.J., 2004. Image analysis of the shape of granulated powder grains. *J. Pharm. Sci.*, 93(3), 621-634.

Almeida-Prieto, S., Blanco-Mendez, J., Otero-Espinar, F.J., 2006. Microscopic image analysis techniques for the morphological characterization of pharmaceutical particles: Influence of process variables. *J. Pharm. Sci.*, 95(2), 348-357.

Baert, L., Remon, J.P., 1993. Influence of amount of granulation liquid on the drug release rate from pellets made by extrusion spheronization. *Int. J. Pharm.* 95, 135-146.

Bataille, B., Ligarski, K., Jacob, M., Thomas, C., Duru, C., 1993. Study of the influence of spheronization and drying conditions on the physico-mechanical

properties of neutral spheroids containing Avicel PH-101 and lactose. *Drug Dev. Ind.*

Pharm., 19, 653-671.

Bhrany, U.N., Johnson, R.T., Myron, T.L., Pelczarski, E.A., 1962. Dynamics of pelletization. In: Knepper, W.A. (Ed.), *Agglomeration*, Wiley-Interscience, New York, pp. 223-249.

Bohning, D., Seidel, W., 2003. Editorial: recent developments in mixture models.

Comput. Statist. Data Anal., 41, 349-357.

Bommareddy, G.S., Parker-Leggs, S., Saripella, K.K., Neau, S.H., 2006. Extruded and spheronized beads containing Carbopol 974P to deliver nonelectrolytes and salts of weakly basic drugs. *Int. J. Pharm.*, 321, 62-71.

Bornhoft, M., Thommes, M., Kleinebudde, P., 2005. Preliminary assessment of carrageenan as excipient for extrusion/spheronisation. *Eur. J. Pharm. Biopharm.*, 59, 127-131.

Boutell, S., Newton, J.M., Bloor, J.R., Hayes, G., 2002. The influence of liquid binder on the liquid mobility and preparation of spherical granules by the process of extrusion/spheronization. *Int. J. Pharm.*, 238, 61-76.

- Bury, K.V., 1999. *Statistical Distributions in engineering*, Cambridge University Press, New York.
- Chatchawalsaisin, J., Podczeck, F., Newton, J.M., 2004. The influence of chitosan and sodium alginate and formulation variables on the formation and drug release from pellets prepared by extrusion/spheronisation. *Int. J. Pharm.*, 275, 41-60.
- Chatchawalsaisin, J., Podczeck, F., Newton, J.M., 2005. The preparation by extrusion/spheronization and the properties of pellets containing drugs, microcrystalline cellulose and glyceryl monostearate. *Eur. J. Pharm. Sci.*, 24, 35-48.
- Chukwumezie, B.N., Wojcik, M., Malak, M., D'Amico, F., Adeyeye, M.C., 2004. Factorial design in the spheronization of ibuprofen microparticulates using the rotor disk fluid-bed technology. *Pharm. Dev. Technol.*, 9(1), 49-62.
- Conine, J. W., Hadley, H.R., 1970. Preparation of small solid pharmaceutical spheres. *Drug Cosm. Ind.*, 106 April, 38-41.
- Dyer, A.M., Khan, K.A., Aulton, M.E., 1994. Effect of the drying method on the mechanical and drug release properties of pellets prepared by extrusion-spheronization. *Drug Dev. Ind. Pharm.* 20, 3045-3065.

- Eriksson, M., Alderborn, G., Nystrom, C., Podczeck, F., Newton, J.M., 1997. Comparison between and evaluation of some methods for the assessment of the sphericity of pellets. *Int. J. Pharm.* 148, 149-154.
- Fielden, K.E., Newton, J.M., 1992. Extrusion and extruders. In: Swarbrick, J., Boyland, J.C. (Eds.), *Encyclopedia of Pharmaceutical Technology*, Vol. 5, Marcel Dekker Inc., New York, pp. 395-442.
- Fielden, K.E., Newton, J.M., Rowe, R.C., 1989. The effect of lactose particles particle size on the extrusion properties of microcrystalline cellulose-lactose mixture. *J. Pharm. Pharmacol.*, 41, 217-221.
- Galland, S., Ruiz, T., Delalonde, M., Krupa, A., Bataille, B., 2005. A texturing the spherical granular system influence of the spheronisation stage. *Powder Technol.*, 157, 156-162.
- Gu, L., Liew, C.V., Soh, J.L.P., Heng, P.W.S., 2006. Feasibility of eliminating premixing for the production of pellets in a rotary processor. *Pharm. Devt. Technol.*, 11, 159-165.

- Harris, M.R., Sellassie, I.G., 1989. Formulation variables. In: Sellassie, I.G., (Ed.), *Pharmaceutical pelletization technology*, Marcel Dekker Inc., New York, pp. 217-239.
- Hellen, L., Yliruusi, J., Muttonen, E., Kristoffersson, E., 1993. Process variables of the radial screen extruder: Part II – Size and size distributions of pellets. *Pharm. Tech. Int.*, Jan, 44-53.
- Heng, P.W.S., Koo, O.M.Y., 2001. A study of the effects of the physical characteristics of microcrystalline cellulose on performance in extrusion spheronization. *Pharm. Res.*, 18(4), 480-487.
- Heng, P.W.S., Liew, C.V., Gu, L., 2002. Influence of teardrop studs on rotating frictional base plate on spheroid quality in rotary spheronization. *Int. J. Pharm.*, 241, 173-184.
- Heng, P.W.S., Wan, L.S.C., Tan, Y.T.F., 1996. Optimization of spheroid production by centrifugal rotary processing. *Int. J. Pharm.*, 143, 107-112.
- Holm, P., Bonde, M., Wigmore, T., 1996. Pelletization by granulation in a roto-processor RP-2. Part I: Effect of process and product variables on granule growth. *Pharm. Technol. Eur.*, 8(8), 22-36.

Hoornaert, F., Wauters, P,A,L., Meesters, G.M.H., Pratsinis, S.E., Scarlett, B., 1998. Agglomeration behaviour of powders in a lödige mixer granulator. *Powder Technol.*, 96, 116-128.

Howard, M.A., Neau, S.H., Sack, M.J., 2006. PEO and MPEG in high drug load extruded and spheronized beads that are devoid of MCC. *Int. J. Pharm.*, 307, 66-76.

Iveson, S.M., Litster, J.D., Hapgood, K., Ennis, B.J., 2001. Nucleation, growth and breakdown phenomena in agitated wet granulation processes: a review. *Powder Technol.*, 117, 3-39.

Kleinebudde, P., 1994. Shrinking and swelling properties of pellets containing microcrystalline cellulose and low substituted hydroxylpropylcellulose: I. Shrinking properties. *Int. J. Pharm.*, 109, 209-219.

Kleinebudde, P., Schroder, M., Schultz, P., Muller, B.W., Waaler, T., Nymo, L., 1999. Importance of the fraction of microcrystalline cellulose and spheronization speed on the properties of extruded pellets made from binary mixtures. *Pharm. Devt. Technol.*, 4(3), 397-404.

- Koo, O.M.Y., Heng, P.W.S., 2001. The influence of microcrystalline cellulose grade on shape and shape distributions of pellets produced by extrusion-spheronization. *Chem. Pharm. Bull.*, 49(11), 1383-1387.
- Krejčová, K., Rabisková, M., Věchy, D., Polásek, E., 2006. The influence of drug solubility and particle size on the pellet formulation in a rotoprocessor. *Drug Dev. Ind. Pharm.*, 32, 585-593.
- Kristensen, J., 2005. Direct pelletization in a rotary processor controlled by torque measurements. III. Investigation of microcrystalline cellulose and lactose grade. *AAPS PharmSciTech.* 1(4), Article 62.
- Kristensen, J., Schæfer, T., 2000. Direct pelletization in a rotary processor controlled by torque measurements. II: Effects of changes in the content of microcrystalline cellulose. *AAPS Pharmsci.*, 2(3), Article 24.
- Kristensen, J., Schæfer, T., Kleinebudde, P., 2000. Direct pelletization in a rotary processor controlled by torque measurements. I. Influence of process variables. *Pharm. Dev. Technol.*, 5(2), 247-256.
- Leuenberger, H., Imanidis, G., 1986. Monitoring mass transfer processes to control moist agglomeration. *Pharm. Tech.*, 3, 56-73.

Liew, C.V., Gu, L., Heng, P.W.S., 2002. The influence of operational variables on mean size and size distribution of spheroids produced by rotary spheronization using teardrop studs. *Int. J. Pharm.* 242, 345-348.

Liew, C.V., Gu, L., Soh, J.L.P., Heng, P.W.S., 2005. Functionality of cross-linked polyvinylpyrrolidone as a spheronization aid: A promising alternative to microcrystalline cellulose. *Pharm. Res.*, 22(8), 1387-1398.

Liew, C.V., Heng, P.W.S., Wan, L.S.C., 2000. Role of base plate rotational speed in controlling spheroid size distribution and minimizing oversize particle formation during spheroid production by rotary processing. *Int. J. Pharm.*, 26(9), 953-963.

Liew, C.V., Wan, L.S.C., Heng, P.W.S., 1998. Influence of polytetrafluoroethylene on spheroid production by rotary processing. *STP Pharma Sci.*; 8(5), 297-302.

Linder, H., Kleinbudde, P., 1994. Use of powder cellulose for the production of pellets by extrusion/spheronization. *J. Pharm. Pharmacol.*, 46, 2-7.

Linkson, P.B., Gastonbury, J.R., Duffy, G.J., 1973. The mechanism of granule growth in wet pelletizing. *Trans, Instn. Chem. Engrs.*, 51, 251-259.

MacRitchie, K.A., Newton, J.M., Rowe, R.C., 2002. The evaluation of the rheological properties of lactose/microcrystalline cellulose and water mixture by controlled stress rheometry and the relationship to the production of spherical pellets by extrusion/spheronization. *Eur. J. Pharm. Sci.*, 17, 43-50.

Mehrotra, V.P., Sastry, K.V.S., 1986. Moisture requirements and role of ash and microporosity in pelletization of coal fines. *Powder Techno.*, 47, 51-59.

Morris, N.J., Warburton, B., 1984. Particle size analysis of microcapsules. *J. Pharm. Pharmacol.*, 36, 73-76.

MunozRuiz, A., Paronen, P., 1997. Particle and powder properties of cyclodextrins. *Int. J. Pharm.*, 148, 33-39.

Newton, J.M., Chapman, S.R., Rowe, R.C., 1995a. The influence of process variables on the preparation and properties of spherical granules by process of extrusion and spheronization. *Int. J. Pharm.*, 120, 101-109.

Newton, J.M., Chapman, S.R., Rowe, R.C., 1995b. The assessment of the scale-up performance of the extrusion/spheronisation process. *Int. J. Pharm.*, 120, 95-99.

Newton, J.M., Chow, A.K., Jeewa, K.B., 1992. The effect of excipients source on spherical granules made by extrusion/spheronization. *Pharm. Tech. Int.*, 4 Oct., 52, 54-56.

Pinto, J.F., Abreu, C.N., 2006. Evaluation of the performance of a new continuous spheronizer. *Drug Dev. Ind. Pharm.*, 32, 1061-1078.

Pisek, R., Sicra, J., Svanjak, G., Srcic, S., 2001. Comparison of rotor direct pelletization (fluid bed) and extrusion/spheronization method for pellet production. *Pharm. Ind.*, 63(11), 1202-1209.

Podczeck, F., Knight, P., 2006. The evaluation of formulation for the preparation of pellets with high drug loading. *Pharm. Dev. Technol.*, 11, 263-274.

Podczeck, F., Newton, M.J., 1994. A shape factor to characterize the quality of spheroids. *J. Pharm. Pharmacol.* 46, 82-85.

Podczeck, F., Rahman, S.H., Newton, M.J., 1999. Evaluation of a standardised procedure to assess the shape of pellets using image analysis. *Int. J. Pharm.*, 192(2), 123-138.

Reynolds, A.D., 1970. A new technique for the production of spherical particles.

Manuf. Chem. Aerosol News., 41 June, 40-43.

Robinson, R.L., Hollenbeck, R.G., 1991. Manufacture of spherical acetaminophen pellets: Comparison of rotary processing with multiple-step extrusion and spheronization. Pharm. Technol., 15(May), 48, 50-54, 56.

Rough, S.L., Wilson, D.L., 2005. Extrudate fracture and spheronisation of microcrystalline cellulose pastes. J. Mat. Sci., 40, 4199-4219.

Rowe, R.C., 1985. Spheronization: a novel pill-making process? Pharm. Int., 6, 119-123.

Sastry, K.V.S., Fuerstenau, D.W., 1973. Mechanism of agglomerate growth in green pelletization. Powder Technol., 7, 97-105.

Sastry, K.V.S., Fuerstenau, D.W., 1977. Kinetic and process analysis of the agglomeration of particulate materials by green pelletization. In: Sastry, K.V.S. (Ed.), Agglomeration, AIME, 77, 381-402.

REFERENCES

Schmidt, C., Kleinebudde, P., 1998. Comparison between a twin-screw extruder and a rotary ring die press. Part II: Influence of process variables. *Eur. J. Pharm. Biopharm.*, 45, 173-179.

Schwartz, J.B., 1988. Granulation. *Drug Dev. Ind. Pharm.* 14, 2071-2090.

Scott, A.C., Hounslow, M.J., Instone, T., 2000. Direct evidence of heterogeneity during high-shear granulation. *Powder Technol.*, 113, 205-213.

Sellassie, I.G., Gordon, R.H., Fawzi, M.B., Nesbitt, R.U., 1985. Evaluation of a high speed pelletization process and equipment. *Drug Dev. Ind. Pharm.*, 11, 1523-1541.

Sellassie, I.G., 1989a. Pellets: a general overview. In: Sellassie, I.G., (Ed.), *Pharmaceutical Pelletization Technology*, Marcel Dekker Inc., New York, pp. 1-13.

Sellassie, I.G., 1989b. Mechanism of pellet formation and growth. In: Sellassie, I.G., (Ed.), *Pharmaceutical Pelletization Technology*, Marcel Dekker Inc., New York, pp. 123-143.

Sellassie, I.G., 1994. Preface. In: Sellassie, I.G., (Ed.), *Multiparticulate oral drug delivery*, Marcel Dekker Inc., New York, pp. iii-iv.

Shah, R.D., Kabadi, M., Pope, D.G., Ausburger, L.L., 1994. Physicomechanical characterization of the extrusion-spheronization process. Part I: Instrumentation of the Extruder. *Pharm. Res.*, 11(3), 355-360.

Shah, R.D., Kabadi, M., Pope, D.G., Ausburger, L.L., 1995. Physico-mechanical characterization of the extrusion-spheronization process. Part II: Rheological determinants for successful extrusion and spheronization. *Pharm. Res.*, 12(4), 496-507.

Sherrington, P.J., Oliver, R., 1981a. Introduction. In: *Granulation*, Heyden, London, pp. 1-6.

Sherrington, P.J., Oliver, R., 1981b. Compaction and other granulation methods. In: *Granulation*, Heyden, London, pp. 141-152.

Soh, J.L.P., Liew, C.V., Heng, P.W.S., 2006. Torque rheological parameters to predict pellet quality in extrusion-spheronization. *Int. J. Pharm.*, 315, 99-109.

Sousa, J.J., Sousa, A., Podczek, P., Newton, J.M., 2002. Factors influencing the physical characteristics of pellets obtained by extrusion-spheronization. *Int. J. Pharm.*, 232, 91-106.

- Souto, C., Rodriguez, A., Parajes, S., Martinez-Pacheco, R., 2005. A comparative study of the utility of two superdisintegrants in microcrystalline cellulose pellets prepared by extrusion-spheronization. *Eur. J. Pharm. Biopharm.*, 61(1-2), 94-99.
- Steckel, H, Mindermann-Nogly, F., 2004. Production of chitosan pellets by extrusion/spheronization. *Eur. J. Pharm. Biopharm.*, 57, 107-114.
- Tho, I., Sande, S.A., Kleinbudde, P., 2002. Pectinic acid, a noval excipient for production of pellets by extrusion/spheronizations: preliminary studies. *Eur. J. Pharm. Biopharm.*, 54, 95-99.
- Tho, I., Sande, S.A., Kleinebudde, P., 2005. Cross-linking of amidated low-methoxylated pectin with calcium during extrusion/spheronisation: Effect on particle size and shape. *Chem. Eng. Sci.*, 60, 3899-3907.
- Thoma, K., Ziegler, I., 1998. Investigations on the influence of the type of extruder for pelletization by extrusion-spheronization. II. Sphere characteristics. *Drug Dev. Ind. Pharm.*, 24(5), 413-422.
- Thommes, M., Kleinebudde, P., 2006a. Use of κ -carrageenan as alternative pelletisation aid to microcrystalline cellulose in extrusion/spheronisation. I. Influence of type and fraction of filler. *Eur. J. Pharm. Biopharm.*, 63, 59-67.

Thommes, M., Kleinebudde, P., 2006b. Use of κ -carrageenan as alternative pelletisation aid to microcrystalline cellulose in extrusion/spheronisation. II. Influence of drug and filler type. *Eur. J. Pharm. Biopharm.*, 63, 68-75.

Tomer, G., Podczeck, F., Newton, J.M., 2002. The influence of model drugs on the preparation of pellets by extrusion/spheronization: II Spheronization parameters. *Int. J. Pharm.*, 231, 107-119.

Umprayn, K., Chitropas, P., Amarekajorn, S., 1999. Influence of process variables on physical properties of pellets using extruder and spheronizer. *Drug Dev. Ind. Pharm.*, 25(1), 45-61.

Verbeek, J.J., Vlassis, N., Krose, B., 2003. Efficient greedy learning of Gaussian mixture models. *Neural Comput.*, 15, 469-485.

Vertommen J., Rombaut P., Michoel A., Kinget R., 1998. Estimation of amount of the water removed by gap and atomization air streams during pelletization in a rotary processor. *Pharm Devt Technol.*, 3(1), 63-72.

Vervaet, C., Baert, L., Remon, J.P., 1995. Extrusion-spheronization, A literature review. *Int. J. Pharm.*, 116, 131-146.

Vervaet, C., Remon, J.P., 1996. Influence of impeller design, method of screen perforation and perforation geometry on the quality of pellets made by extrusion spheronization. *Int. J. Pharm.*, 133, 29-37.

Wan, L.S.C., Heng, P.W.S., Liew, C.V., 1993. Spheronization conditions on spheroid shape and size. *Int J Pharm.*, 96:59-65.

Wan, L.S.C., Heng, P.W.S., Liew, C.V., 1994. The role of moisture and gap air pressure in the formation of spherical granules by rotary processing. *Drug Dev. Ind. Pharm.*, 20(16), 2551-2561.

Wanibe, Y., Itoh, T., 1998. Distribution of particle sizes. In: Wanibe, Y., Itoh, T. (Eds.), *New quantitative approach to powder technology*, John Wiley & Sons, New York, pp. 29-47.

LIST OF PUBLICATIONS/POSTER PRESENTATIONS

LIST OF PUBLICATIONS/POSTER PRESENTATIONS

Liew, C.V., **Chua, S.M.**, Heng, P.W.S., 2007. Elucidation of spheroid formation with and without the extrusion step. *AAPS PharmSciTech.*, 8(1), Article 10.

Chua, S.M., Liew, C.V., Heng, P.W.S., 2004, Comparison of roundness descriptors for quantifying the spheronization process of extrudates in a spheronizer. Inaugural AASP Conference, Beijing, China. (Poster)

Heng, P.W.S., **Chua, S.M.**, Liew, C.V., 2003, Analysis of size distribution of spheroids produced by Extrusion-Spheronization. AAPS Annual Meeting and Exposition, Salt Lake City, Utah, U.S. (Poster)